The University of Texas at Dallas
Center for Quantum Electronics
The Gamma-Ray Laser Project
Quarterly Report
January-March 1988

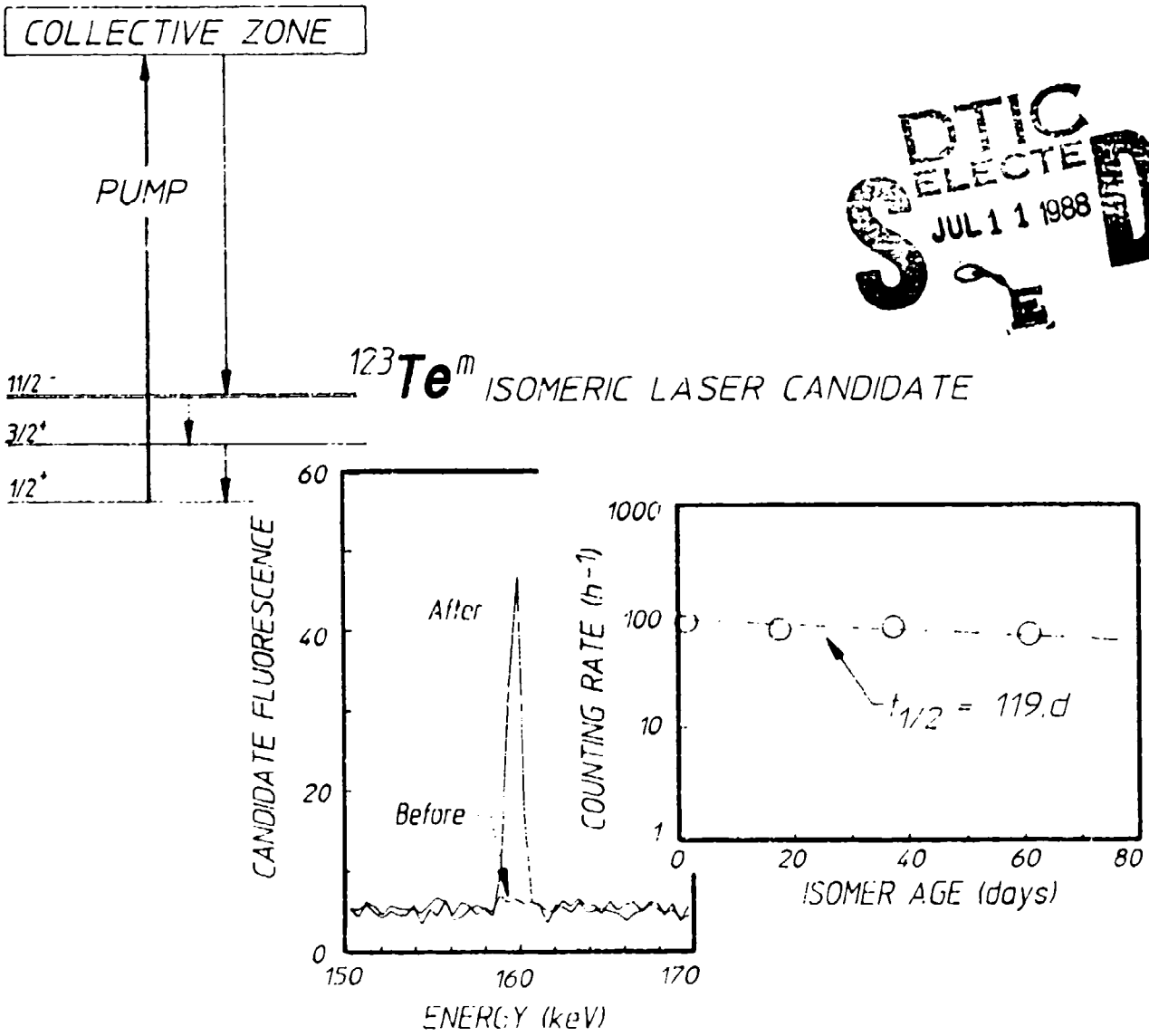

Report GRL/8704

PROOF OF THE FEASIBILITY OF COHERENT AND INCOHERENT SCHEMES FOR PUMPING A GAMMA-RAY LASER

Principal Investigator: Carl B. Collins
The University of Texas at Dallas
Center for Quantum Electronics
P.O. Box 830688
Richardson, Texas 75083-0688

April 1988

Quarterly Technical Progress Report
1 January 1988 through 31 March 1988
Contract Number N00014-86-C-2488

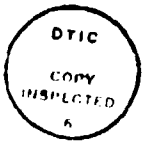

Prepared for
INNOVATIVE SCIENCE AND TECHNOLOGY DIRECTORATE
OF STRATEGIC DEFENSE INITIATIVE ORGANIZATION

Contracting Officer's Technical Representative
Dr. Paul Kepple, Code 4720
Naval Research Laboratory
4555 Overlook Avenue, SW
Washington, DC 20375-5000

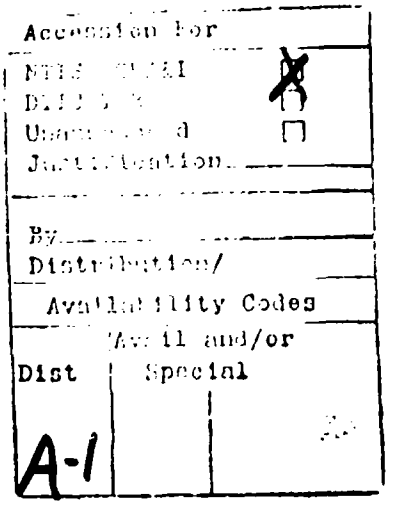

SECURITY CLASSIFICATION OF THIS PAGE (When Data Entered)

REPORT DOCUMENTATION PAGE

READ INSTRUCTIONS BEFORE COMPLETING FORM

1. REPORT NUMBER: GRL/8704	2. GOVT ACCESSION NO.
3. RECIPIENT'S CATALOG NUMBER	
4. TITLE (and Subtitle): PROOF OF THE FEASIBILITY OF COHERENT AND INCOHERENT SCHEMES FOR PUMPING A GAMMA-RAY LASER	5. TYPE OF REPORT & PERIOD COVERED: Quarterly Technical Progress 1/1/88 - 3/31/88
	6. PERFORMING ORG. REPORT NUMBER
7. AUTHOR(s): C. B. Collins	8. CONTRACT OR GRANT NUMBER(s): N00014-86-C-2488
9. PERFORMING ORGANIZATION NAME AND ADDRESS: University of Texas at Dallas, Center for Quantum Electronics, P.O. Box 830688 Richardson, TX 75083-0688	10. PROGRAM ELEMENT, PROJECT, TASK AREA & WORK UNIT NUMBERS
11. CONTROLLING OFFICE NAME AND ADDRESS: INNOVATIVE SCIENCE AND TECHNOLOGY DIRECTORATE OF STRATEGIC DEFENSE INITIATIVE ORGANIZATION	12. REPORT DATE: April 1988
	13. NUMBER OF PAGES: 92
14. MONITORING AGENCY NAME & ADDRESS(if different from Controlling Office): Dr. Paul Kepple, Code 4720, Naval Research Laboratory, 4555 Overlook Avenue, SW, Washington, DC 20375-5000	15. SECURITY CLASS. (of this report): Unclassified
	15a. DECLASSIFICATION/DOWNGRADING SCHEDULE

16. DISTRIBUTION STATEMENT (of this Report)

This document has been approved for public release and sale; its distribution is unlimited.

17. DISTRIBUTION STATEMENT (of the abstract entered in Block 20, if different from Report)

18. SUPPLEMENTARY NOTES

19. KEY WORDS (Continue on reverse side if necessary and identify by block number)

20. ABSTRACT (Continue on reverse side if necessary and identify by block number)

Recent approaches to the problem of the gamma-ray laser have focused upon upconversion techniques in which metastable nuclei are pumped with long wavelength radiation. At the nuclear level the storage of energy can approach tera-Joules (10^{12} J) per liter for thousands of years. However, any plan to use such a resource for a gamma-ray laser poses problems of a broad interdisciplinary nature requiring the fusion of concepts taken
(continued next page)

DD FORM 1 JAN 73 1473 EDITION OF 1 NOV 65 IS OBSOLETE

SECURITY CLASSIFICATION OF THIS PAGE (When Data Entered)

20. Abstract (continued)

from relatively unrelated fields of physics. Our research group has described several means through which this energy might be coupled to the radiation fields with cross sections for stimulated emission that could reach 10^{-17} cm^2. Such a stimulated release could lead to output powers as great as 3×10^{21} Watts/liter. Since 1978 we have pursued an approach for the upconversion of longer wavelength radiation incident upon isomeric nuclear populations that can avoid many of the difficulties encountered with traditional concepts of single photon pumping. Recent experiments have confirmed the general feasibility and have indicated that a gamma-ray laser is feasible if the right combination of energy levels and branching ratios exists in some real material. Of the 1886 distinguishable nuclear materials, the present state-of-the-art has been adequate to identify 29 first-class candidates, but further evaluation cannot proceed without remeasurements of nuclear properties with higher precision. A laser-grade database of nuclear properties does not yet exist, but the techniques for constructing one have been developed under this contract and are now being utilized. Resolution of the question of the feasibility of a gamma-ray laser now rests upon the determination of: 1) the identity of the best candidate, 2) the threshold level of laser output, and 3) the upconversion driver for that material.

This quarter's report focuses upon continued development of one of the new technologies for the screening of the laser candidates. It is the nuclear analog of the optical double resonance methods which produced much of the database at the molecular level that was of such essential use in the development of conventional lasers. Applied most recently to the study of levels which might be used in dumping isomeric populations into freely radiating states, it produced an unexpected result of major importance. In several test isotopes, a class of extremely useful states was discovered that could radiatively couple to both normal and isomeric states of a nucleus spanning large changes of angular momentum.

The achievements of this quarter culminated in the major milestone demonstration of the excitation of populations of the second of the 29 actual candidates for a gamma-ray laser. Another of the less attractive of the 29 isomers because of a large change in angular momentum of 5 h, $^{123}Te^m$ was one of the few which had both a radioactive signature sufficiently distinctive for detection and a stable ground state from which to fabricate a target. Pumped with the bremsstrahlung from a medical linear accelerator having its maximum output near 2 MeV, an astonishingly large cross section of 10,000 was found on the scale where unity results in a large yield. This corresponds to a partial width for the useful pumping of this isomer of 0.05 eV, a value nearly 10^5 in excess of the rule-of-thumb supposed to limit the useful absorption widths to 1 μeV for the pumping of nuclei with flash x-rays. The extent of the success with this relatively poor candidate together with the earlier achievement in pumping $^{180}Ta^m$ considerably strengthens the probabilities that a more suitable isomer for a gamma-ray laser exists among the better candidates.

TABLE OF CONTENTS

PREFACE

The nuclear analog of the ruby laser embodies the simplest concepts for a gamma-ray laser. Not surprisingly, the greatest rate of achievement in the quest for a subAngstrom laser continues in that direction. This quarterly report focuses upon the third major milestone achieved in FY-1987. The first had shown that bandwidth funneling works at the nuclear level, just as it did for ruby on the molecular scale. Experiments pumping ^{77}Se and ^{79}Br produced eleven orders of magnitude increase in fluorescence intensity over what could have been obtained by direct excitation. The second milestone demonstrated great success in optically pumping the first of the 29 actual candidates for a gamma-ray laser, $^{180}Ta^{m}$. Not a particularly attractive candidate, <u>a priori</u>, $^{180}Ta^{m}$ had been the only one for which a macroscopic sample was available. The need to span a formidably large $\Delta J = 8$ between isomer and fluorescence level supported little initial enthusiasm for this nucleus. However, when actually pumped, it showed the largest integrated cross section ever reported for interband transfer in any material, 4×10^{-22} cm^2 eV. This corresponded to a partial width for absorption from $^{180}Ta^{m}$ isomer to fluorescence was measured to be about 0.5 eV, *a value far exceeding the 1 μeV usually offered as a rule of thumb that would limit the interband transfer of nuclear population.*

The major milestone achieved in the current reporting period demonstrated that the successes with $^{180}Ta^{m}$ could be extended to another of the 29 candidate isomers. While milligram sized samples are not available for any of the remaining 28 candidates, one admits an alternative procedure for testing. Instead of dumping the isomer it can be produced by pumping it up from the ground state with flashes of x-rays. The candidate $^{123}Te^{m}$ is one of the few which has both a radioactive signature sufficiently distinctive to permit the unequivocal detection of such a long-lived isomer and a stable ground state from which to fabricate a target. In this case the ^{123}Te is a rare, but naturally occurring isotope with 0.91% abundance. Reported in this quarter is the excitation of ^{123}Te to the candidate isomer $^{123}Te^{m}$ with flash x-rays through an integrated cross section of 10,000 units. This corresponds to a partial width of 0.05 eV, another enormous value. The inverse could easily approach the 0.5 eV measured for the dumping of $^{180}Ta^{m}$ since pumping down in energy should be more favorable than pumping up.

These results with seemingly unattractive candidates indicate the probabilities should be raised for the full success of one of the other 27 materials. Two out of two candidates examined to date have narrowly missed being acceptable. They performed 10^3 to 10^4 times better than would have been expected theoretically. Perhaps, as suggested two quarters ago, collective oscillations which break the symmetries of the nuclei provide this major windfall making it easier to dump isomers by mixing single particle states needed in the transfer process. Much more experimentation will be needed to identify whether this is the actual mechanism responsible and to understand if the lessons taught by these first two materials are generally applicable in the pool of candidate isomers.

Continuing the preparation of this report as an "in-house" journal, this series presents material to reflect the individual contributions of the teams of research faculty and graduate students involved in these phases of the research. In this regard I wish to thank all our staff for their splendid efforts in supporting the preparation of these manuscripts to a rather demanding timetable.

- C. B. Collins
- Director
- Center for Quantum Electronics

MAJOR MILESTONE REPORT

Strengthening the Feasibility of a Gamma-Ray Laser

February 8, 1988

C. B. Collins, Center for Quantum Electronics, University of Texas at Dallas

Achievement

Discovered in the first of the 29 candidate isomers to be tested for a gamma-ray laser was a critical nuclear structure enabling performance to approach the ideal. Now a similar arrangement has been found in the second of the 29 candidates.

Technical Background

The nuclear analog of the ruby laser embodies the simplest concepts for a gamma-ray laser. Not surprisingly, the greatest rate of achievement in the quest for a subAngstrom laser continues in that direction. For ruby the identification and exploitation of a bandwidth funnel were the critical keys in the development of the first laser. There was a broad absorption band linked through efficient cascading to the narrow laser level.

Recently we reported a major milestone which showed that comparable structure existed at the nuclear scale in the first of the 29 candidate isomers available for testing, $^{180}Ta^{m}$. Populations of the isomer were successfully pumped down with flashes of x-rays absorbed through an astonishingly large cross section of 40,000 on the usual scale ($\times 10^{-29}$ cm^2 keV) where 10 describes a fully allowed process. This corresponded to a partial width for useful absorption of 0.5 eV, even better than what had been assumed for idealized nuclei. Such extremely favorable attributes allowed us to perform those experiments with as little as one milligram of $^{180}Ta^{m}$.

Milligram sized samples are not available for any of the remaining 28 candidates. However, one admits an alternative procedure for testing. Instead of dumping them, the isomers can be produced by pumping them up from the ground state with flashes of x-rays. The candidate $^{123}Te^{m}$ is one of the few which has both a radioactive signature sufficiently distinctive to permit the unequivocal detection of such a long-lived isomer and a stable ground state from which to fabricate a target. In this case the ^{123}Te is a rare, but naturally occurring isotope with 0.91% abundance.

Reported here is the excitation of ^{123}Te to the candidate isomer $^{123}Te^{m}$ with flash x-rays through an integrated cross section of 10,000 units.

Report

The excitation of $^{123}Te^{m}$ can be detected by the 159 keV photon emitted with 84% efficiency as part of the decay scheme of this isomer, as shown in Fig. 1. After pumping, the intensity of this spectral line should decay with the characteristic 119.7 day half-life of the isomer. In this major milestone experiment, 171 milligrams of the ground state ^{123}Te diluted in 32.4 grams of natural tellurium were irradiated with the bremsstrahlung from a 6 MeV linac. The accumulated dose at 2 MeV near the peak of the spectrum was 5.6×10^{10} photons/cm^2/keV delivered in a sequence of pulses each having a peak intensity of about 4 W/cm^2 at the sample.

The excitation energy of the gateway state was assumed to be 2000 keV in order to obtain a minimum value for the cross section, since smaller fluxes were available at even higher energies. Data shown in Figs. 2 and 3 determined the integrated cross section for the process to be about 10,200 of the usual units ($\times 10^{-29}$ cm^2 keV). This is an enormous value exceeded only by the cross section for the inverse process of dumping the only other laser candidate tested to date.

Significance

There is a threefold significance to this demonstration of the efficiency for producing populations of the second laser candidate to be considered.

1) The first and second real isomers to be tested for a gamma-ray laser were successfully destroyed and created, respectively, by optical pumping with astonishingly large cross sections. The partial width for creating the $^{123}Te^{m}$ isomer corresponds to 0.05 eV, an enormous value, and the inverse could easily approach the 0.5 eV measured for the dumping of $^{180}Ta^{m}$, since pumping down in energy should be more favorable than pumping up.

2) The nuclear analog to the ruby laser is a fully viable scheme for a gamma-ray laser, and both $^{180}Ta^{m}$ and $^{123}Te^{m}$ narrowly missed being acceptable candidates. They performed about 10^{4} and at least 10^{3} times better than would have been expected theoretically.

3) These results with seemingly unattractive candidates indicate the probabilities should be raised for full success of one of the other 27 materials.

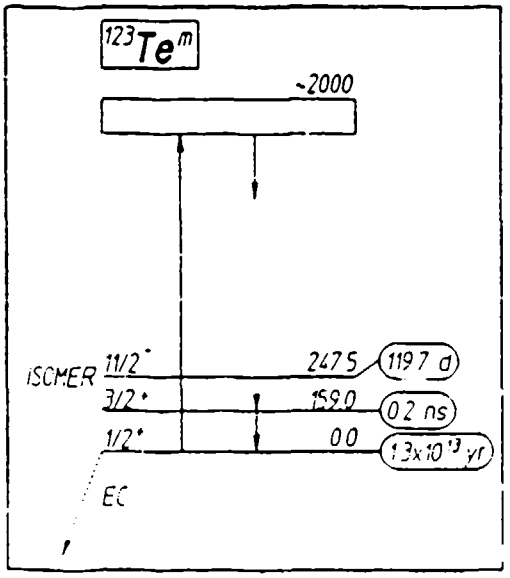

Figure 1: Schematic energy level diagram of ^{123}Te. Half-lives are shown in ovals to the right of the levels, and energies are in keV. The pump band is shown by the arrow pointing upward to the broad state represented by the rectangle. Cascade from this gateway is not known, but leads finally to the isomeric state. The resulting population of the laser candidate $^{123}Te^{m}$ is detected by the 159 keV fluorescence with a 119.7 day half-life.

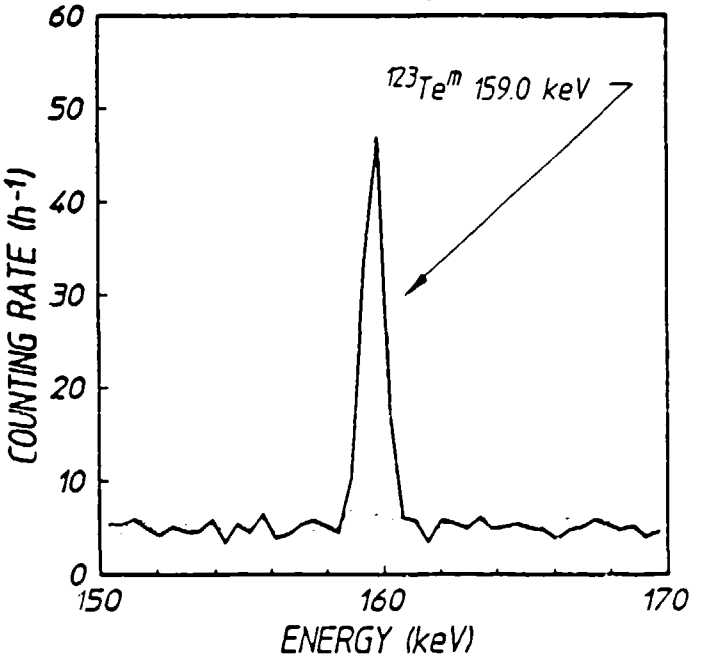

Figure 2 (top, right): Dotted and solid curves show, respectively, the spectra obtained before and after pumping some of the 171 mg of ^{123}Te to the isomeric $^{123}Te^{m}$.

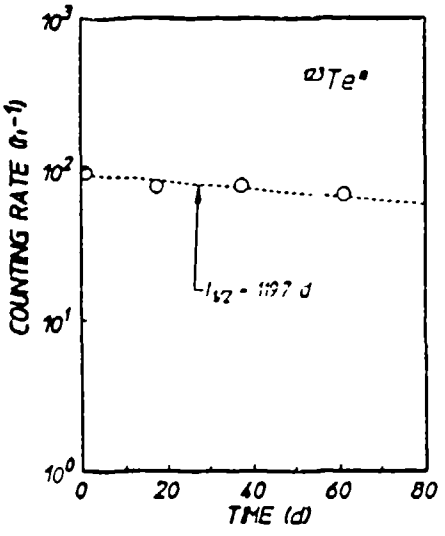

Figure 3 (bottom, left): Plot of the time decay of the activity of the $^{123}Te^{m}$ pumped into the target by the irradiation with the x-rays. The size of the plotted points represents 1 σ deviation, and the slope corresponds to the expected 119.7 day half-life.

RADIATIVE COUPLING TO THE ISOMERIC STATE $^{123}Te^{m}$

by J. A. Anderson, C. D. Eberhard, J. F. McCoy, K. N. Taylor, J. J. Carroll, M. J. Byrd, and C. B. Collins
University of Texas at Dallas

E. C. Scarbrough and P. P. Antich
University of Texas Southwestern Medical Center at Dallas

The first observation[1] of a (γ,γ') reaction leading to the deexcitation of an isomeric population revealed an unexpected large cross section for the process. The reaction $^{180}Ta^{m}(\gamma,\gamma')^{180}Ta$ was found to proceed through a partial width of 0.5 eV when pumped with the bremsstrahlung from a medical linear accelerator (linac). This is an enormous value which exceeds anything previously reported for (γ,γ') reactions[2-4] by two to three orders of magnitude. Such a high probability for deexcitation had been least expected for this isomer because of the unlikely change of $\Delta J = 8$ between $^{180}Ta^{m}$ and its ground state. For this reason it had been considered one of the poorest of the 29 candidates for a gamma-ray laser.

The extremely large size of the integrated cross section for the deexcitation of $^{180}Ta^{m}$, 4.8×10^{-22} cm^2 eV allowed us to perform those experiments with as little as one milligram of $^{180}Ta^{m}$. Unfortunately, even milligram sized samples are not available for any of the remaining 28 candidates so the general applicability of the lessons taught by the tantalum experiment cannot be directly examined. However, $^{123}Te^{m}$ is one of the few candidates for which indications can be found by less direct means. It has both a radioactive signature sufficiently distinctive to permit its unequivocal detection and a stable ground state from which to fabricate a target. In this case the ground state ^{123}Te is a rare, but naturally occurring radioactive isotope with 0.91% natural abundance and a half-life of 1.3×10^{13} years. Thus, instead of deexciting the isomeric state to the ground state, the inverse reaction can be studied.

In fact, experimental difficulties remain because of the combination of the low natural abundance of ^{123}Te in the ground state and a long half-life of 119.7 days for the emission of the fluorescence. Before there was any reason to expect that such negative factors could be compensated by a great width to the process, there was little motivation to try to examine the reaction $^{123}Te(\gamma,\gamma')^{123}Te^{m}$ and it was not reported in the previous general survey.[5] In the experiments described here it

was found that a large width did compensate the other difficulties and substantial amounts of fluorescence were observed.

The energy level diagram of ^{123}Te is shown in Fig. 1, together with a schematic representation of the individual steps in the excitation and detection of the $^{123}Te(\gamma,\gamma')^{123}Te^{m}$ reaction. As can be seen in Fig. 1, detection of the isomer depends on observing the 159 keV line from the lowest lying excited state in ^{123}Te, which is populated by the decay of $^{123}Te^{m}$ through an M4 transition. The efficiency for the emission of 159 keV photons relative to the number of $^{123}Te^{m}$ decays is about[6] 84%.

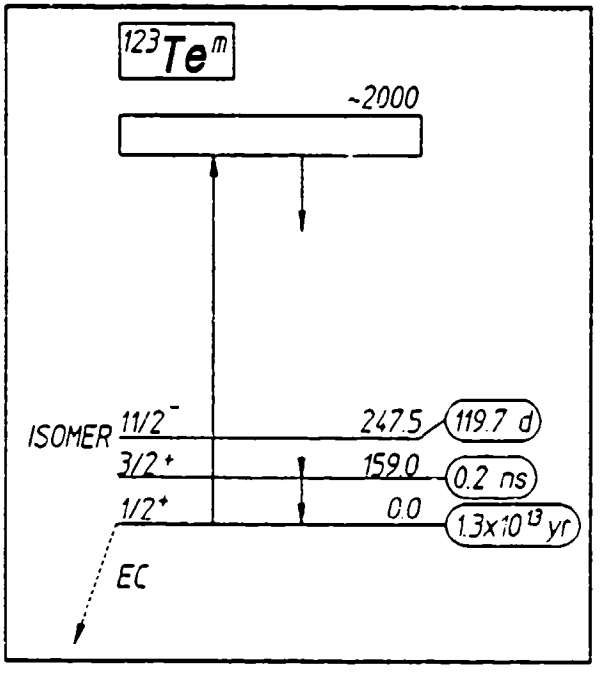

Figure 1: Schematic energy level diagram of ^{123}Te. Half-lives are shown in ovals to the right of the levels, and energies are in keV. The pump band is shown by the arrow pointing upward to the broad state represented by the rectangle. The cascade from this gateway is not known, but leads finally to the isomeric state. The resulting population of the laser candidate $^{123}Te^{m}$ is detected by the 159 KeV fluorescence with a 119.7 day half-life.

The target used in these experiments was a planchet of elemental tellurium in natural abundance. It was 5.2 cm in diameter and 0.47 cm

thick. The sample consisted of 32.4 g of tellurium, containing 0.294 g of ^{123}Te in its ground state.

The sample was exposed to bremsstrahlung radiation from a Varian Clinac 1800 linear accelerator (linac) operated with an end-point energy of 6 MeV. This device has been well characterized,[7,8] and its output dose rate is maintained in calibration with an accuracy of ± 3%. The accumulated dose at 2 MeV near the peak of the spectrum was 5.6×10^{10} photons/cm^2/keV delivered in a sequence of pulses each having a peak intensity of about 4 W/cm^2 at the sample. After irradiation, the sample was counted with an N-type, HPGe spectrometer having a beryllium entrance window. Conventional techniques were used to calibrate the counting system with isotopic standards.

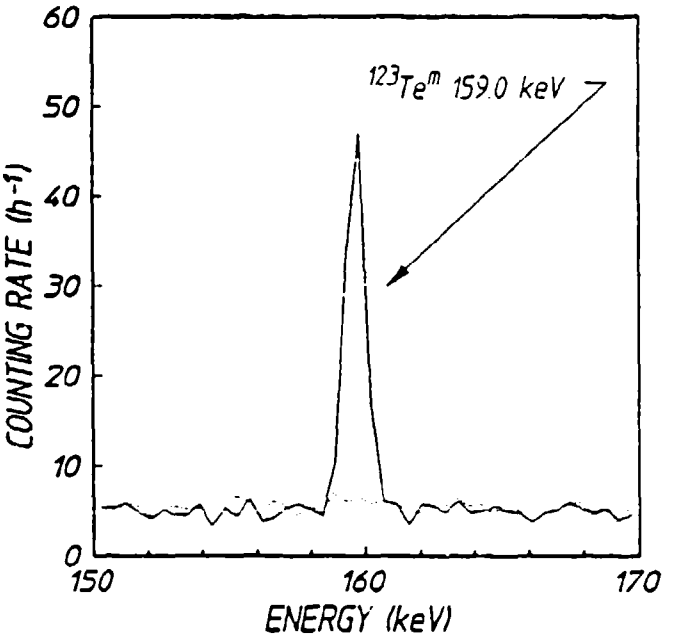

Figure 2: Dotted and solid curves show, respectively, the spectra obtained before and after pumping some of the 294 mg of ^{123}Te to the isomeric $^{123}Te^m$.

Figure 2 shows the spectra of the target before and after 4.0 hours irradiation. Figure 3 shows the dependence upon time of the counting rate observed in the 159 keV peak after irradiation. Data points are plotted to have a size comparable to the 1σ statistical error in the number of counts accumulated during the measurement periods. The figure

shows the close agreement of the measured rates to the decay expected for a half-life assumed to be 119.7 days.

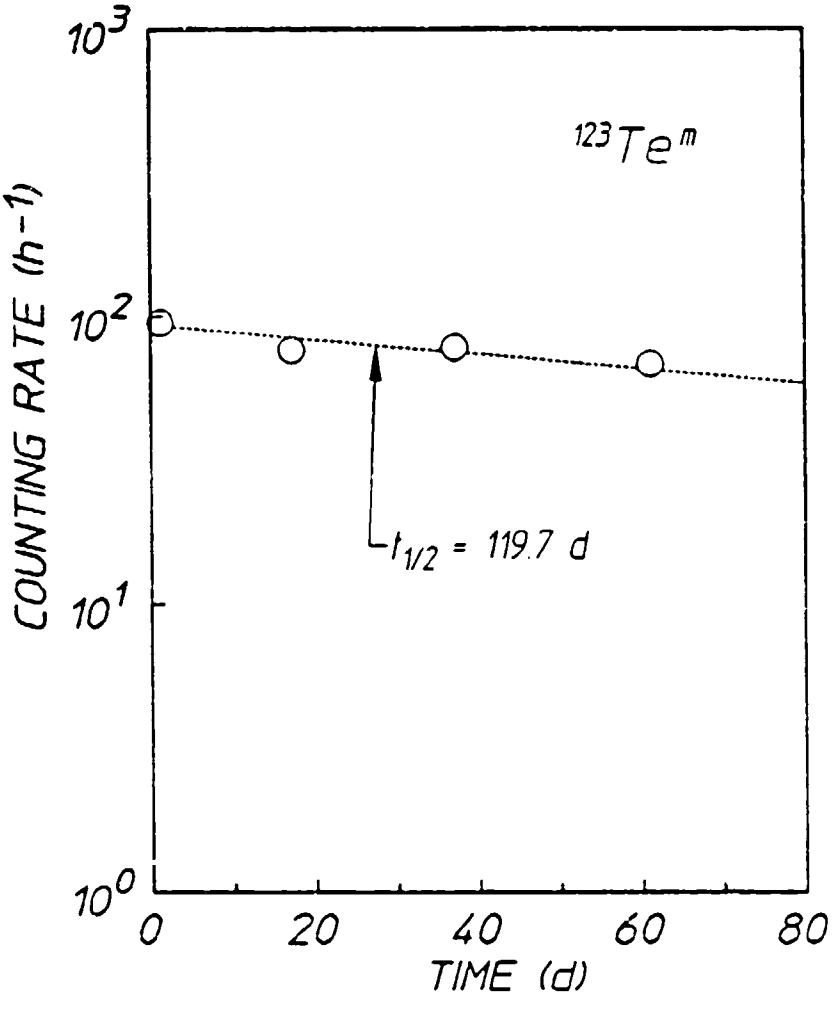

Figure 3: Plot of the time decay of the activity of the $^{123}Te^m$ produced in the target by irradiation with x-rays. The size of the plotted points is comparable to a 1 σ deviation, and the slope indicates the expected 119.7 day half-life.

The spectrum of the bremsstrahlung pumping the fluorescence seen in Fig. 2 was taken from the literature[7] and was normalized to the total dose measured in this experiment. In this way the time integrated spectral intensity producing the fluorescence was found to vary no more than a factor of two over the range 1-5 MeV, being approximately 1.0 *

10^{14} keV/(keV cm^2). The number of counts observed in the 159 keV line was corrected for finite irradiation and counting times. The total number of excitations was then calculated based on the 84% emission intensity of the 159 keV line from ^{123}Te, the calculated 59% probability for uncollided escape of the photon from the sample, and the calibrated absolute peak efficiency for the detector. From such data the integrated cross section for the deexcitation of the isomer can be readily calculated if the reaction is assumed to occur through a gateway state narrow in comparison to the range of energies spanned by the irradiation. A value of $\sigma\Gamma = 1.0 \times 10^{-25}$ cm^2 keV is obtained for the integrated cross section if the gateway energy is arbitrarily assumed to be near the lowest value consistent with prior[10] negative results, 2.0 MeV. Even larger cross sections would result from the assumption that the gateway lies at higher energies where the pumping flux is decreased. Once the gateway energy is fixed, experimental error in the integrated cross section is bounded by a total uncertainty of 15% contributed by the calibrations of source and detector.

As in the case of the deexcitation of ^{180}Ta^m, the cross section for the excitation of ^{123}Te^m is an enormous value. Moreover, the straightforward path of analyses shown schematically in Fig. 4 leads to rather astonishing conclusions.

Along the path of analysis of Fig. 4, assumptions are shown in ovals and derived results in rectangles. The most conservative results continue to be obtained by supposing the energy of the gateway band to which absorption first occurs to lie around 2 MeV. As shown in Fig. 4, this assumption together with the measured number of decays of ^{123}Te^m gives the value being reported for the integrated cross section, $(\pi b_a b_o \Gamma \sigma_o/2)$.

To obtain the partial width in the third row of Fig. 4 requires the Breit-Wigner cross section which peaks at

$$\sigma_o = \frac{\lambda^2}{2\pi} \frac{2I_e+1}{2I_g+1} \frac{1}{\alpha_p+1} , \qquad (1)$$

where λ is the wavelength in cm of the gamma ray at the resonant energy, E_i; I_e and I_g are the nuclear spins of the excited and ground states, respectively; and α_p is the total internal conversion coefficient of the gateway level. The value of α_p is essentially zero for a 2 MeV transition which is highly allowed; and even were it not, σ_o would be reduced

further and the partial width would become even larger. Nothing is known about the spin of the gateway state, but it is most reasonable to expect it to lie between that for the initial and final states. In that case $I_e > I_g$, since the process is starting on the $1/2^+$ state. From Eq. (1) it can be seen that the assumption $I_e = 3/2$ results in a possible underestimation of σ_0 but not by more than 50%.[11] As shown in Fig. 4, the partial width for pumping the isomer down to the ground state becomes,

$$b_a b_0 \Gamma = 0.05 \text{ eV} \quad . \qquad (2)$$

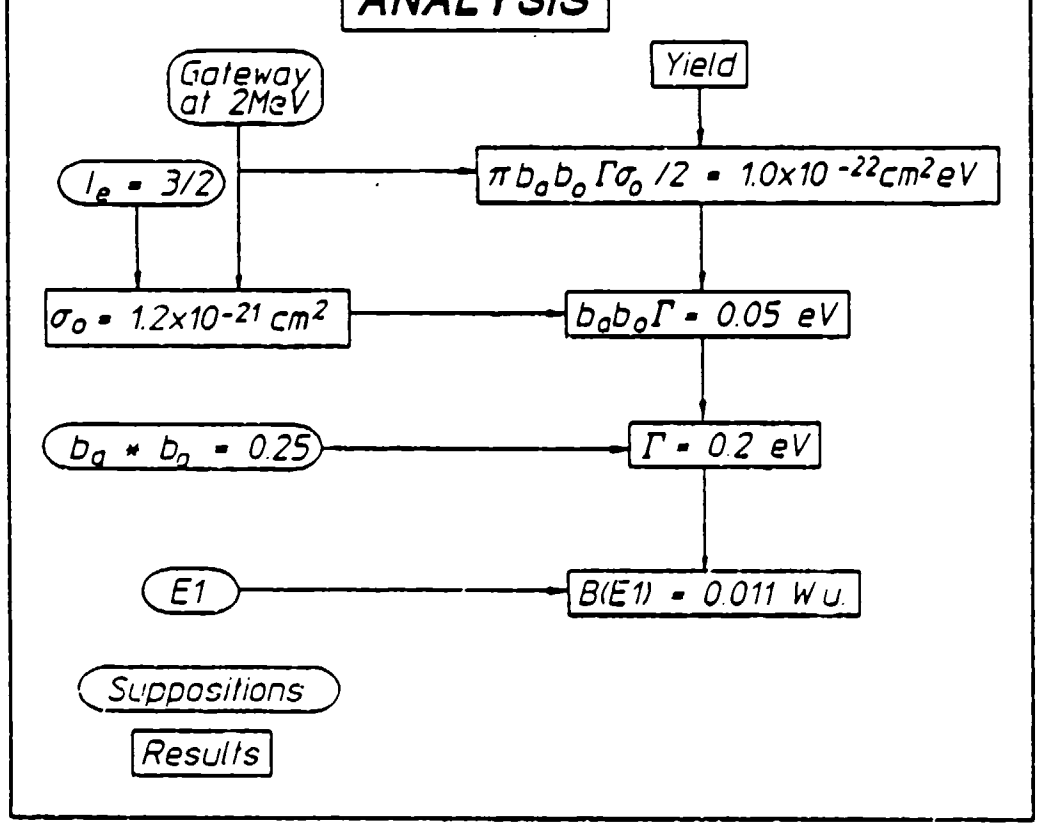

Figure 4: Flow chart showing the interrelation of assumptions and conclusions reached in the analysis of the tellurium data.

If this product is further analyzed as representing the width of a single state coupled to the ground state toward the isomer as shown in Fig. 1, it must be concluded that the width of the gateway state is at least 0.2 eV, as shown in Fig. 4. From the uncertainty principle,

$$\Gamma = \hbar/\tau_1 \quad , \tag{3}$$

where τ_1 is the lifetime of the funneling state, it is found,

$$t_{1/2}(\text{gateway}) = 2.2 \text{ fs} \quad . \tag{4}$$

To be consistent with the assumption $b_a \times b_o = 0.25$ it must be concluded that the total width of 0.2 eV for the funneling level is contributed equally by two transitions, each of 0.1 eV width. As shown in Fig. 1, one must connect to the ground and one to some other level with angular momentum more nearly comparable to that of the isomer. Transition strengths are often measured in Weisskopf units (W.u.) since 1.0 W.u. is the maximum possible for the transition of a single nucleon for a given multipolarity.[12] Converted into those units the transition probability B(M) for one of the component steps of 0.1 eV width would become,

$$B(E1) = 0.0058 \text{ W.u.} \quad , \tag{5}$$

and

$$B(M1) = 0.6 \text{ W.u.} \quad , \tag{6}$$

respectively, depending upon whether the multipolarity M were E1 or M1.

Again, these are enormous strengths, being almost without precedent. The expected[13] value for an electric dipole transition lies in the range 5×10^{-7} to 6×10^{-5} W.u. for heavy nuclei and fewer than ten are known[13,14] to approach 0.1 W.u. at these energies. For those exceptional cases, the width of the upper level is entirely due to the contribution from a single transition. Prior to the results with $^{180}Ta^m$ there were no cases known where two transitions of such strength added comparable components of width to the same upper state.

The situation is little changed if the transitions are assumed to be mediated by the magnetic dipole, M1 operator. Generally not as hindered as E1 transitions,[13] M1 strengths approach 0.1 W.u. in many cases. However, the scale of the W.u. for an M1 transition is smaller

in physical units of width; so our measured widths correspond to a much larger number of W.u., thus presenting the equivalent problem. Fewer than ten M1 transitions are known[13] to have B(M1) > 1.0 W.u. and none are paired to share a common level.

While the width of the transfer process is difficult to interpret in the context of a single funneling state in a single particle model, a puzzle of comparable complexity is found in the efficiency with which ΔJ is transferred. It is an interesting speculation that at certain energies of excitation collective oscillations of the core nucleons could break some of the symmetries upon which rest the identification of the pure single particle states. If single particle states of differing angular momenta were mixed in this way, the possibility for transferring larger amounts of ΔJ with greater partial widths might be enhanced. Some support for such a speculation was found in the unexpected enhancements measured for the excitation of ^{167}Er, as discussed in a previous quarterly report.[15].

Whatever the cause, the significance of these results is clear. Two of the poorest examples of the 29 candidates for gamma-ray materials were found to have very strong radiative connections between ground and isomeric states. The partial width for creating the $^{123}Te^{m}$ isomer corresponds to 0.05 eV, an enormous value, and the inverse could easily approach the 0.5 eV measured for the dumping of $^{180}Ta^{m}$, since pumping down in energy should be more favorable than pumping up. It appears that both $^{180}Ta^{m}$ and $^{123}Te^{m}$ narrowly missed being acceptable candidates. They performed about 10^4 and at least 10^3 times better than would have been expected theoretically. These results with seemingly unattractive candidates indicate the probabilities should be raised for full success of one of the other 27 materials.

References

1. C. B. Collins, C. D. Eberhard, J. W. Glesener, and J. A. Anderson, Phys. Rev. C (May 1988).

2. E. C. Booth and J. Brownson, Nucl. Phys. A98, 529 (1967).

3. M. Boivin, Y. Cauchois and Y. Henc, Nucl. Phys. A137, 520 (1971).

4. M. Boivin, Y. Cauchois and Y. Heno, Nucl. Phys. A176, 626 (1971).

5. H. R. Lukins, J. W. Otvos, and C. D. Wagner, Int. J. of Appl. Rad. and Isotopes 11, 30 (1961).

6. E. Browne and R. B. Firestone, Table of Radioactive Isotopes, edited by V. S. Shirley, (J. Wiley, New York, 1986) p. 180-2.

7. R. Mohan, C. Chui, and L. Lidofsky, Med. Phys. 12, 595 (1985).

8. N. C. Ikoro, D. A. Johnson, and P. P. Antich, Med. Phys. 14, 93 (1987).

9. Since the spectral intensity is roughly constant, the flux decreases as E^{-1} toward the end point with a final more rapid drop between 5 and 6 MeV.

10. C. B. Collins and J. A. Anderson, Proof of the Feasibility of Coherent and Incoherent Schemes for Pumping a Gamma-Ray Laser, University of Texas at Dallas, Report #GRL/8701, Innovative Science and Technology Directorate of Strategic Defense Initiative Organization, July 1987, pp. 35-53.

11. It is unlikely I_e could be greater than 5/2 and still support such a highly allowed transition from the ground state.

12. P. J. Brussard and P. W. M. Glaudemans, Shell-Model Applications in Nuclear Spectroscopy, (North-Holland, Amsterdam, 1977) Ch. 10.

13. A. deShalit and H. Feshbach, Theoretical Nuclear Physics Vol. I: Nuclear Structure (J. Wiley, New york, 1974) Ch. 8 Section 11.

14. C. F. Perdrisat, Rev. Mod. Phys. 38, 41 (1966).

15. C. B. Collins, J. M. Carroll, and J. A. Anderson, in Center for Quantum Electronics Report #GRL/8702, University of Texas at Dallas, 1987 (unpublished), pp. 13-44.

N00014-86-C-2488
UTD #24522-964

PHOTOTACTIVATION OF SHORT-LIVED ISOMERS WITH BREMSSTRAHLUNG RADIATION FROM A MEDICAL LINEAR ACCELERATOR

by J. A. Anderson, C. D. Eberhard, J. F. McCoy, K. N. Taylor, J. J. Carroll, M. J. Byrd, and C. B. Collins
University of Texas at Dallas

E. C. Scarbrough and P. P. Antich
University of Texas Southwestern Medical Center at Dallas

Recently, a renaissance was launched in the study of (γ,γ') reactions by the availability of medical linear accelerators (linacs) which can serve as intense and stable bremsstrahlung sources with particularly well-characterized spectra.[1,2] The total doses which they can deposit in reasonable working periods have made possible the examination of (γ,γ') reactions involving rare materials for which target masses are limited to milligrams. In this way, the first (γ,γ') reaction leading to the deexcitation of an isomeric sample was studied,[3] with rather unexpected results. Requiring an unlikely change of $\Delta J = 8$, this isomer $^{180}Ta^{m}$ was dumped through a partial width of at least 0.5 eV, an enormous value exceeding anything previously reported for (γ,γ') reactions at comparable energies by two to three orders of magnitude. Subsequently, the reactions producing some other long-lived isomers were found[4] to proceed through nearly comparable partial widths of 0.05 eV. Such a large value was also found for the isomer $^{123}Te^{m}$. With a 119.7 day half-life it becomes the longest lived isomer produced in a (γ,γ') reaction.

The integrated cross sections for either pumping or dumping of nuclear isomers are usually expressed as $\pi b_a b_o \sigma_o \Gamma/2$ where Γ is the natural width in keV of the i-th pump band,

$$\Gamma = \hbar/\tau_p \quad , \tag{1}$$

where τ_p is the natural lifetime and the branching ratios b_a and b_o give the probabilities for the decay of the broad level back into the initial and fluorescence level, respectively. The pump energy E_i is in keV and σ_o is the amplitude of the Breit-Wigner cross section for the absorption transition,

$$\sigma_o = \frac{\lambda^2}{2\pi} \quad \frac{2I_e+1}{2I_g+1} \quad \frac{1}{\alpha_p+1} \quad , \tag{2}$$

where λ is the wavelength in cm of the gamma ray at the resonant energy E_i; I_e and I_g are the nuclear spins of the excited and ground states, respectively; and α_p is the internal conversion coefficient of the absorption transition. If there is more than one pump band linking initial and final states, products of integrated cross section and input flux must be summed over the appropriate bands.

The combination, Γ_x

$$\Gamma_x = b_a b_o \Gamma \quad , \tag{3}$$

is the partial width for excitation (or deexcitation) of an isomeric sample. Because of the possibility of cascading transitions being involved in the reaction, a partial width measured in one sense does not necessarily characterize the inverse process.

Integrated cross sections for the archetype cases[5,6] of ^{115}In and ^{111}Cd were of the order of 10 in the conventional units of 10^{-29} cm^2 keV. Such values for excitation through a gateway near 1 MeV are characteristic of products of branching ratios $b_a b_o$ somewhat degraded from the optimal value of 0.25. One transition is primarily responsible for the favorable width of the gateway. The other transition is parasitic, contributing lesser additional width. Whether this is simply coincidental for these two cases or the result of a general principle is not known.

Very early data[7,8] indicated that yields from (γ,γ') reactions increased as higher energy gateway states were accessed. Evidence was accumulated[7,8] in the form of increases in the slopes of curves showing product yields as functions of the end point energies of the bremsstrahlung used to pump the reactions, but the changes were not dramatic. The largest value found[8] was 580 units for the (γ,γ') excitation of ^{87}Sr^m from the ground state through a gateway at 2.66 MeV.

Systematic studies[9] have shown that collective octupole oscillations of the nuclear core can unhinder E1 transitions, making very short lived states available for (γ,γ') reactions excited from ground states at energies between 1 and 2 MeV. However, the literature[10] suggests that the branching for such a collective state would almost entirely favor the initial transition so that a diminishing product, $b_a b_o$, would largely offset the greatly increased width Γ in expressions for the

integrated cross section for a (γ,γ') reaction excited through such a collective state. Such an expectation is supported by the early data mentioned above.

Since the density of states is considerably elevated at energies of 1 to 2 MeV above the ground state, an alternate speculation is attractive. A strong collective oscillation of the core might serve to mix enough single particle states so that radiative branches to several different lower levels would become comparable. In this case a very large integrated cross section of (γ,γ') reactions producing isomers from ground state nuclei might be found to be only slightly dependent upon the detailed single particle assignments of neighboring nuclei. Just such an observation was recently reported.[4] Integrated cross sections of the order of 10,000 in the units of 10^{-29} cm^2 keV were found for the excitation of isomers of ^{111}Cd, ^{113}In, and ^{115}In through resonant gateways pumped by bremsstrahlung from a linear accelerator producing most of its intensity near 2 MeV.

Confirmed in a subsequent report was an extension of those studies to the excitation of very long-lived isomers having half-lives varying from hours to weeks. Pumped with a linac having its end point energy at 6 MeV, the (γ,γ') reactions had to proceed through channels providing for changes of angular momentum ranging from $\Delta J = 4$ to 6. Five nuclides were examined: ^{87}Sr, ^{117}Sn, ^{135}Ba, ^{195}Pt, and ^{199}Hg. Integrated cross sections were found to range from 1,000 to 20,000 in the usual units of 10^{-29} cm^2 keV, the facility for excitation showing no correlation with ΔJ. The largest occurred for ^{195}Pt$(\gamma,\gamma')^{195}$Pt^m which requires $\Delta J = 6$ to excite a 4 day isomer.

Reported here is a further extension of these studies to the excitation of short-lived isomers having half-lives varying from 2.3 to 153 seconds. Pumped with the same linac as used with the longer-lived isomers, these (γ,γ') reactions proceeded through channels providing for changes of angular momentum ranging from $\Delta J = 3$ to 5. Eight isomers were successfully activated and studied in this work: ^{167}Er, ^{79}Br, ^{191}Ir, ^{183}W, ^{197}Au, ^{89}Y, ^{77}Se, and ^{137}Ba. In addition, silver was photoactivated, but the limited resolution of our NaI(Tl) spectrometer was inadequate to separate the contributions of ^{107}Ag ($T_{1/2}$ = 44.2 s, E = 93.2 keV) and 109Ag ($T_{1/2}$ = 39.6 s, E = 88.0 keV). Six other isomers, ^{207}Pb, ^{90}Zr, ^{177}Hf, ^{178}Hf, ^{176}Yb, and ^{190}Os, exhibited no measurable activation.

Because of the short half-lives a pneumatic system was needed to transfer the samples from the site of the irradiation to the counting system. Since the activation saturated after a few half-lives for the isomeric population, irradiation times were short and only (γ,γ') reactions proceeding through highly allowed channels could be studied. Nevertheless, integrated cross sections were generally found to be as large for the short-lived isomers as had been found for the longer-lived ones, ranging from 2000 to 100,000 in the usual units of 10^{-29} cm^2 keV. In contrast to the previous work[11] with the long-lived isomers, these studies showed some roughly inverse correlation of cross section with the magnitude of ΔJ that had to be spanned between ground state and isomer. While the energies of the responsible gateways still cannot be determined, the pervasiveness of such large partial widths for the exchange of substantial amounts of angular momentum remains surprising for any energies below the thresholds for (γ,n) reactions.

Experimental Procedures

The relevant energy levels for the ten nuclei of interest in these experiments are shown in Fig. 1. With two exceptions, they were present in targets fabricated from materials containing natural isotopic abundances in the form of either powders held in cylindrical polyethylene vials or in metallic foils. In some cases the samples were sufficiently thick that self-absorption of the output transition necessitated a correction of significant magnitude. The samples of ^{167}Er and ^{77}Se were isotopically enriched materials.

Targets were exposed for times on the order of a few minutes to the output of a Varian Clinac 1800 linear accelerator at the Department of Radiology of the University of Texas Southwestern Medical Center at Dallas. This linear accelerator was operated with an end point energy of 6 MeV. After irradiation, the samples were transferred to a counting system with the same pneumatic arrangement described in previous reports of experiments conducted on e-beam sources of bremsstrahlung.[12] The transit time was logged and all samples were counted in a well-type NaI(Tl) crystal spectrometer.

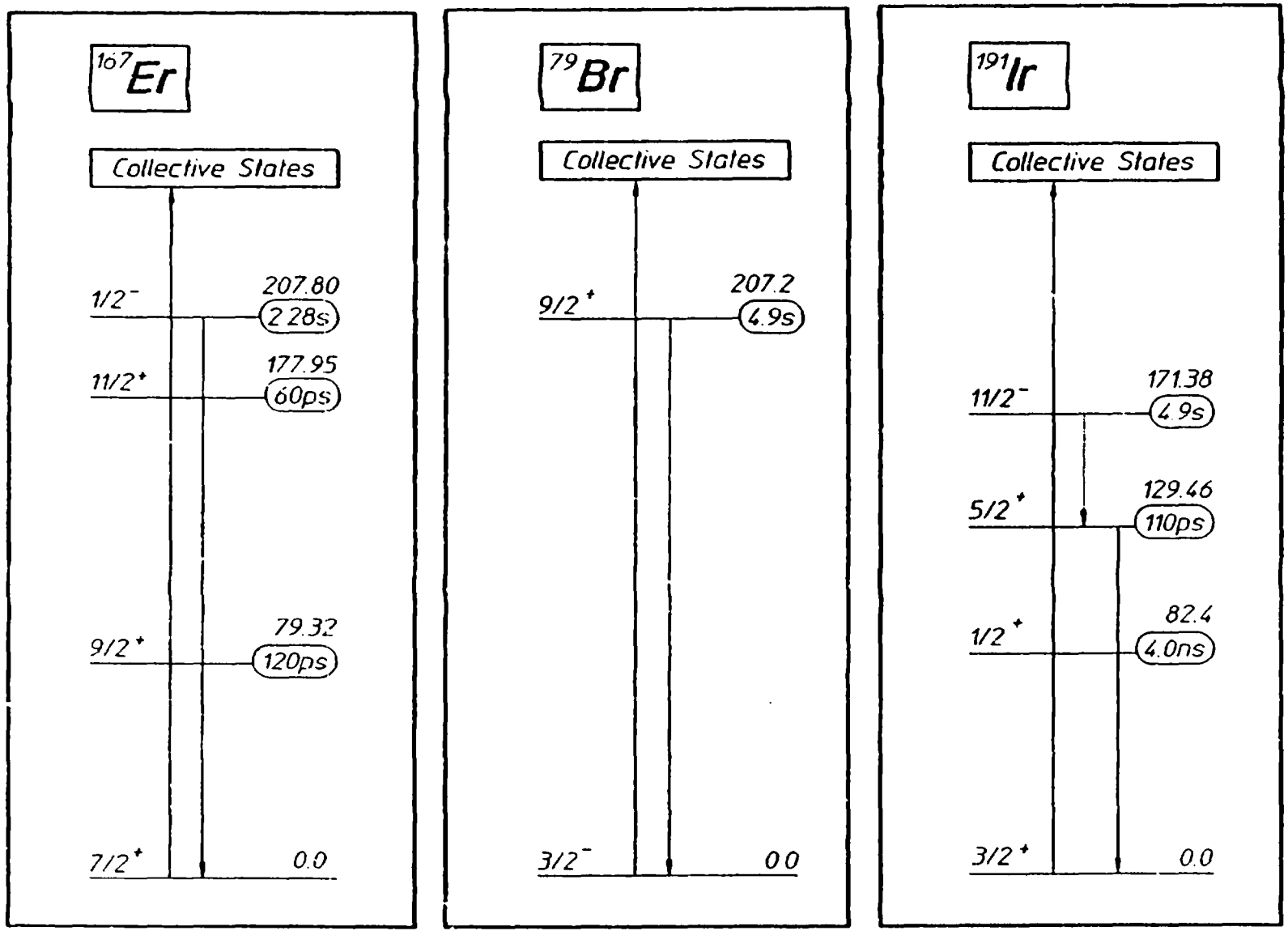
^{167}Er
Collective States
1/2⁻
207.80
2.28s
11/2⁺
177.95
60ps
9/2⁺
79.32
120ps
7/2⁺
0.0
^{79}Br
Collective States
9/2⁺
207.2
4.9s
3/2⁻
0.0
^{191}Ir
Collective States
11/2⁻
171.38
4.9s
5/2⁺
129.46
110ps
1/2⁺
82.4
4.0ns
3/2⁺
0.0

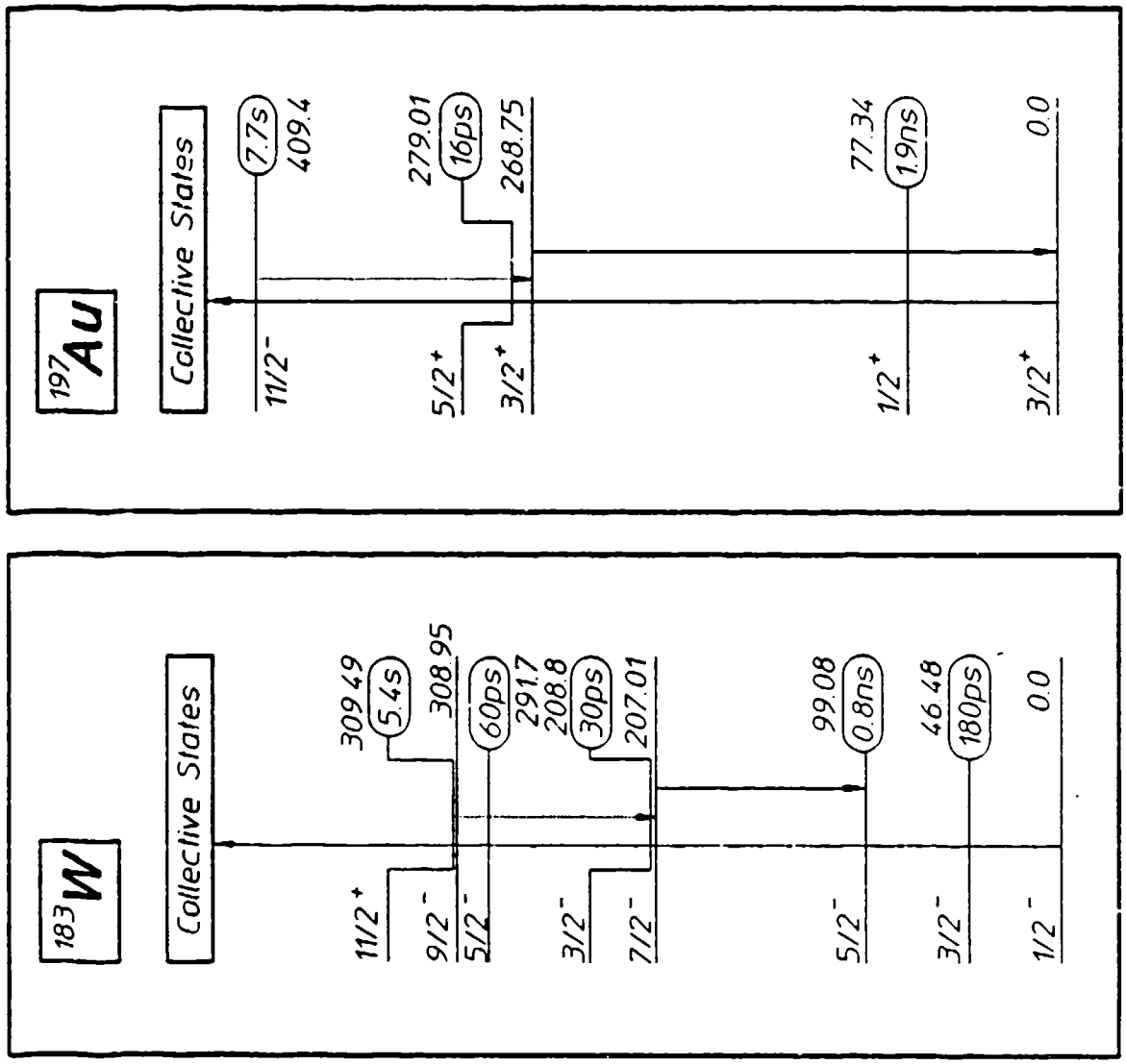

Figure 1: Energy level diagrams of the excited states important to the production and detection of the isomers of the nuclei shown. Half-lives of the states are shown to the right of each, together with their energies in keV. Downward arrows locate transitions used in the detection of populations of the isomers produced by the absorption transitions indicated by the upward arrows. The locations of the gateways through which the (γ,γ') reactions proceed are not to scale, and the details of the cascades downward to the isomers are unknown. Shown by dotted arrows are components of cascades from the product isomers useful in feeding the transitions used for detection. a), b) and c) (opposite from left): Transitions important to the study of (γ,γ') reactions producing the isomers $^{167}Er^{m}$, $^{79}Br^{m}$, and $^{191}Ir^{m}$. d), and e) (from left): Transitions important to the study of (γ,γ') reactions producing the isomers $^{183}W^{m}$, and $^{197}Au^{m}$.

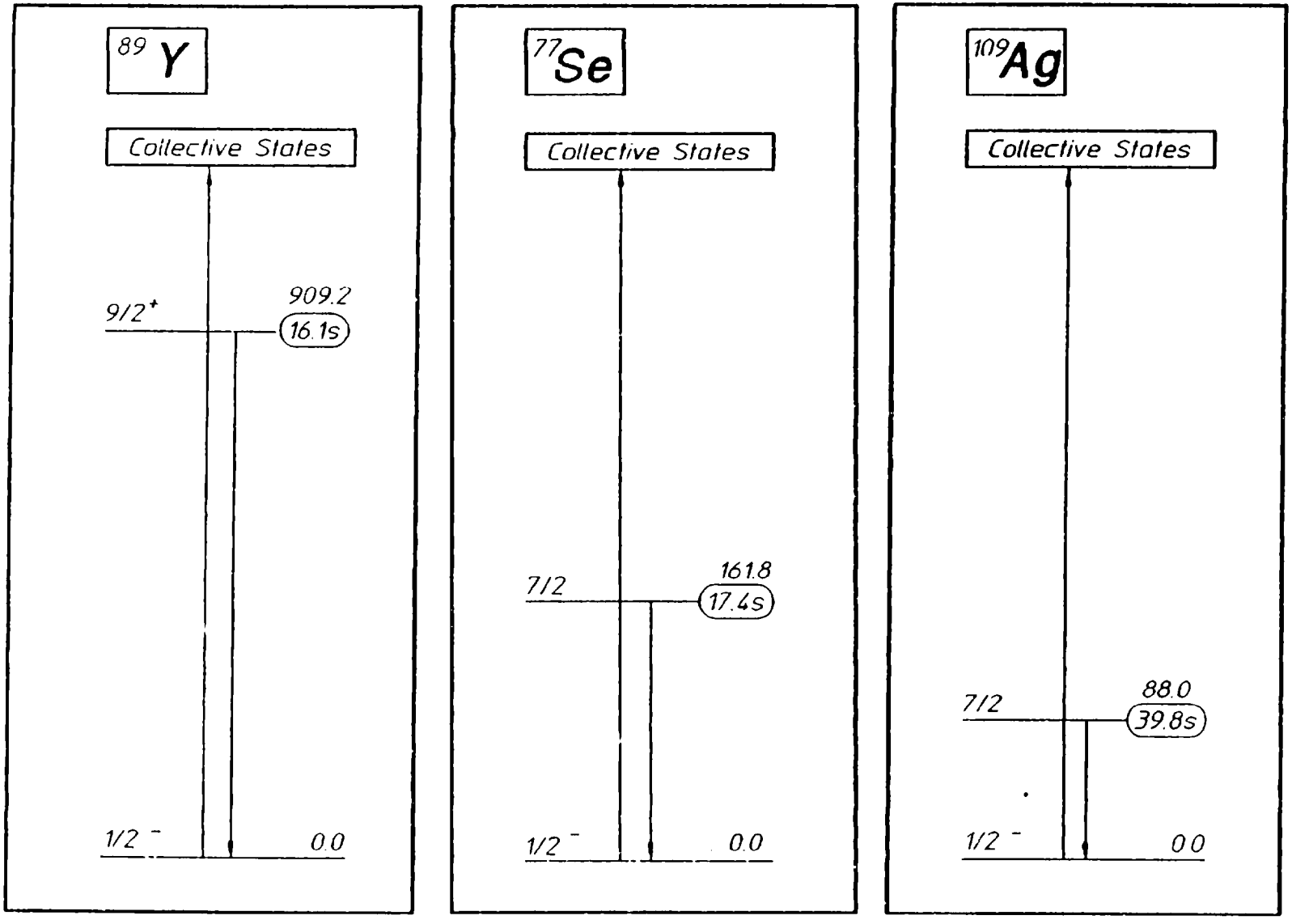
89 Y
Collective States
9/2+
909.2
16.1s
1/2 -
0.0
77Se
Collective States
7/2
161.8
17.4s
1/2 -
0.0
109Ag
Collective States
7/2
88.0
39.8s
1/2 -
0.0

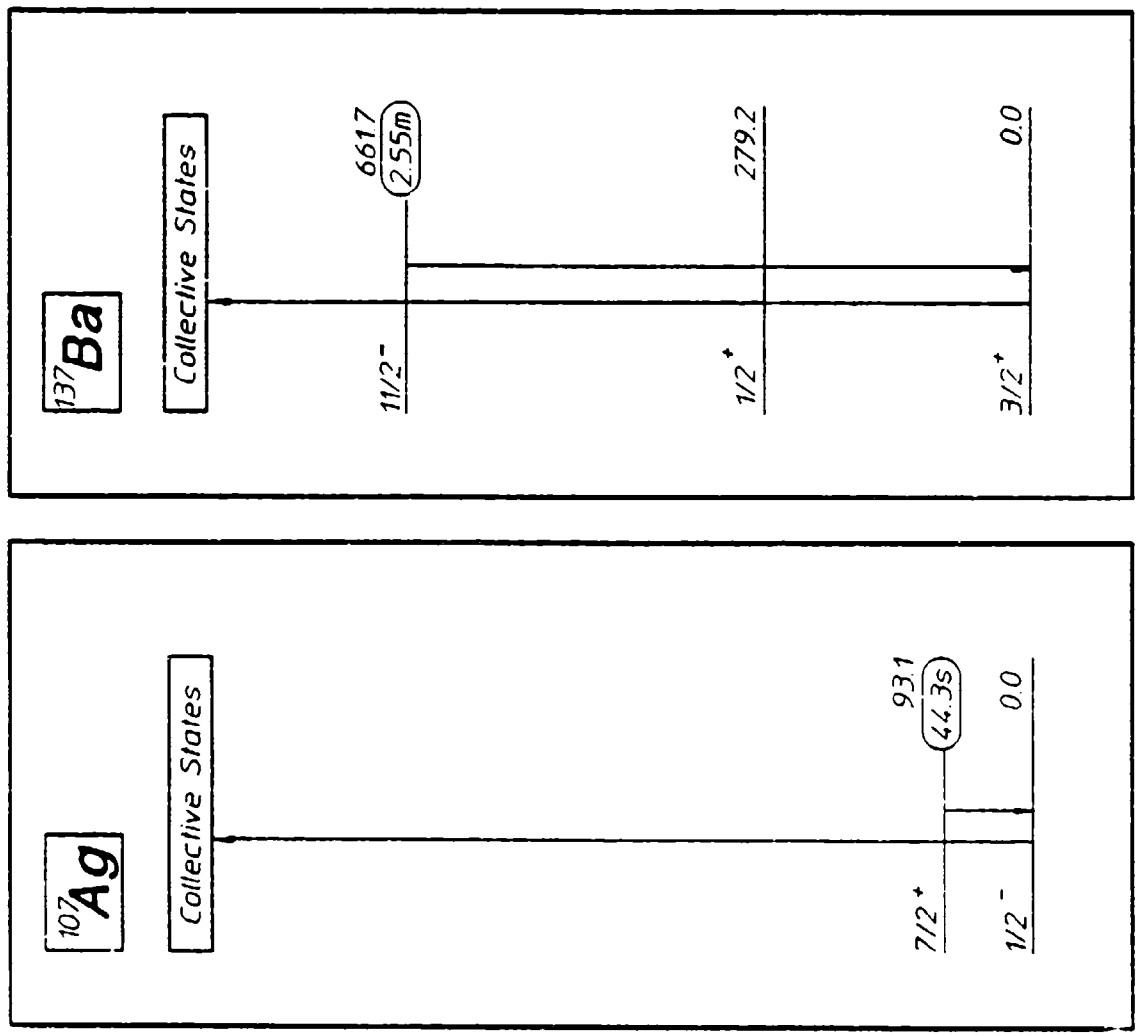

Figure 1: (continued) Energy level diagrams of the excited states important to the production and detection of the isomers of the nuclei shown. Half-lives of the states are shown to the right of each, together with their energies in keV. Downward arrows locate transitions used in the detection of populations of the isomers produced by the absorption transitions indicated by the upward arrows. The locations of the gateways through which the (γ,γ') reactions proceed are not to scale, and the details of the cascades downward to the isomers are unknown. Shown by dotted arrows are components of cascades from the product isomers useful in feeding the transitions used for detection. f), g), and h) (opposite from left): Transitions important to the study of (γ,γ') reactions producing the isomers $^{89}Y^{m}$, $^{77}Se^{m}$, and $^{109}Ag^{m}$. i) and j), (from left): Transitions important to the study of (γ,γ') reactions producing the isomers $^{107}Ag^{m}$ and $^{137}Ba^{m}$.

Target parameters are summarized in Table I, together with the corrections for self-absorption computed from the counting geometry, sample composition, and sample density. The validity of the self-absorption calculation was verified by comparing cross-section results obtained for idential materials using samples that presented different geometrical conditions.

TABLE I

LINAC Short-lived Isomer Study
Sample Parameters for Nuclides in LINAC Study

Nuclide	Abundance (%)	Chemical Form	Sample Mass (g)	Half-life (s)	Exposure Time (s)	Count Time (s)	Principal Fluorescence (keV)	Fluorescence Intensity (%)	Transparency
^{96}Zr	91.54	ZrO_2	9.08	2.28	25	5	207.79	41.70	0.579
^{79}Br	50.69	LiBr	12.83	4.86	50	10	207.70	75.80	0.842
^{191}Ir	37.30	Ir	3.97	4.94	50	10	129.43	25.70	0.0793
^{185}W	14.30	W	20.75	5.15	50	10	107.93	18.40	< 0.0384
^{197}Au	100.00	Au		7.80	80	20	279.11	73.00	0.399 - 0.092
^{89}Y	100.00	YF_3	10.23	16.06	160	32	909.15	99.14	0.965
^{77}Se	94.38	Se	3.38	17.45	150	40	161.92	52.40	0.837
^{109}Ag	48.16	Ag	53.05	39.60	400	80	88.03	3.60	
^{107}Ag	51.84	Ag	53.05	44.30	400	80	93.15	4.67	
^{137}Ba	11.74	BaF_2	7.48	153.08	599	300	661.66	90.10	0.953

Typical nuclear fluorescence spectra from the isomers excited in this work by the irradiations are shown in Figs. 2a - 2i. The low resolution of the NaI(Tl) system necessitated a greater level of concern over the identity of the various prominent features in the spectra than would have been necessary had the data been taken with an HPGe spectrometer. Confirmation that the fluorescence peaks were the signatures of the respective isomers was obtained by examining the decays of the counting rates as functions of the times elapsed from the cessation of the irradiation. These decay data are shown in Fig. 3a - 3i, together with curves reflecting expectations based upon literature values of the half-lives. For each of the ten nuclides studied, both spectral and temporal content of the fluorescence were consistent with the expected signatures.

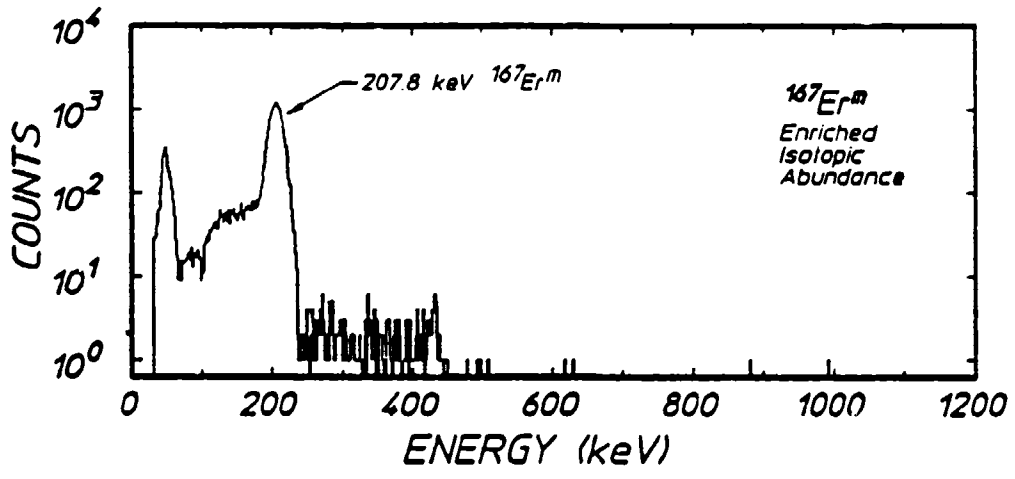
207.8 keV 167Er m
167Er m
Enriched
Isotopic
Abundance
COUNTS
ENERGY (keV)

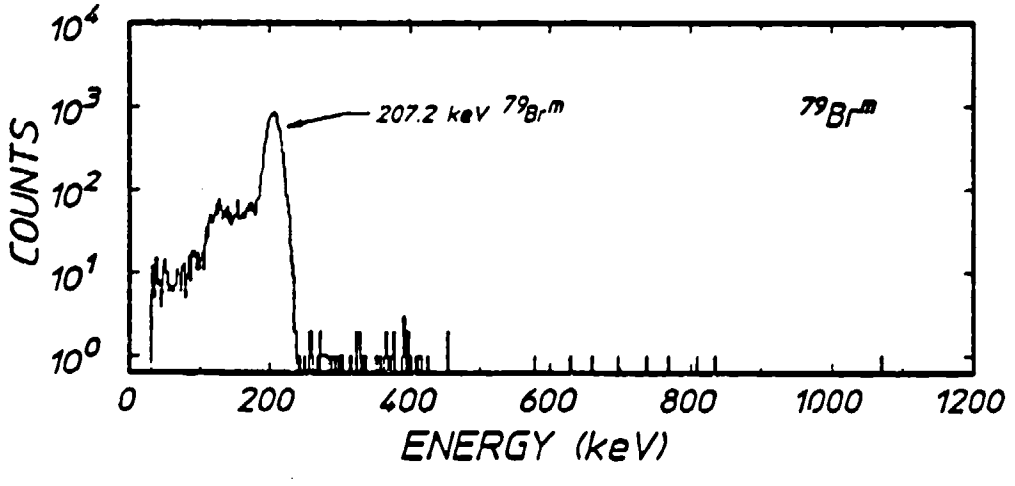
207.2 keV 79Br m
79Br m
COUNTS
ENERGY (keV)

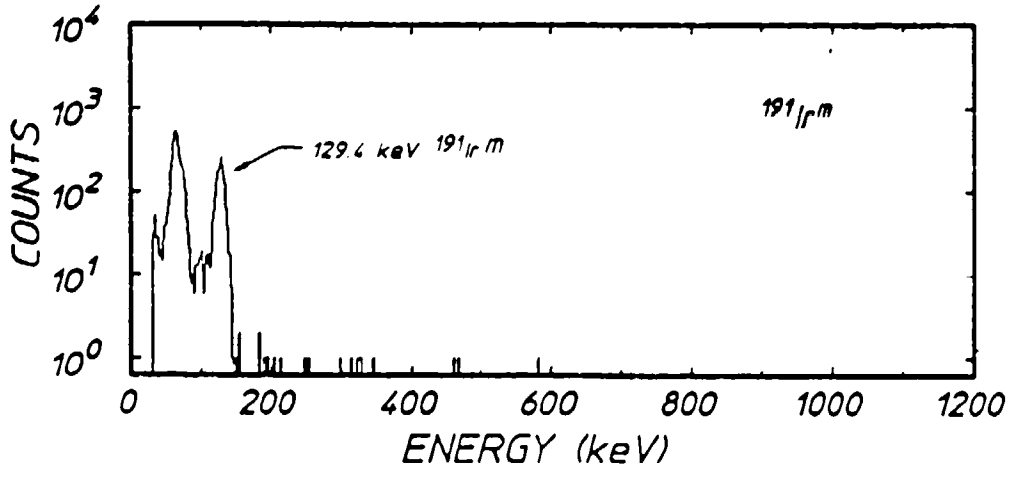
129.4 keV 191Ir m
191Ir m
COUNTS
ENERGY (keV)

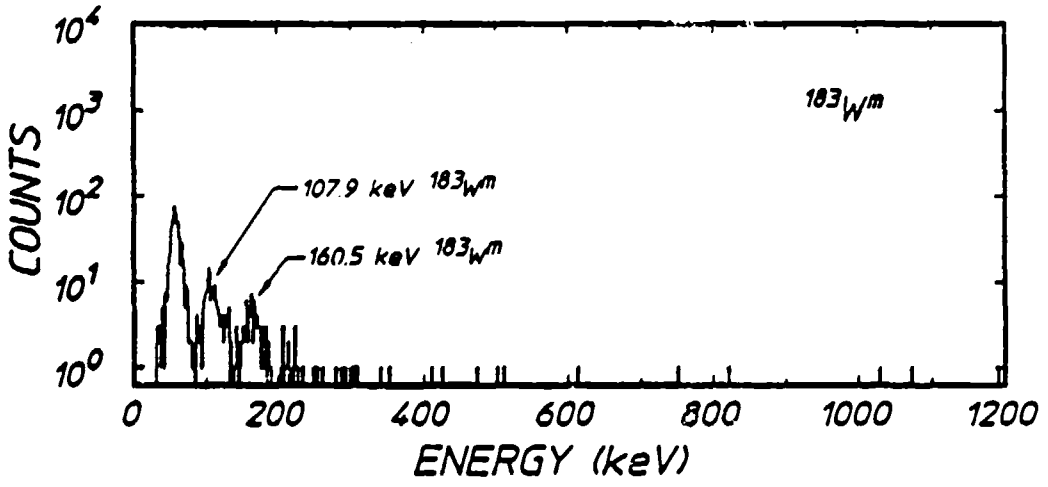
COUNTS
10^4
10^3
10^2
10^1
10^0
$^{183}W^m$
107.9 keV $^{183}W^m$
160.5 keV $^{183}W^m$
0
200
400
600
800
1000
1200
ENERGY (keV)

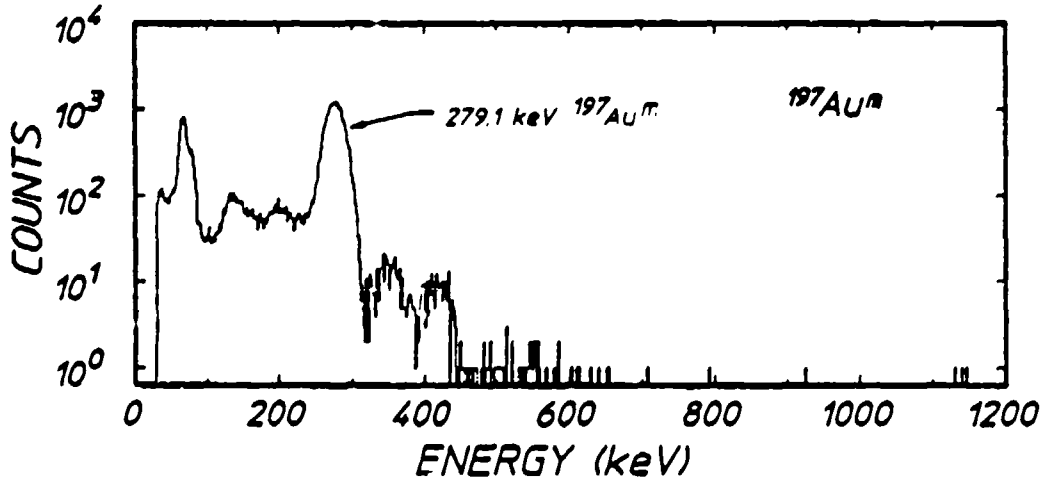
COUNTS
10^4
10^3
10^2
10^1
10^0
279.1 keV $^{197}Au^m$
$^{197}Au^m$
0
200
400
600
800
1000
1200
ENERGY (keV)

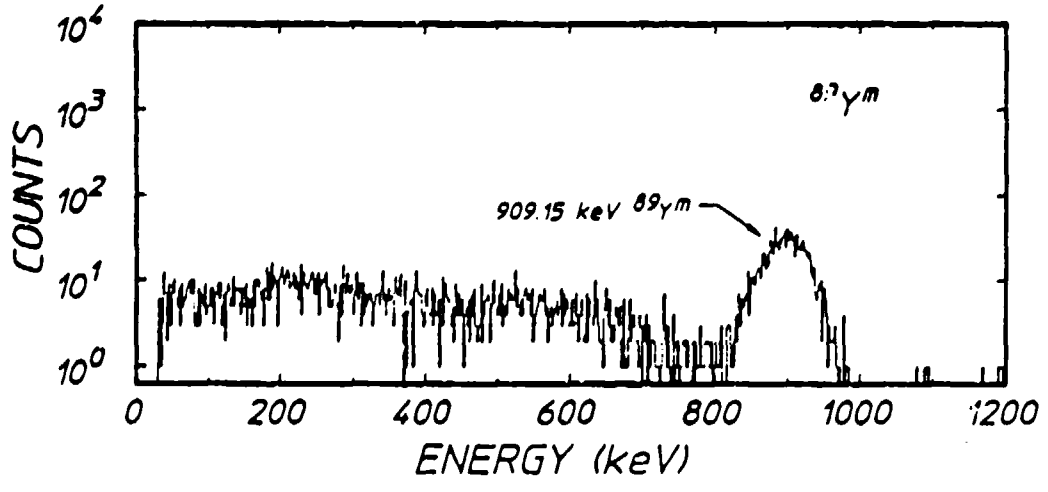
COUNTS
10^4
10^3
10^2
10^1
10^0
909.15 keV $^{89}Y^m$
0
200
400
600
800
1000
1200
ENERGY (keV)

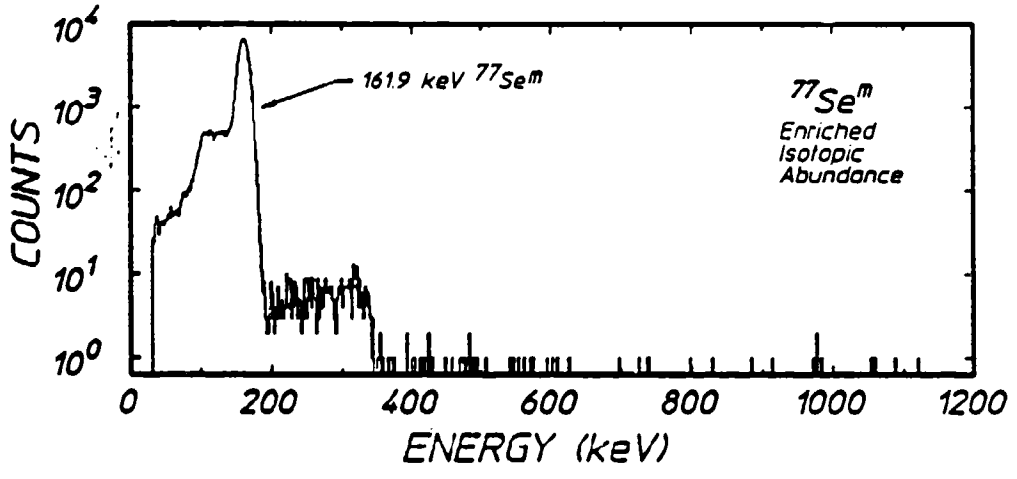
COUNTS
10^4
10^3
10^2
10^1
10^0
161.9 keV $^{77}Se^m$
$^{77}Se^m$
Enriched
Isotopic
Abundance
0
200
400
600
800
1000
1200
ENERGY (keV)

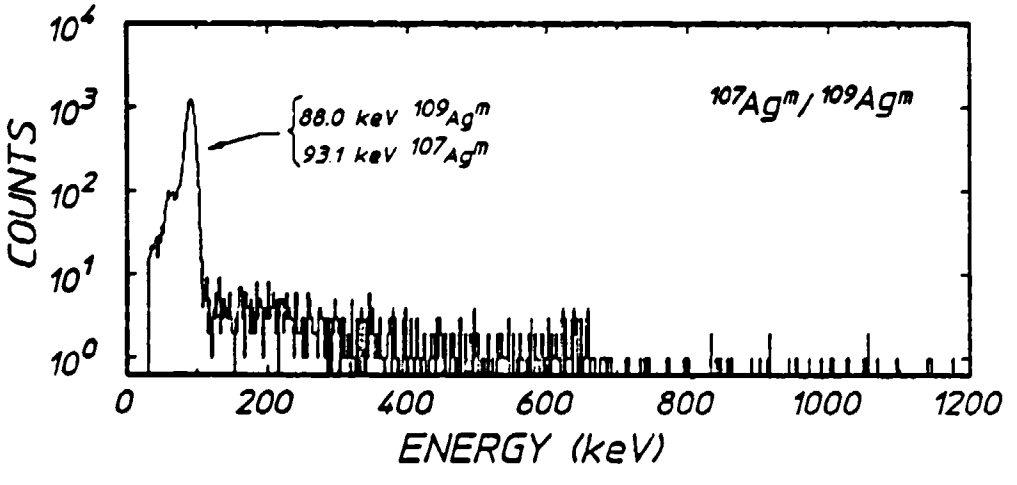
COUNTS
10^4
10^3
10^2
10^1
10^0
88.0 keV $^{109}Ag^m$
93.1 keV $^{107}Ag^m$
$^{107}Ag^m$ / $^{109}Ag^m$
0
200
400
600
800
1000
1200
ENERGY (keV)

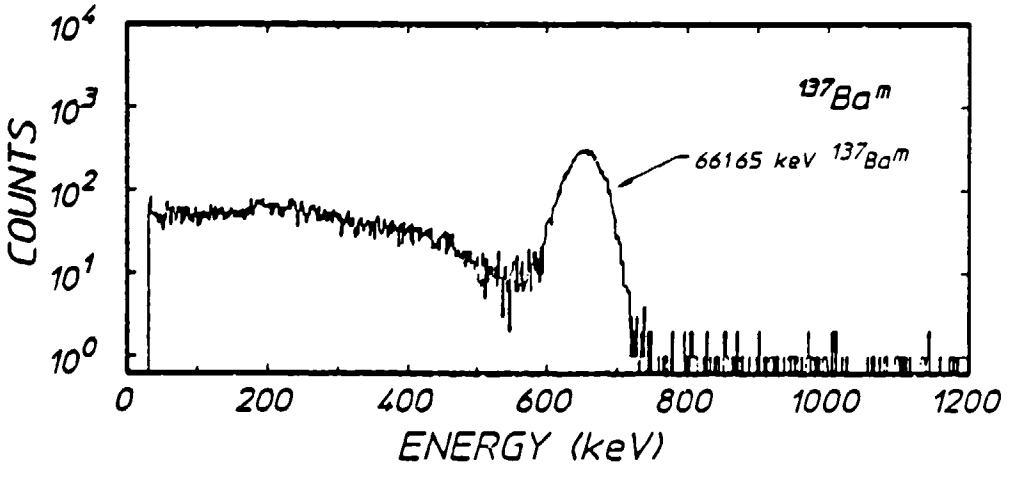
COUNTS
10^4
10^3
10^2
10^1
10^0
$^{137}Ba^m$
66165 keV $^{137}Ba^m$
0
200
400
600
800
1000
1200
ENERGY (keV)

Figure 2: Characteristic energy spectra for isomeric decays obtained in this work with a 7.6 cm × 7.6 cm diameter NaI(Tl) detector having a 5.1 cm × 2.5 cm diameter well. Transitions shown in Figs. 1a - 1i for the detection of the isomers are identified by the arrows. Counting times are given in Table I and the times elapsed between irradiation and counting are as follows:
a), b) and c) (third preceding page) ^{167}Er, ^{79}Br, *and* ^{191}Ir: *Delays of 2.06, 2.06, and 1.77 sec.*
d), e) and f) (second preceding page) ^{183}W, ^{197}Au, *and* ^{89}Y: *Delays of 2.31, 1.63, and 2.00 sec.*
g), h) and i) (preceding page) ^{77}Se, $^{107}Ag/^{109}Ag$, *and* ^{137}Ba: *Delays of 2.00, 3.04, and 1.84 sec.*

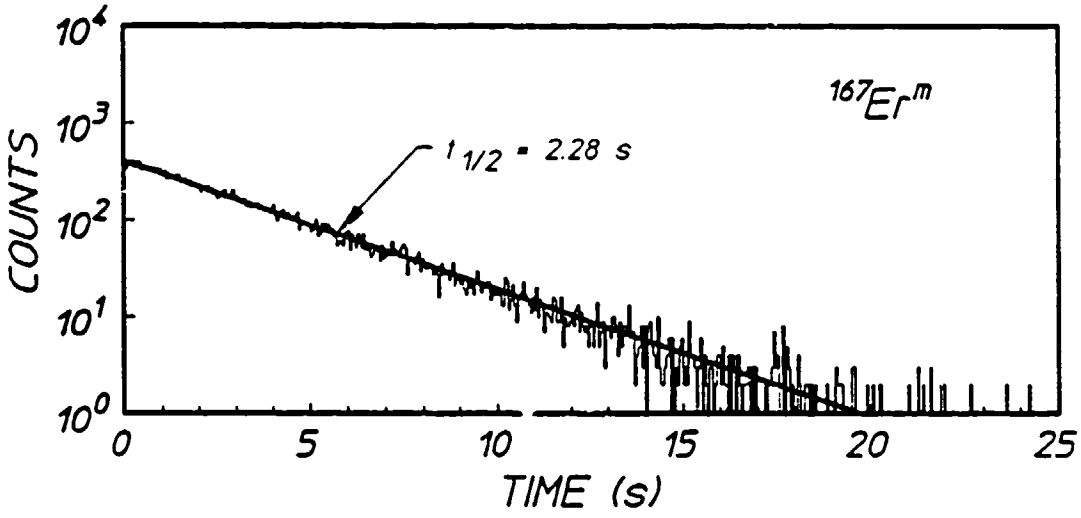
$^{167}Er^{m}$
$t_{1/2}$ = 2.28 s
COUNTS
TIME (s)

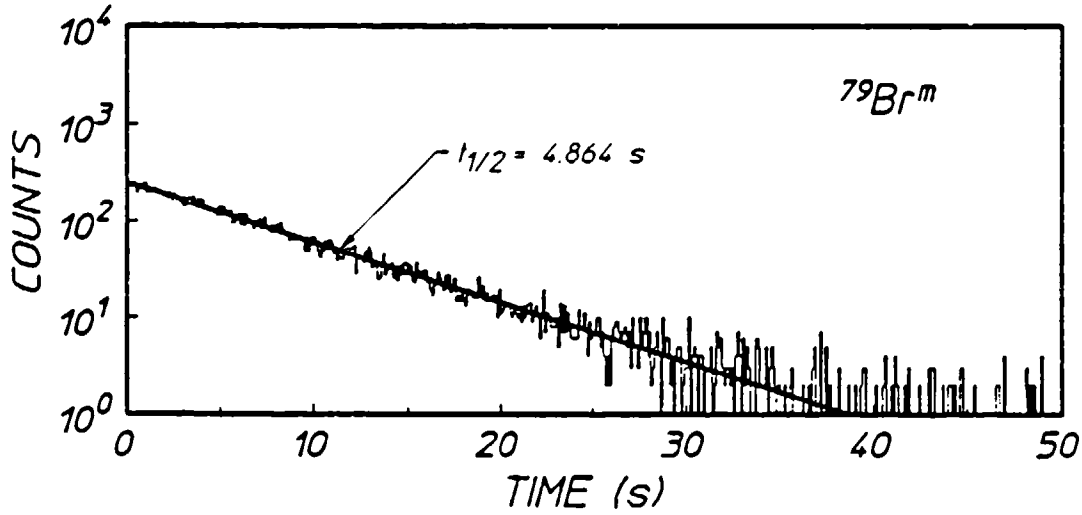
$^{79}Br^{m}$
$t_{1/2}$ = 4.864 s
COUNTS
TIME (s)

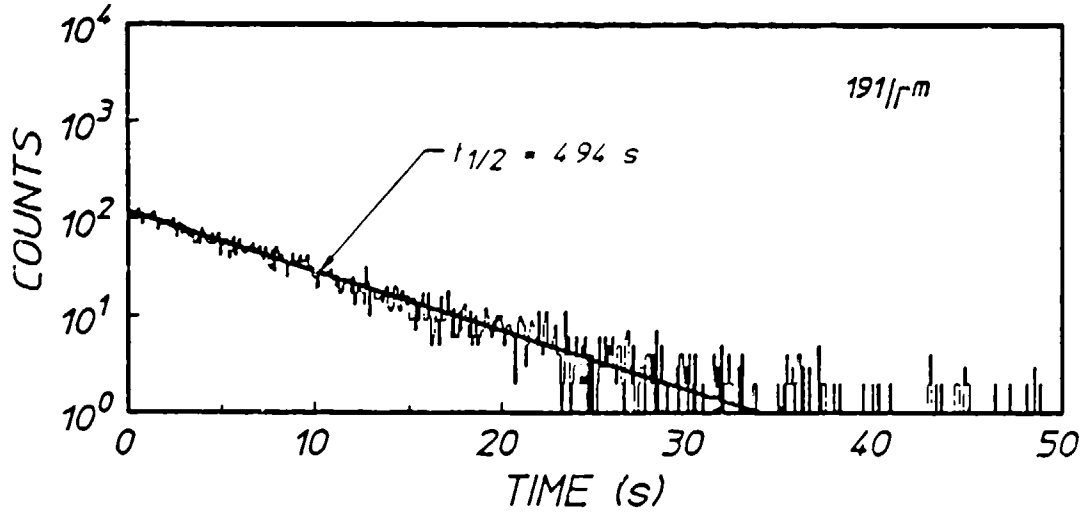
$^{191}Ir^{m}$
$t_{1/2}$ = 4.94 s
COUNTS
TIME (s)

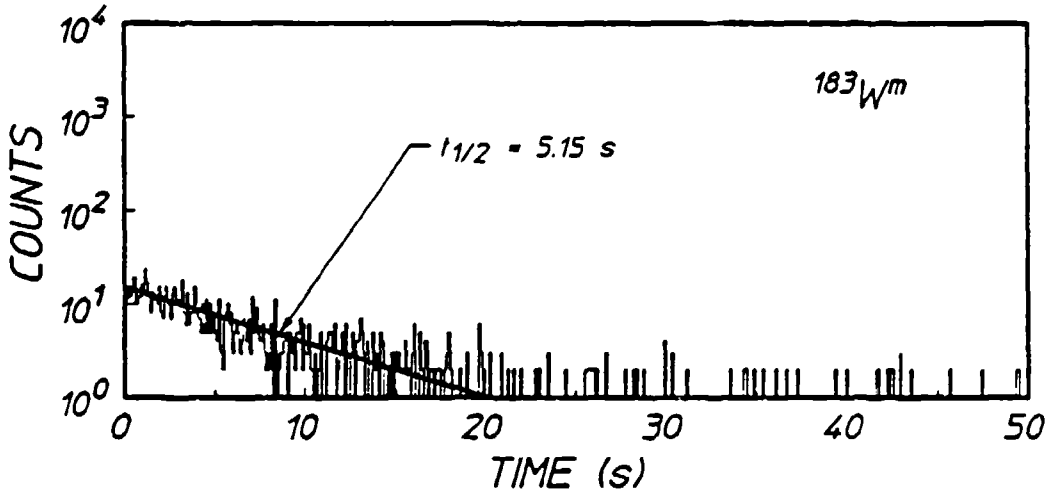
10^4
10^3
10^2
10^1
10^0
COUNTS
$^{183}W^m$
$t_{1/2}$ = 5.15 s
0
10
20
30
40
50
TIME (s)

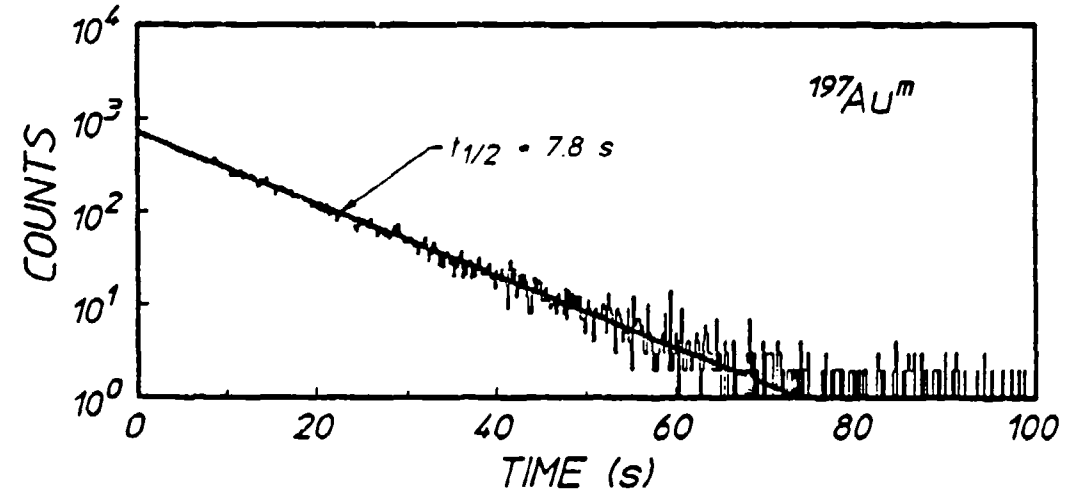
10^4
10^3
10^2
10^1
10^0
COUNTS
$^{197}Au^m$
$t_{1/2}$ = 7.8 s
0
20
40
60
80
100
TIME (s)

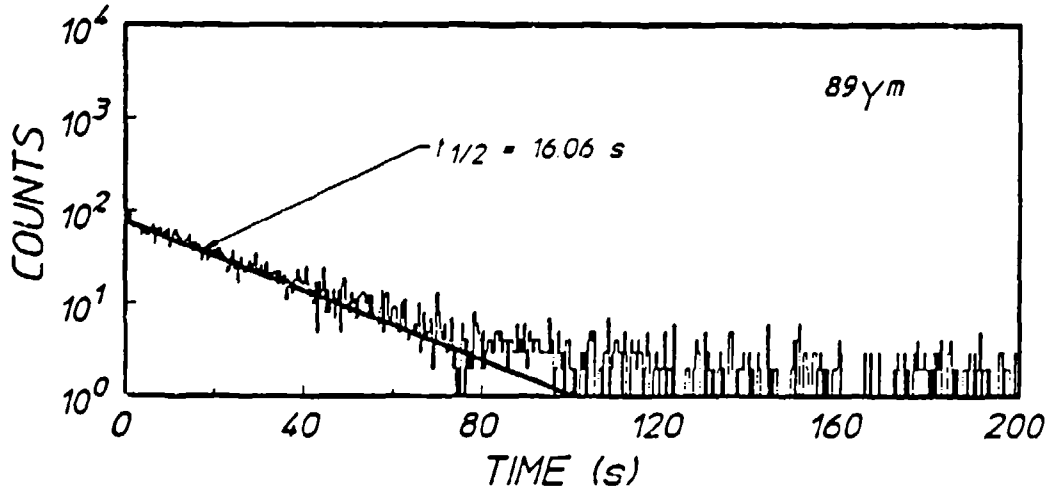
10^4
10^3
10^2
10^1
10^0
COUNTS
$^{89}Y^m$
$t_{1/2}$ = 16.06 s
0
40
80
120
160
200
TIME (s)

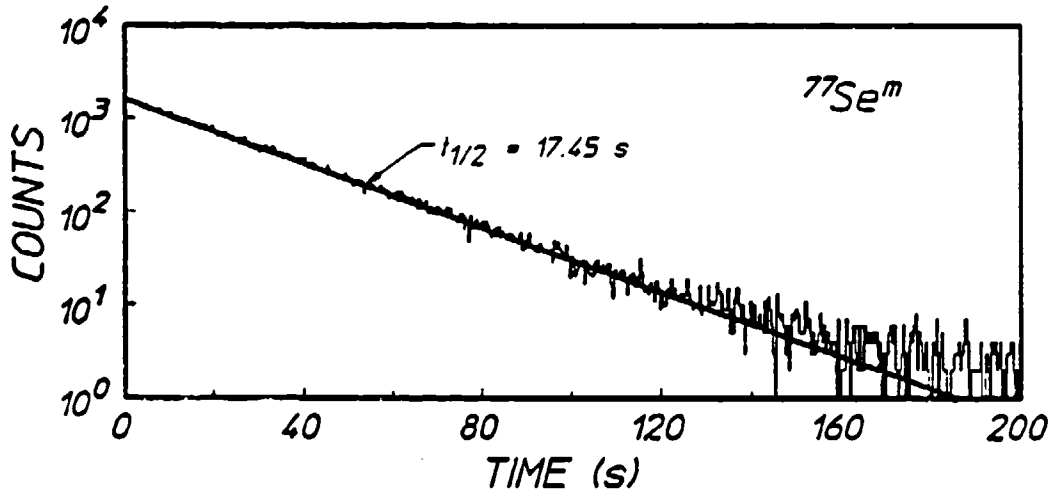
$^{77}Se^{m}$
$t_{1/2}$ = 17.45 s
COUNTS
TIME (s)

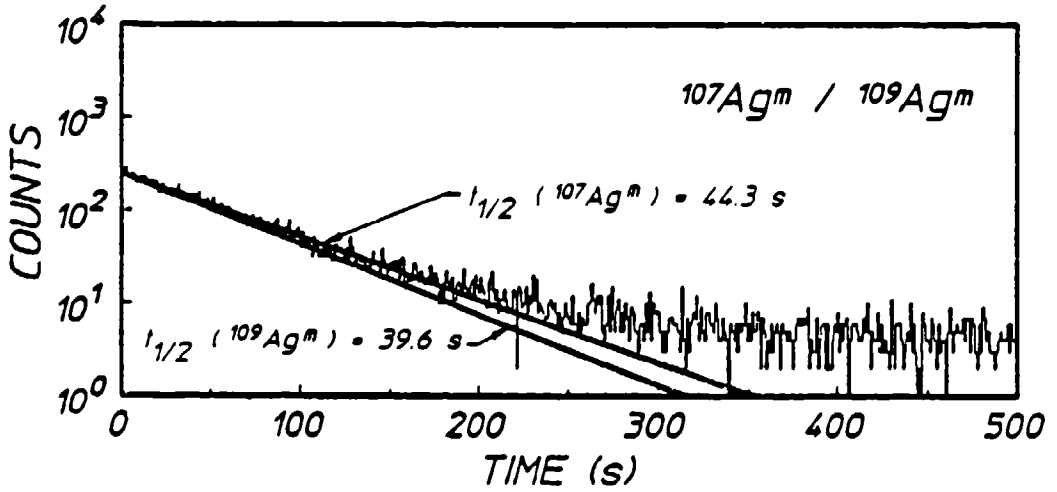
$^{107}Ag^{m}$ / $^{109}Ag^{m}$
$t_{1/2}$ ($^{107}Ag^{m}$) = 44.3 s
$t_{1/2}$ ($^{109}Ag^{m}$) = 39.6 s
COUNTS
TIME (s)

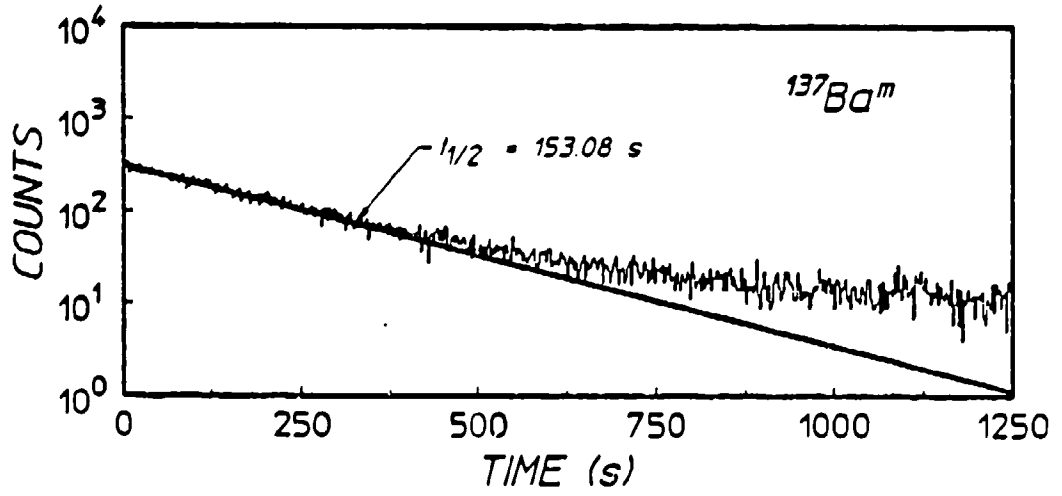
$^{137}Ba^{m}$
$t_{1/2}$ = 153.08 s
COUNTS
TIME (s)

Figure 3: Plots of the total counting rate as a function of time elapsed from the start of counting for the isomers studied in this work. Plots are presented as total counts observed in successive dwell intervals of the multichannel scaler. All events above a chosen lower level discriminator are recorded. The dotted lines show the decay curves expected from the literature values of the half-lives.
a), b), and c) (third preceding page) Fluorescence decay curves for $^{167}Er^{m}$, $^{79}Br^{m}$, and $^{191}Ir^{m}$. Dwell times are 0.05, 0.1, and 0.1 seconds per channel.
d), e), and f) (Second preceding page) Fluorescence decay curves for $^{183}W^{m}$, $^{197}Au^{m}$, and $^{89}Y^{m}$. Dwell times are 0.1, 0.2, and 0.4 seconds per channel.
g), h), and i) (preceding page) Fluorescence decay curves for $^{77}Se^{m}$, $^{107}Ag^{m}/^{109}Ag^{m}$, and $^{137}Ba^{m}$. Dwell times are 0.4, 1.0, and 2.5 seconds per channel. The presence of photoactivated $^{135}Ba^{m}$ ($T_{1/2}$ = 28.7 h) is indicated by the elevated background at long times.

Results

From the numbers of counts in the fluorescence spectra of Figs. 2a - 2i, the numbers of activations in the samples were obtained by well-established procedures. The efficiency of the spectrometer was determined with calibrated sources and was found to conform to nominal specifications. The self-absorption corrections used in these calculations are listed as transparencies in Table I. Fluorescence intensities were taken from the literature.[13]

The rates of activations of the samples, dN/dt, were obtained by dividing the observed numbers of activations by the irradiation times after correcting for finite counting and irradiation times. Literature values of the half-lives were used in making these corrections.[14]

The excitation rate is

$$\frac{dN}{dt} = N_o \sum_i (\pi \Gamma_x \sigma_o / 2)_i \, \phi_i \quad , \qquad (4)$$

where the parameters in parentheses comprise the integrated cross section for pumping the (γ,γ') reaction through the i-th gateway, ϕ_i is the photon flux at the energy needed to excite that gateway, and N_o is the number of target nuclei. In our experiment, the spectrum of irradiation, $\phi_i(E)$, cannot yet be varied in a controlled manner so that the sum of Eq. (4) cannot be decomposed from the experimental measurements of dN/dt into components from each of the contributing bands. An interesting alternative is to extract the effective cross section $\sigma(E)$

which would be necessary to produce the observed activation through a single gateway,

$$\sigma(E) = \frac{dN/dt}{N_0\phi(E)} \quad . \qquad (5)$$

The spectral distribution from the Clinac 1800 medical linac is considered to be well-known[1,2] and is normalized by a measurement of the total dose delivered during the irradiation. The expected distribution is shown in Fig. 4. From the $\phi(E)$ determined in this way, the effective, integrated cross section can be determined from the measured activation rate as shown in Eq. (5). The $\sigma(E)$is a function of the energy E at which the effective gateway is assumed to lie. Results for the eight isotopes characterised in these experiments are shown in Figs. 5a - 5h. In each case the possible values of energies for the gateways are limited at the lower end by prior reports of much smaller cross sections for (γ,γ') reactions known to occur through gateways lying between 1 and 1.5 MeV.

Conclusions

From Figs. 5a - 5h it can be seen that the integrated cross sections for isomeric excitation in these eight species through channels open to 6 MeV bremsstrahlung reach values exceeding almost all previous results by two to three orders of magnitude, continuing the trend found in the excitation of the longer-lived isomers.[11] However, most earlier work was conducted with sources having end point energies lying below 3 MeV so it might be initially supposed that these larger cross sections describe channels open near the threshold for (γ,n) reactions where state density is high. A troubling aspect is the large change of angular momentum spanned by these reactions and the lack of correlation of reaction probabilities with minimal changes in J. Figure 6 presents a summary of the results of this work which suggests some groupings of the magnitudes of these cross sections.

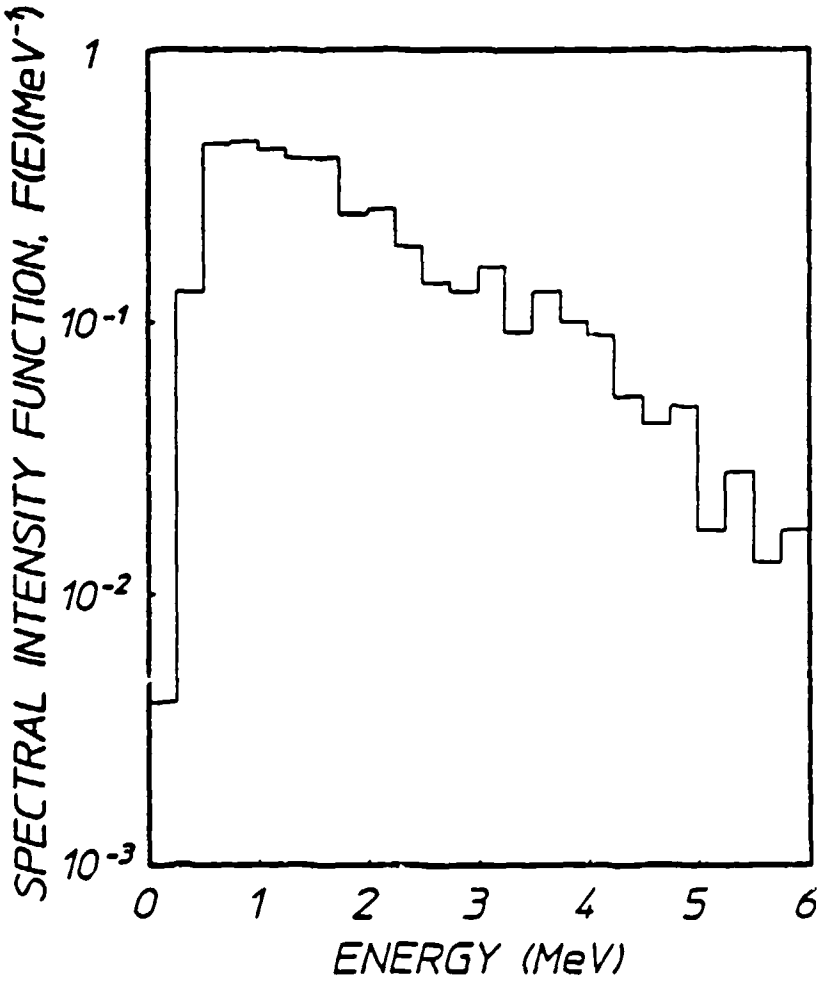

Figure 4: Relative spectral intensities of the bremsstrahlung used for irradiation in these experiments normalized so that the integral under the curve is unity.

The pervasiveness of the unexpectedly large values of integrated cross sections for the transfers of such large amounts of angular momenta continues to suggest some type of core property varying only slowly with increasing nuclear size. In such a case, however, there would seem to be the need for a mixing of several single particle states so the decay of the gateway state could occur into several different cascades with comparable probabilities. In any case, the integrated cross sections found in this experiment correspond to remarkably large partial widths. Derived values are summarized in Table II. Such widths

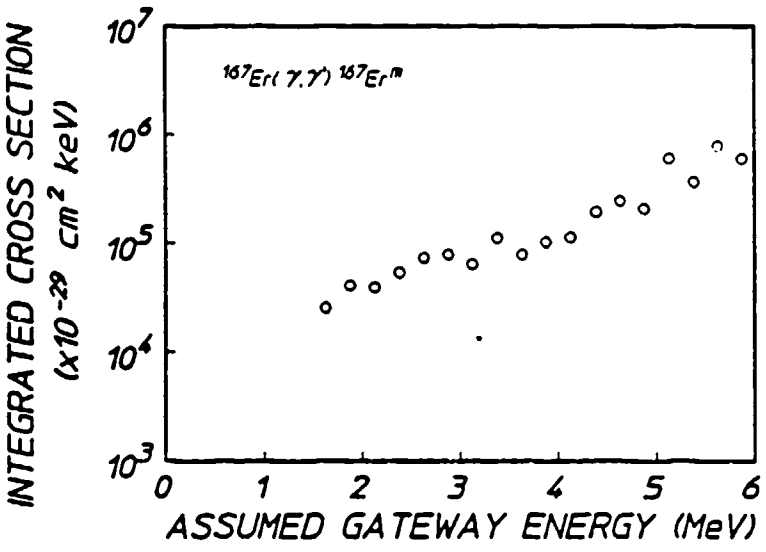
$^{167}Er(\gamma,\gamma')^{167}Er^m$
INTEGRATED CROSS SECTION
(x10^{-29} cm^2 keV)
10^7
10^6
10^5
10^4
10^3
0 1 2 3 4 5 6
ASSUMED GATEWAY ENERGY (MeV)

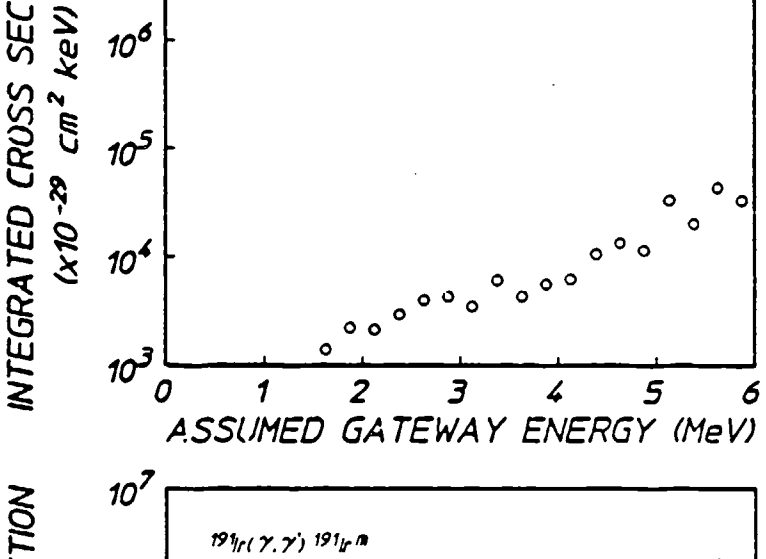
$^{79}Br(\gamma,\gamma')^{79}Br^m$
INTEGRATED CROSS SECTION
(x10^{-29} cm^2 keV)
10^7
10^6
10^5
10^4
10^3
0 1 2 3 4 5 6
ASSUMED GATEWAY ENERGY (MeV)

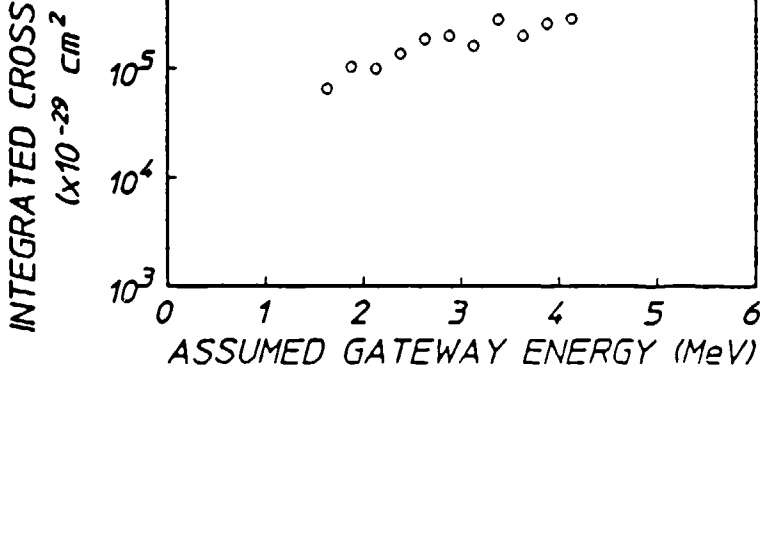
$^{191}Ir(\gamma,\gamma')^{191}Ir^m$
INTEGRATED CROSS SECTION
(x10^{-29} cm^2 keV)
10^7
10^6
10^5
10^4
10^3
0 1 2 3 4 5 6
ASSUMED GATEWAY ENERGY (MeV)

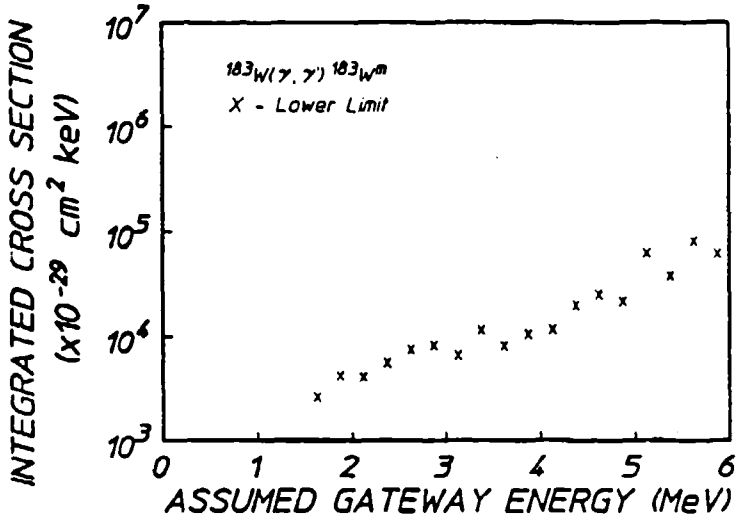
INTEGRATED CROSS SECTION
(x10^-29 cm^2 keV)
183W(γ, γ') 183Wm
X - Lower Limit
10^7
10^6
10^5
10^4
10^3
0 1 2 3 4 5 6
ASSUMED GATEWAY ENERGY (MeV)

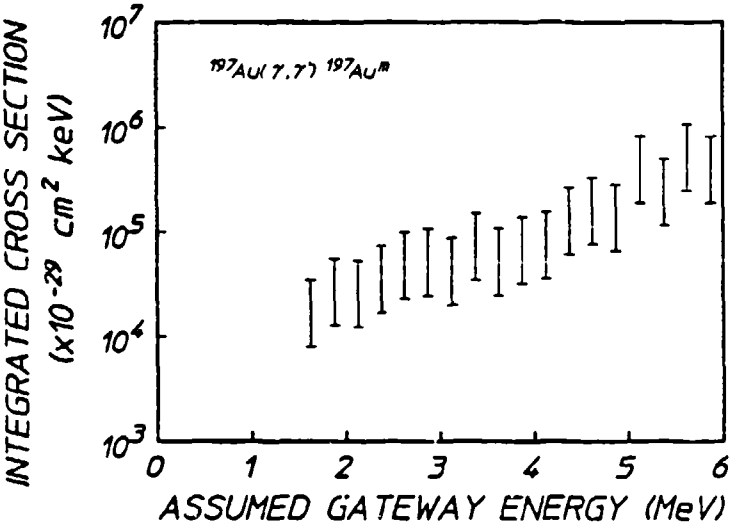
INTEGRATED CROSS SECTION
(x10^-29 cm^2 keV)
197Au(γ, γ') 197Aum
10^7
10^6
10^5
10^4
10^3
0 1 2 3 4 5 6
ASSUMED GATEWAY ENERGY (MeV)

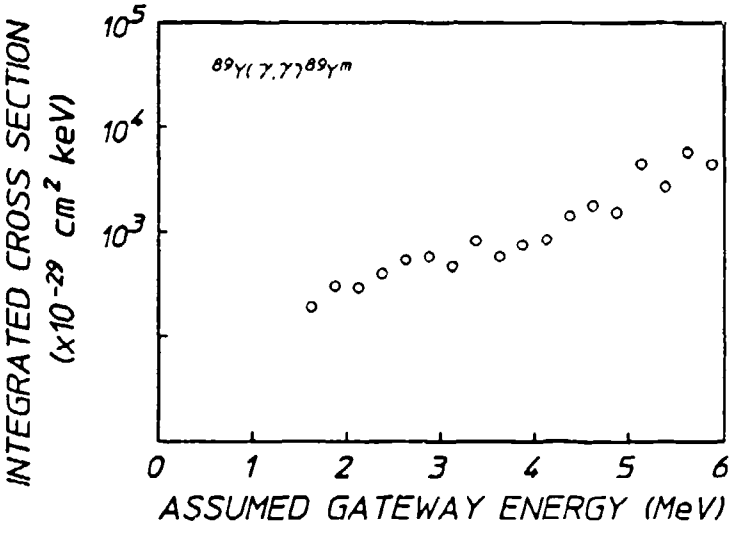
INTEGRATED CROSS SECTION
(x10^-29 cm^2 keV)
89Y(γ, γ')89Ym
10^5
10^4
10^3
0 1 2 3 4 5 6
ASSUMED GATEWAY ENERGY (MeV)

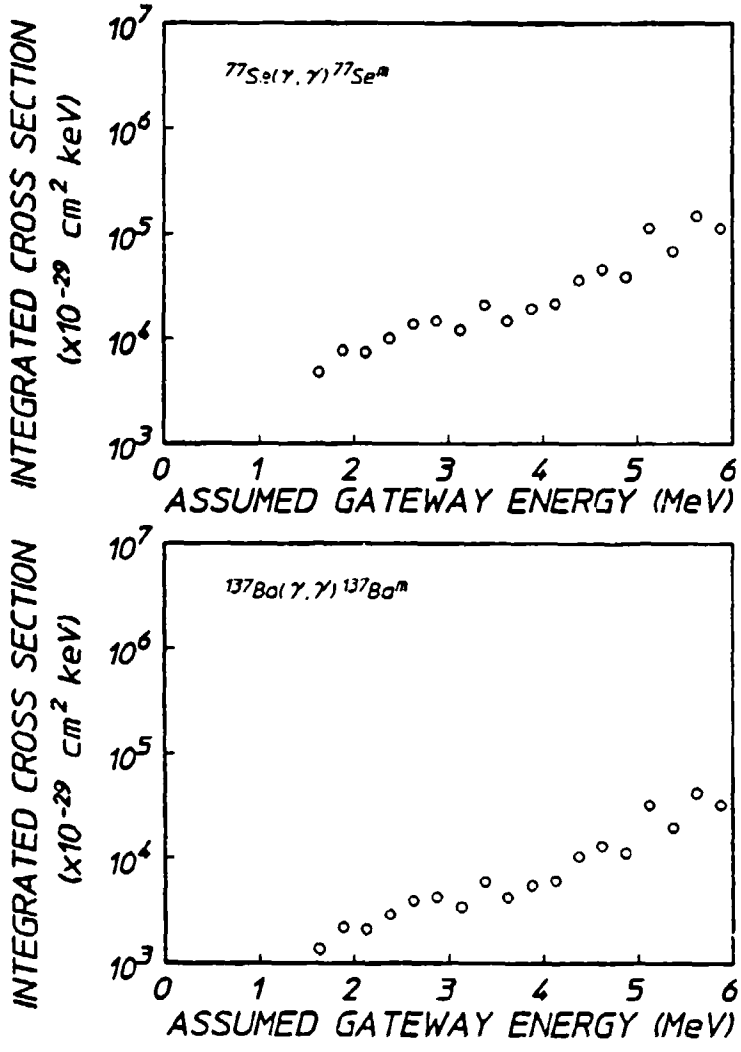

Figure 5: The circles plot integrated cross sections for the (γ,γ') reactions shown on each panel through single, unknown gateway states as functions of the energies at which they could be assumed to lie. Literature values preclude the possibilities that these gateways could lie at energies below the minima shown. As shown in two cases, ^{183}W and ^{197}Au uncertainties in the computations of target transparencies introduced probable errors which were larger than the plotted sizes of the symbols.

a), b) and c) (second preceding page) Reactions of ^{167}Er, ^{79}Br, and ^{191}Ir.

d), e) and f) (preceding page) Reactions of ^{183}W, ^{197}Au, and ^{89}Y.

g) and h) (above) Reactions of ^{77}Se and ^{137}Ba.

are characteristic of relatively unhindered E1 transitions and motivate further investigation of their occurrence.

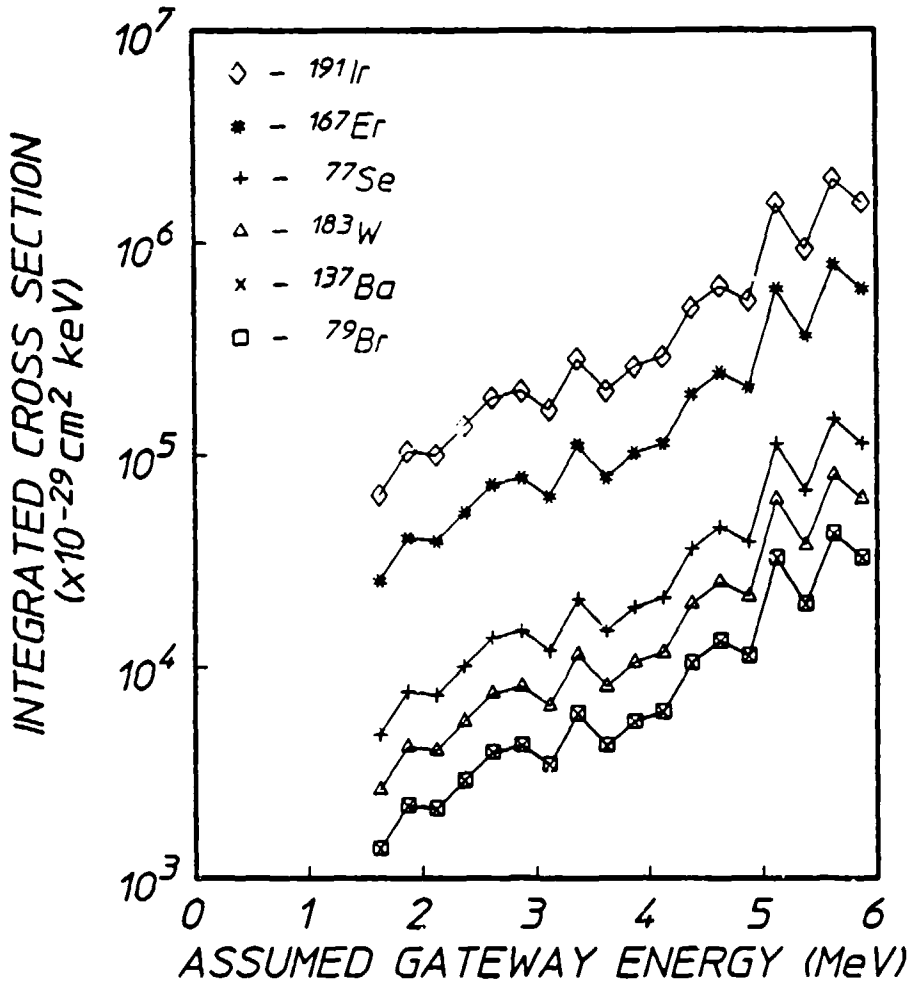

Figure 6: Summary of the integrated cross sections for the (γ,γ') reactions producing the isomers of the species shown, plotted as functions of the energies at which a single gateway state could be assumed for each. For simplicity the range of values possible for ^{197}Au were not shown and the data for ^{183}W must be considered to be lower limits.

Table II

Summary of the partial widths for the (γ,γ') reactions producing the isomers of the species shown. Values were obtained from the integrated cross sections by assuming the gateway energies lay at 2 MeV, near the bremsstrahlung maximum, and that statistical weights were the same in the ground and gateway states, so that $\sigma_0 = 6.1 \times 10^{-22}$ cm^2.

Nuclide	$\pi\sigma_0(b_a b_0 \Gamma)/2$ at 2 MeV ($\times 10^{-29}$ cm^2 keV)	Partial width (meV)
^{167}Er	36,000	380
^{79}Br	2,000	21
^{191}Ir	91,000	950
^{183}W	> 3,700	> 38
^{197}Au	11,000 - 49,000	110 - 510
^{89}Y	270	2.8
^{77}Se	6,700	70
^{137}Ba	2,000	21

References

1. R. Mohan, C. Chui, and L. Lidofsky, Med. Phys. 12, 595 (1985).

2. N. C. Ikoro, D. A. Johnson, and P. P. Antich, Med. Phys. 14, 93 (1987).

3. C. B. Collins, C. D. Eberhard, J. W. Glesener, and J. A. Anderson, Phys. Rev. C 37, 2267 (1988).

4. C. D. Eberhard, J. W. Glesener, Y. Paiss, J. A. Anderson, C. B. Collins, W. L. Hodge, E. C. Scarbrough, and P. P. Antich, Phys. Rev. C (pending).

5. C. B. Collins, J. A. Anderson, Y. Paiss, C. D. Eberhard, R. J. Peterson, and W. L. Hodge, Phys. Rev. C (pending).

6. J. A. Anderson, M. J. Byrd, and C. B. Collins, Phys. Rev. C (pending).

7. M. L. Wiedenbeck, Phys. Rev. 67, 92 (1945).

8. E. C. Booth and J. Brownson, Nucl. Phys. A 98, 529 (1967).

9. A. deSchalit and H. Feshbach, Theoretical Nuclear Physics Vol. 1: Nuclear Structure (J. Wiley, New York, 1974) pp. 488-491.

10. C. F. Perdrisat, Rev. Mod. Phys. 38, 41 (1966).

11. C. B. Collins, J. A. Anderson, C. D. Eberhard, J. F. McCoy, J. J. Carroll, E. C. Scarbrough, and P. P. Antich, Center for Quantum Electronics Report #GRL8703, University of Texas at Dallas, 1988 (unpublished) pp. 37-56.

12. C. B. Collins, J. M Carroll, and J. A. Anderson, Center for Quantum Electronics Report #GRL8702, University of Texas at Dallas, 1987 (unpublished) pp. 13, 44.

13. E. Browne and R. B. Firestone, Table of Radioactive Isotopes, edited by Virginia S. Shirley (Wiley, New York, 1986).

14. Evaluated Nuclear Structure Data File (Brookhaven National Laboratory, Upton, New York, 1986).

N00014-86-C-2488
UTD #24522-964

OPPORTUNITIES FOR THE CALIBRATION OF THE DNA/AURORA ACCELERATOR

by J. A. Anderson, K. N. Taylor, J. M. Carroll, J. F. McCoy, J. J. Carroll, M. J. Byrd, and C. B. Collins

Recently, we have reported[1,2] how effectively our technique of X-Ray Activation of Nuclei (XAN) can be used to calibrate the spectral intensities found in a single pulse of intense bremsstrahlung. Essential to determining the pump intensities used in schemes for exciting a gamma-ray laser,[3] XAN has also been validated as a means of calibrating nuclear simulators having end point energies $E_m < 1.5$ MeV.

As currently implemented, three isotopes, ^{77}Se, ^{79}Br, and ^{115}In, are used to sample narrow spectral slices of the fluence illuminating a target. Information is stored as isomeric excitations to be "read out" later. With three isotopes, XAN accommodates measurements at three photon energies, 433, 761, and 1078 keV. The spectrum from the DNA/PITHON accelerator was calibrated[2] with this system and found to conform closely to expectations.

The key to the development of that technique was the use of a large number of shots to activate test samples in order to resolve experimentally the level of self-consistency among values of basic nuclear parameters in the current database.[4] Five of six critical parameters for these three isotopes were found to be consistent and the sixth was repaired. Lest this give a false sense of security in the use of the existing database for the extension of this technique to a greater range of energies, it must be recognized that these three materials were chosen because it appeared <u>a priori</u> that they were the ones most precisely characterized for $E_m < 1.5$ MeV by the study of particle reactions reported in the literature. The resulting score of 83% for consistency should be considered representative of only the very best group of test nuclei. Fortunately, the level of consistency was this high, or XAN could not have been validated in a practical number of test shots.

The next logical step would be to add more isotopes to the calibration target in order to improve both range and resolution of the photon energies covered, and a number of candidates suggest themselves. During the same series of experiments on the PITHON nuclear simulator during which self-consistency of the basic three was demonstrated, 29 other isotopes were irradiated in a survey mode. Four, ^{167}Er, ^{179}Hf, ^{191}Ir, and

^{197}Au, were found to be particularly promising and others were certainly interesting. The opportunity for using those four to add four more energies below 1.5 MeV to the list for which XAN is applicable was discussed[5] in a previous quarterly report. Unfortunately, of the ten nuclear parameters of importance, *at least five accepted values were found to be drastically erroneous*. An error rate in excess of 50% for this part of the nuclear database, coupled with the lack of foreknowledge of which of the materials should have borne greatest scrutiny, resulted in insufficient data to extract the self-consistent parameters needed for the application of XAN at four additional points.

At higher energies 1.5 MeV < E_M < 6 MeV the situation becomes even more complex.[6] Not only is the accepted database[4] flawed severely, but even basic concepts break down.[7] Most recent experiments[6,7] with the bremsstrahlung from a medical linear accelerator (LINAC) have shown the importance of a new class of giant gateways providing a path for selective excitation of delayed fluorescence about 1000 times greater than anything found earlier.[6] Moreover, conservation principles tending to limit such activations to states requiring that only small changes of angular momentum be imparted together with the x-ray energy seem no longer to apply[7] at the higher end points.

For a sample which is optically thin at the pump wavelength, the number of nuclei produced in levels from which the delayed fluorescence will be radiated for subsequent measurement is given by

$$S = N \sum_i \frac{(\pi b_a b_o \sigma_o \Gamma/2)_i}{E_i} \frac{\phi(E_i)}{A} \quad , \qquad (1)$$

where N is the number of absorbing nuclei in the sample, and the summation is taken over the properties at each of the pump energies E_i for which the intensities are being sampled. Often only one such pump band is assumed to be of dominant importance but there could be several at different E_i, each funneling its population into the same output level.

In Eq. (1) the first ratio in the summation is composed of the nuclear parameters, while the second describes the intensities of the pump x-rays which are assumed to be continuous, at least without structure on the fine scale of the nuclear absorption. In particular, the combination $\phi(E_i)/A$ is the spectral fluence at the energy E_i in units of keV/keV/cm^2. Tacitly, it has been assumed that the duration of the

the pump source is less than the fluorescence lifetime τ_u so that effects of saturation can be neglected.

Of the nuclear parameters, Γ is the natural width in keV of the i-th pump band, through which intensities are sampled

$$\Gamma = \hbar/\tau_p \quad , \tag{2}$$

and the branching ratios, b_s and b_o, give the probabilities for the decay of that broad level back into the initial and fluorescence level, respectively. The pump energy E_i, is in keV, and σ_o is the amplitude of the Breit-Wigner cross section for the absorption transition,

$$\sigma_o = \frac{\lambda^2}{2\pi} \frac{2I_e+1}{2I_g+1} \frac{1}{\alpha_p+1} \quad , \tag{3}$$

where λ is the wavelength in cm of the gamma ray at the resonant energy E_i; I_e and I_g are the nuclear spins of the excited and ground states, respectively; and α_p is the total internal conversion coefficient for the gateway level at E_i.

Equation (1) is the basic expression for evaluating the number of fluorescent nuclei produced by this type of selective absorption that can benefit from bandwidth funneling. The numerator of the first term of Eq. (1) is usually termed the integrated cross section for the photoexcitation of the fluorescent level from the initial state. It is convenient to discuss this quantity in units of 10^{-29} cm^2 keV. On this scale, unity would describe a sampling channel of strength sufficient to give the clear level of nuclear fluorescence described in the previous reports[1,2] from a few grams of material pumped with a source of laboratory scale. For example, the excitation of isomeric $^{77}Se^m$ is mediated by funneling transitions whose strengths total to the order of unity ($\times 10^{-29}$ cm^2 keV) for excitation energies below 1 MeV.

Variability of the integrated cross section is contributed mostly by the product of branching ratios and level widths, $(b_s b_o \Gamma)$. While it has been clear from the beginning that broader funneling levels could be found at higher excitation energies, the concern persisted that the increase in width might be associated only with a stronger transition to the ground state so that the branching ratio to the fluorescent level, b_o, would decrease as Γ increased. This was <u>not</u> found to be the case in

the LINAC experiments and integrated cross sections were reported to be as large as 10,000 in the usual units. [6,7,8]

With the discovery of these giant gateway states for sampling bremsstrahlung fluences above 1.5 MeV, there is a clear motivation to attempt to determine the relevant nuclear parameters and energies, E_i, so that the XAN procedure for calibrating impulsive sources can be extended to the range of photon energies 2 - 6 MeV. Reported here are the results of a series of ranging shots into a target package irradiated by DNA/AURORA. The objective was to determine whether the case could be made for the potential utility of the XAN method for the calibration of the spectral intensity emitted from such a source. Two issues were examined. The first was to determine to what extent the DNA/AURORA could be cross calibrated to the LINAC in terms of relative fluorescence yield from a single target material. The second was to survey a selected group of materials to determine whether they evidenced any individually distinctive dependence of fluorescence efficiency upon bremsstrahlung end point.

Experimental Detail

The relevant energy levels for the six nuclei of interest in these preliminary experiments are shown in Fig. 1a - 1f. They were present in targets fabricated from materials occurring in natural isotopic abundance. Since two were isotopes of indium, there were only five target materials irradiated.

For the resolution of the first experimental issue the indium target was used in the form of a thin foil. It was hung on a test stand 31.5 cm from the plane bounding the outermost projections of the window assemblies of the four triaxial output lines of DNA/AURORA. After irradiation the target was dismounted and dispatched to our counting facility at the Center for Quantum Electronics in Dallas. There, the fluorescence was measured at the endcap window of a 10% relative efficiency, n-type Ge detector. In this geometry some correction had to be made for the reabsorption of the output fluorescence shown in Fig. 1 in the target material. Computations indicated that 95% of the fluorescent photons escaped this self-absorption.

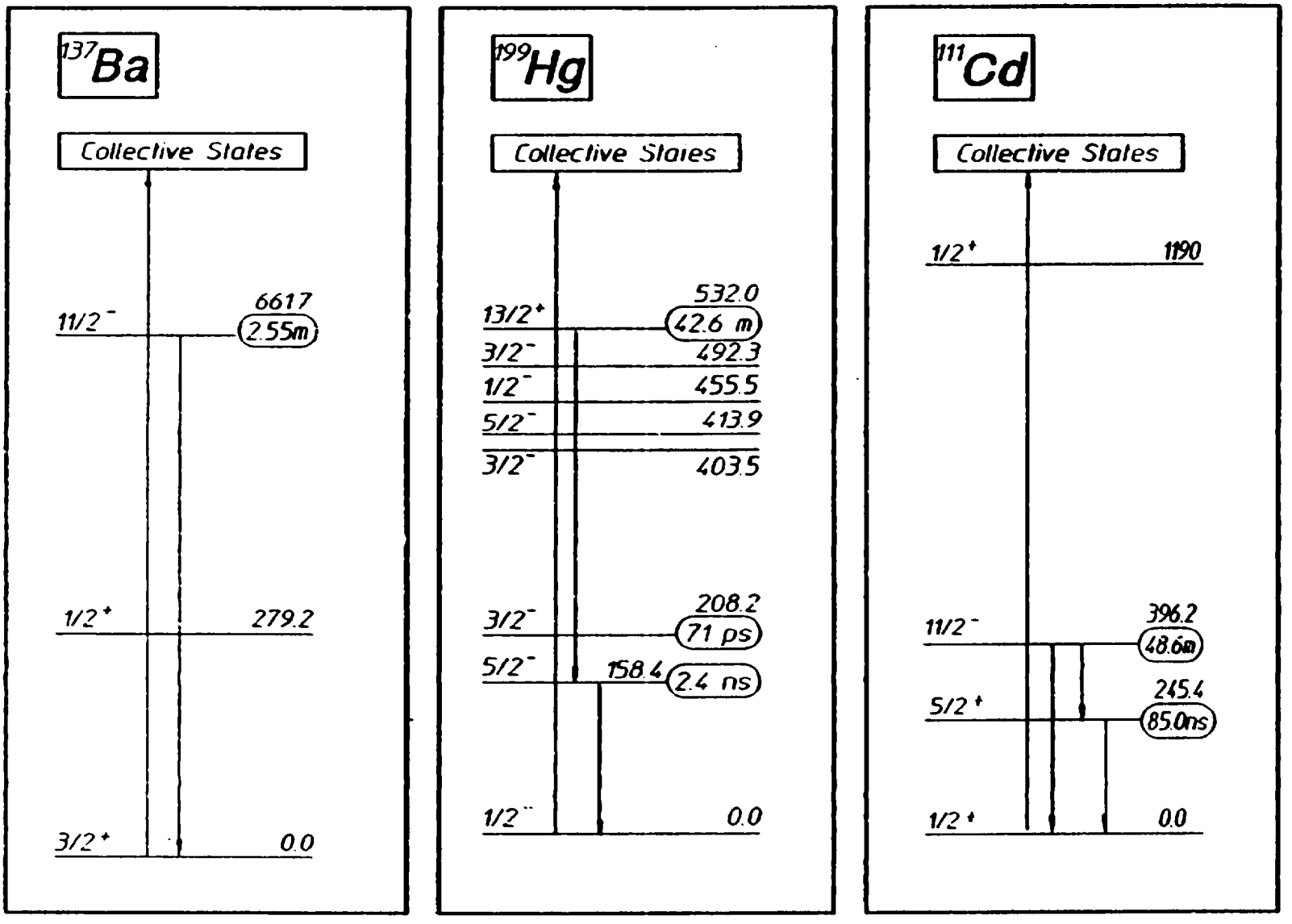
137Ba
Collective States
11/2⁻
661.7
2.55m
1/2⁺
279.2
3/2⁺
0.0
199Hg
Collective States
13/2⁺
532.0
42.6 m
3/2⁻
492.3
1/2⁻
455.5
5/2⁻
413.9
3/2⁻
403.5
3/2⁻
208.2
71 ps
5/2⁻
158.4
2.4 ns
1/2⁻
0.0
111Cd
Collective States
1/2⁺
1190
11/2⁻
396.2
48.6m
5/2⁺
245.4
85.0ns
1/2⁺
0.0

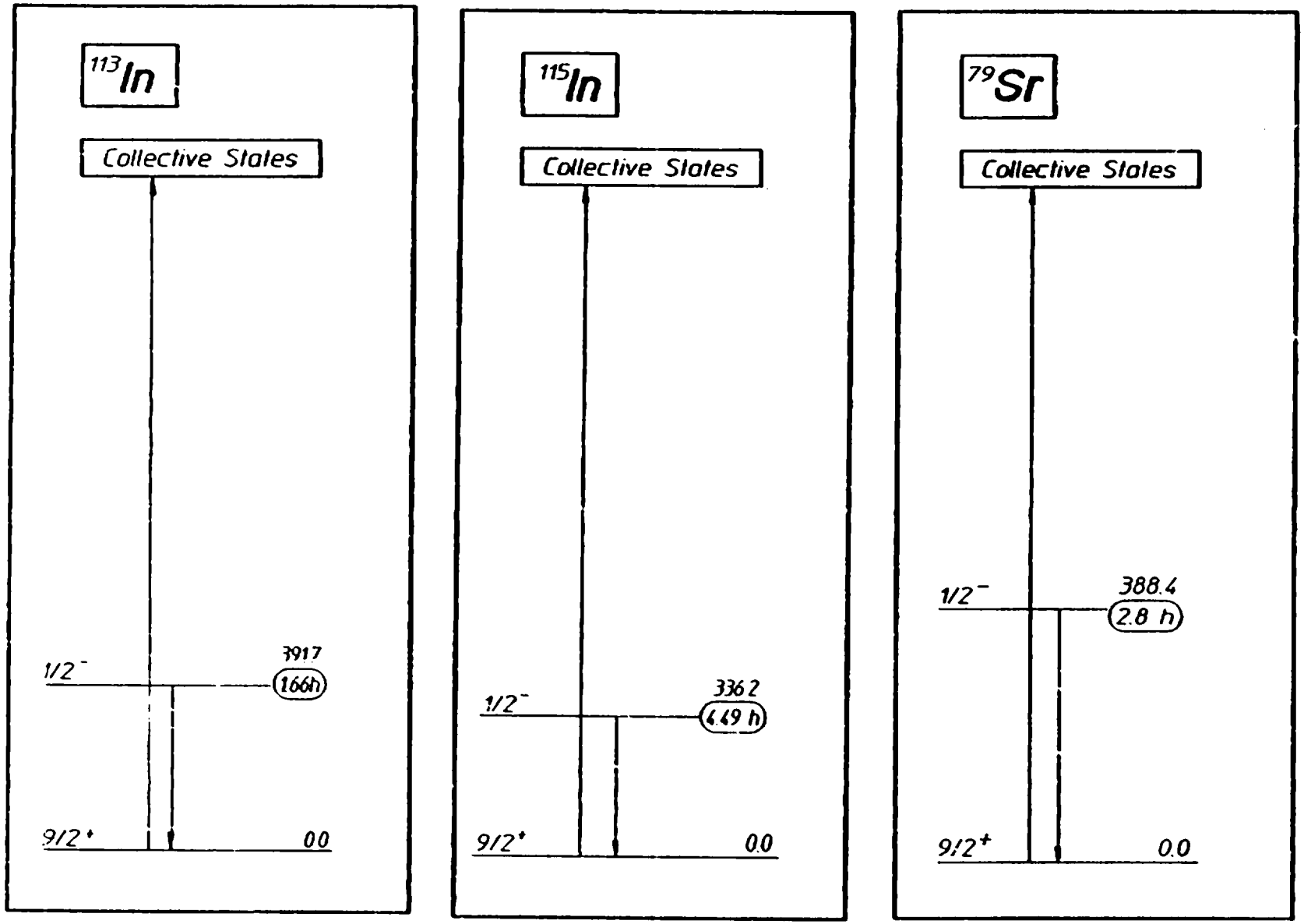
113In
Collective States
391.7
1/2⁻
1.66h
9/2⁺
0.0
115In
Collective States
336.2
1/2⁻
4.49 h
9/2⁺
0.0
79Sr
Collective States
388.4
1/2⁻
2.8 h
9/2⁺
0.0

Figure 1: Energy level diagrams of the excited states important to the production and detection of the isomers of the nuclei shown. Half-lives of the states are shown to the right of each, together with their energies in keV. Downward arrows locate transitions used in the detection of populations of the isomers produced by the absorption transitions indicated by the upward arrows. The locations of the gateways through which the (γ,γ') reactions proceed are not to scale, and the details of the cascades downward to the isomers are unknown.
a), b), and c) (second preceeding page, from left): Transitions important to the study of (γ,γ') reactions producing the isomers $^{137}Ba^{m}$, $^{199}Hg^{m}$, and $^{111}Cd^{m}$.
d), e), and f) (preceeding page, from left): Transitions important to the study of (γ,γ') reactions producing the isomers $^{113}In^{m}$, $^{115}In^{m}$, and $^{87}Sr^{m}$.

The activation induced by the reaction $^{113}In(\gamma,\gamma')^{113}In^{m}$ shown in Fig. 1d was so intense that usable levels of fluorescence were still found in the 1.7 hr isomer of the 4.3% natural fraction of the 7.6 g foil after the 6 hour and 16 minute transit to the counting facility in Dallas.

For the comparative studies, targets of BaF_2, Hg_2Cl_2, and SrF_2 were fabricated from powders, Cd and In from solid pellets, held in cylindrical polyethylene vials. These were hung at the position of the indium foil, and were irradiated perpendicular to the axes of the vials. After irradiation they were dismounted and carried to a locally positioned NaI(Tl) spectrometer. The entire target package was backed with an array of thermoluminescent diodes (TLD's) which were used to determine the morphology of the radiation pattern.

Results-Cross Calibration Studies

From the number of counts in the fluorescence peaks corresponding to the transitions of Figs. 1d and 1e, the numbers of activations in the indium foil sample were obtained by well-established procedures. The efficiency of the spectrometer was determined with calibrated sources and was found to conform closely to nominal specifications. Self-absorption corrections were calculated as discussed and fluorescence efficiencies were taken from the literature.[9] The actual numbers of activations of the samples, S, were obtained by correcting for finite counting and irradiation times. Literature values of the half-lives were used in making these corrections.[4]

The spectral fluence can be obtained if it is assumed that one channel at energy E_1 dominates the excitation so that Eq. (1) can be inverted,

$$\frac{\phi(E_1)}{A} = \frac{SE_1}{N} (\pi b_s b_o \sigma_o \Gamma/2)^{-1}_1 \quad . \qquad (4)$$

As mentioned earlier the term in parentheses is the integrated cross section for the excitation of the fluorescence. Values reported as a result of the linac experiments[8] are shown in Fig. 2 as functions of the energies E_1 at which the pump intensity was being sampled.

Using the data of Fig. 2 in Eq. (4) together with the actual numbers of activations of ^{115}In and ^{113}In gives the values of spectral fluence shown in Fig. 3. Data shown there define the locii of the single measurement of intensity which would result *if the precise energy, E_1, of the dominant gateway were known.*

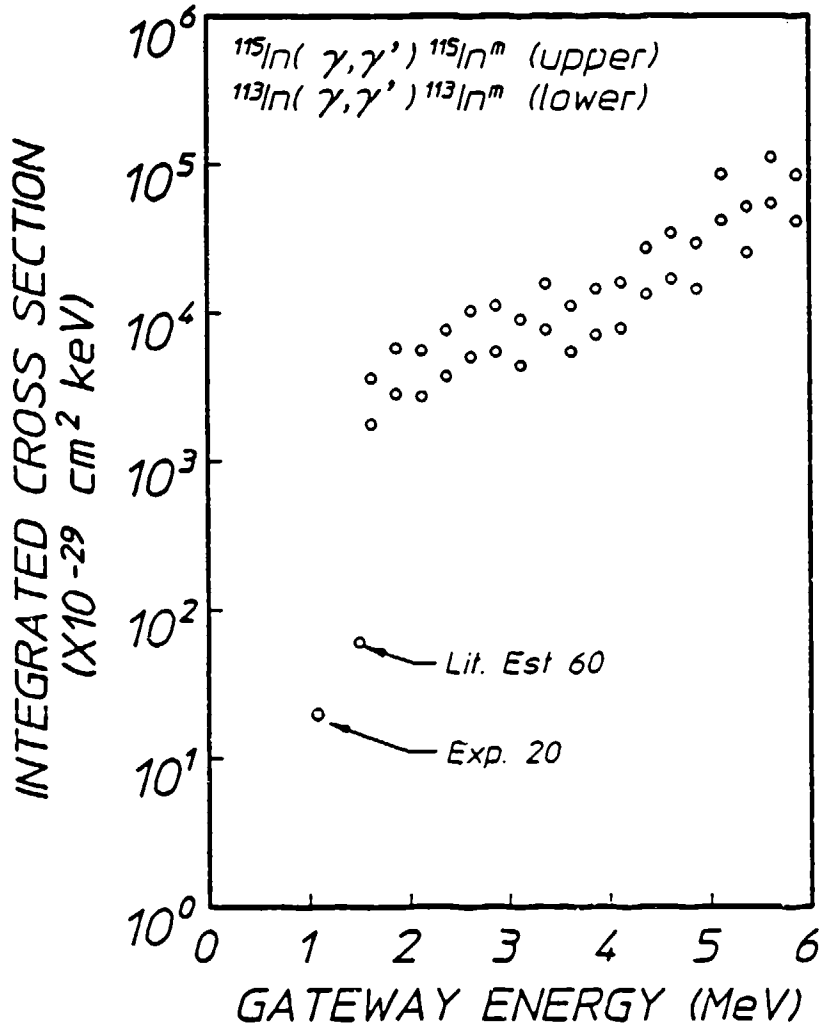

Figure 2: The integrated cross sections reported for the photoactivation of selected nuclei through individual, unknown gateway states as functions of the energies at which they could be assumed to lie. The lower family of points approximated the results obtained for the activation of ^{113}In to within the plotted sizes of the data while the upper characterizes the excitation of ^{115}In. Shown at the successively lower energies are the two points taken from Refs. 4 and 2, respectively.

For comparison, the spectrum indicated by dosimetry is shown in Fig. 3 by the solid line. It was obtained by scaling the results of a theoretical computation of the spectrum[10] to the dose measured with the

TLD's. The dose is defined as the energy absorbed per unit mass of target and is computed from the expression,

$$D = \sum_i \left(\frac{\mu_a}{\rho}\right)_i E_i \left.\frac{d\varphi}{dE}\right|_i \Delta E_i \quad , \tag{5}$$

where

$\left(\frac{\mu_a}{\rho}\right)_i$ - mass energy absorption coefficient[11] for bremsstrahlung at E_i in units of cm^2/g,

E_i - photon energy,

$\left.\frac{d\varphi}{dE}\right|_i$ - spectral flux, derivative with respect to photon energy of the photon fluence; in units of photons/keV/cm^2,

ΔE_i - size of the mesh of energies over which the previous variable is reported.

It is the quantity,

$$G(E_i) = gE_i \left.\frac{d\varphi}{dE}\right|_i \quad , \tag{6}$$

that is reported[11] as a result of computations of the bremsstrahlung. In this expression g is a constant normalizing the intensities to the total measured output. In actual practice it is determined from measurements of the dose at the position of the target being irradiated. Dividing Eq. (6) by g and substituting into Eq. (5) and solving for g gives,

$$g = \frac{1}{D} \sum_i \left(\frac{\mu_a}{\rho}\right)_i G(E_i)\Delta E_i \quad . \tag{7}$$

Finally substituting back into Eq. (6) and solving for $Ed\varphi/dE$,

$$E_i \left.\frac{d\varphi}{dE}\right|_i = DG(E_i) \left[\sum_i \left(\frac{\mu_a}{\rho}\right)_i G(E_i)\Delta E_i\right]^{-1} \quad , \tag{8}$$

which is the quantity for which measurements are reported in Fig. 3.

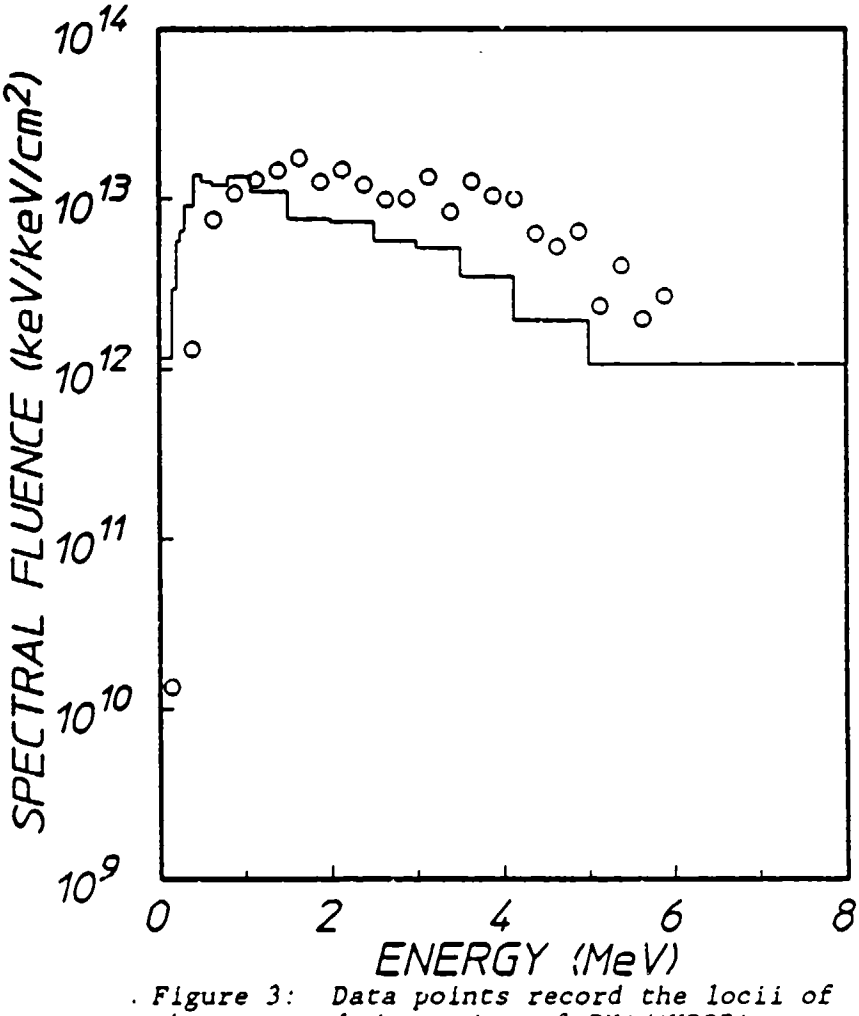

Figure 3: Data points record the locii of the spectral intensity of DNA/AURORA measured at one energy by nuclear activation calibrated in the linac in comparison with the computed spectrum normalized by a dosimeter measurement. The computed spectrum is represented by the solid line. The energy to which the activation procedure is most sensitive is not known but locii record possible values and corresponding intensitites. The bremsstrahlung was produced by DNA/AURORA charged to 90 KV at the Marx input.

Values of G(Ei) were available[11] for charging voltages of 90 kV and 110 kV. Plotted by the solid line in Fig. 3 is the spectral fluence calculated from Eq. (8) for the $G(E_i)$ reported for 90 kV. It is particularly interesting that the functional form of that $G(E_i)$ closely resembles the spectrum[12] from the 6 MeV linac and the resulting spectral

fluence is in rough agreement with the measurements obtained with the indium absorbers.

Results-Target Survey

Since the end point energy of the bremsstrahlung from DNA/AURORA was close to the threshold value for neutron evaporation from (γ,n) reactions, it was necessary to examine the fluorescence spectra from the materials being considered as calibrators for the 2 - 6 MeV range of energies. These spectra are shown in Figs. 4a - 4e. Dominant structures are marked and all correspond to the signatures of the respective (γ,γ') reactions.

The end point energy of the bremsstrahlung could be varied over a limited range at DNA/AURORA by changing the primary charge voltage on the Marx bank while adjusting the spark gaps, correspondingly. If the end point at first lay below the energy of excitation of the first of the giant gateways, relatively little excitation would be expected. Then as it were increased, the activation should "turn-on" when the gateway energy was reached. To search for such evidence of a distinctive gateway characteristic of each target material, fluorescence photons in the peaks of the spectra of Fig. 4a - 4e were counted as functions of the charging voltage of the Marx generator.

Data were corrected to obtain relative numbers of activations by compensating for the delay in the start of the counting period and for its finite duration. An onset of excitation through a gateway is more readily observed if the relative numbers of activations are scaled by the input dose of irradiation measured by the TLD's at the position of the target. In this way the increase in activation simply associated with the greater dose emitted by the accelerator at higher charging voltages is less able to mask the increases resulting from the opening of a new channel for absorption in the nuclei. Shown in Figs. 5a - 5e are the resulting values of the activation per unit dose normalized to the activation at 110 kV, as functions of the charging voltage on the Marx. Due to insufficiently complete transit time information, the ^{137}Ba data could not be reduced to this form.

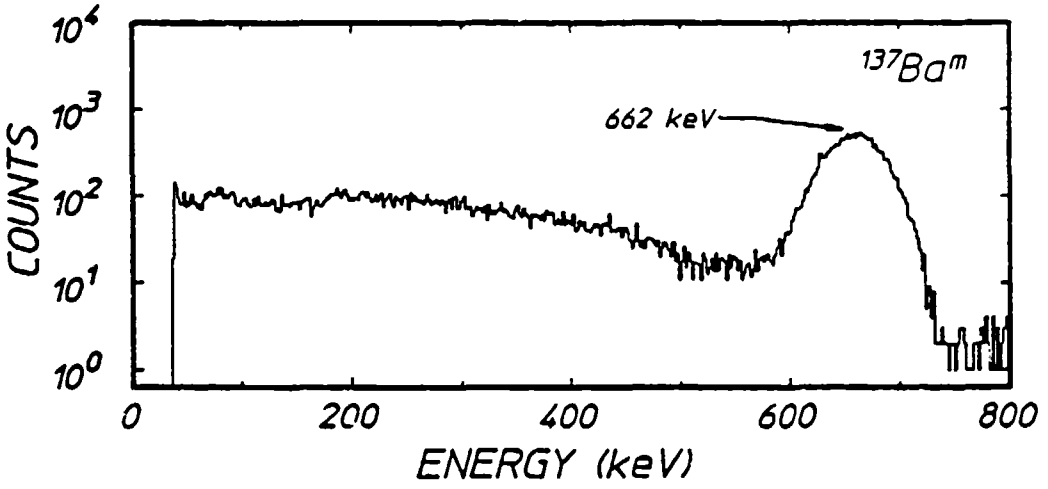
10^4
10^3
10^2
10^1
10^0
COUNTS
$^{137}Ba^m$
662 keV
0
200
400
600
800
ENERGY (keV)

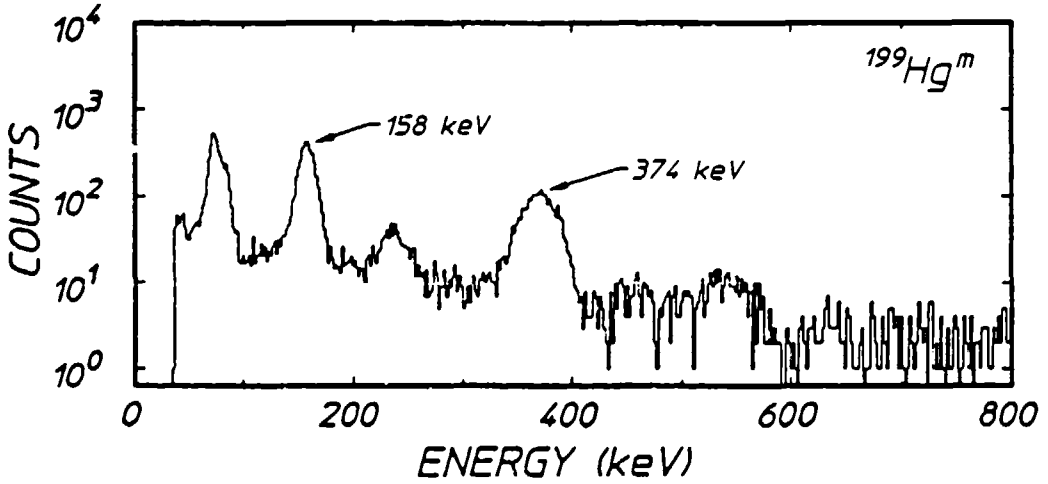
10^4
10^3
10^2
10^1
10^0
COUNTS
$^{199}Hg^m$
158 keV
374 keV
0
200
400
600
800
ENERGY (keV)

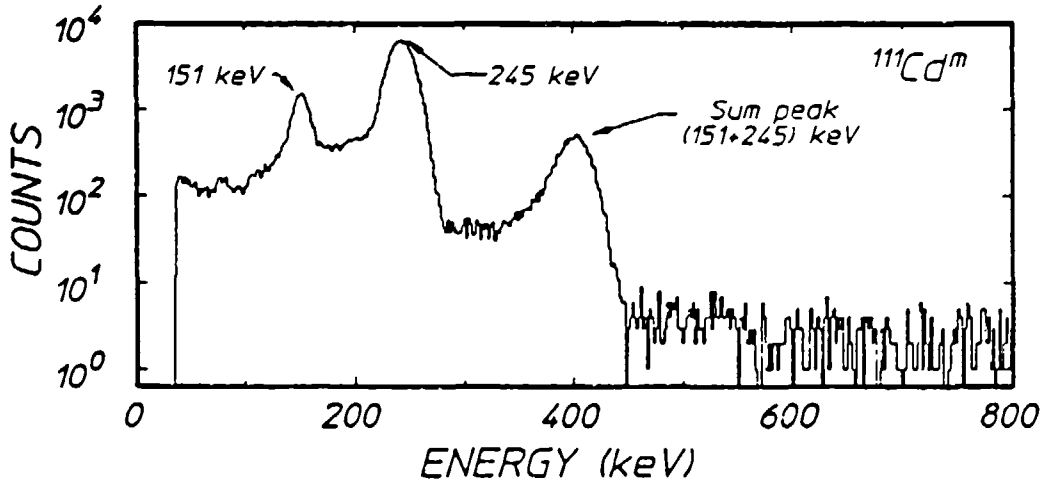
10^4
10^3
10^2
10^1
10^0
COUNTS
$^{111}Cd^m$
151 keV
245 keV
Sum peak
(151+245) keV
0
200
400
600
800
ENERGY (keV)

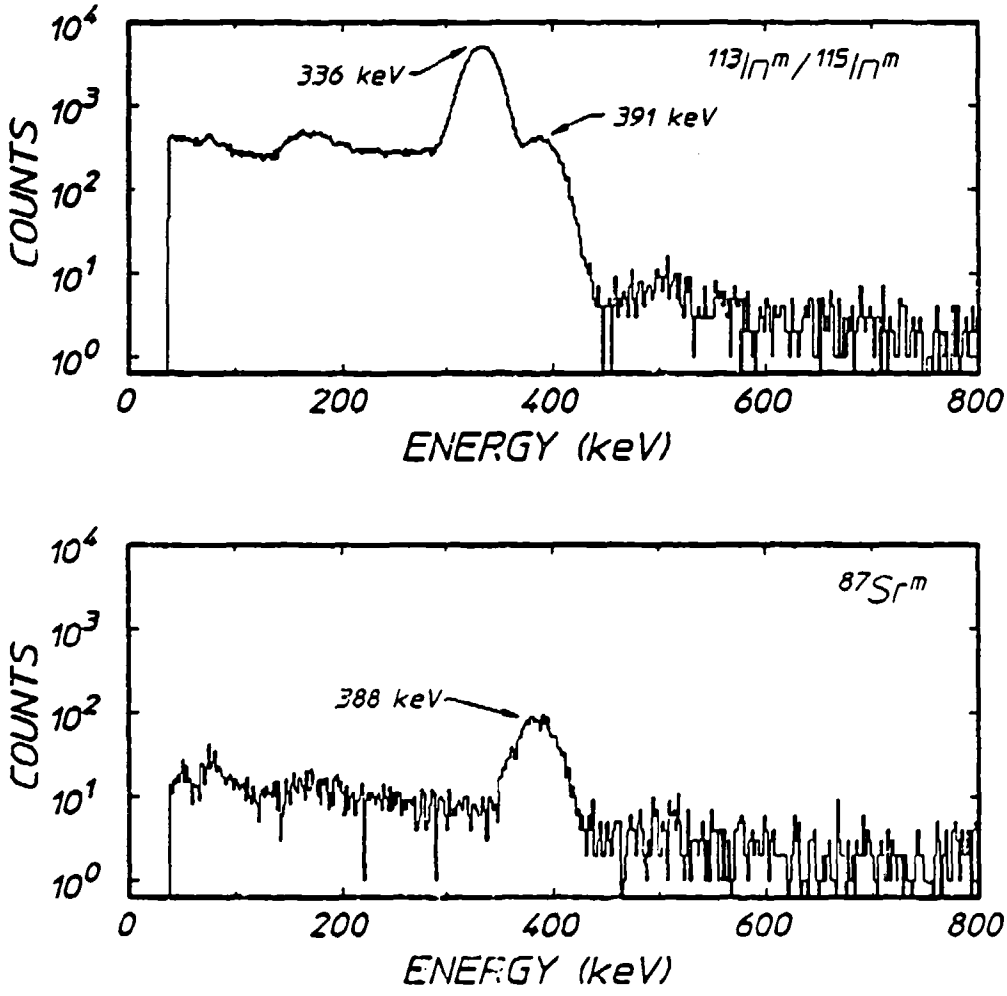

Figure 4: Spectra of the fluorescence detected with an NaI(Tl) detector over the ranfe of energies shown. Transitions shown in Figs. 1a - 1f for the detection of the isomers are identified by the arrows. All samples were counted for 600 s. The elapsed times from irradiation to the start of counting are as follows:
a), b), and c) (preceding page): ^{137}Ba, ^{199}Hg, and ^{111}Cd: Transit times were 6 m, 63 m, and 27 m.
d) and e) (above): $^{113}In/^{115}In$ and ^{87}Sr: Transit times were 45 m and 82 m.

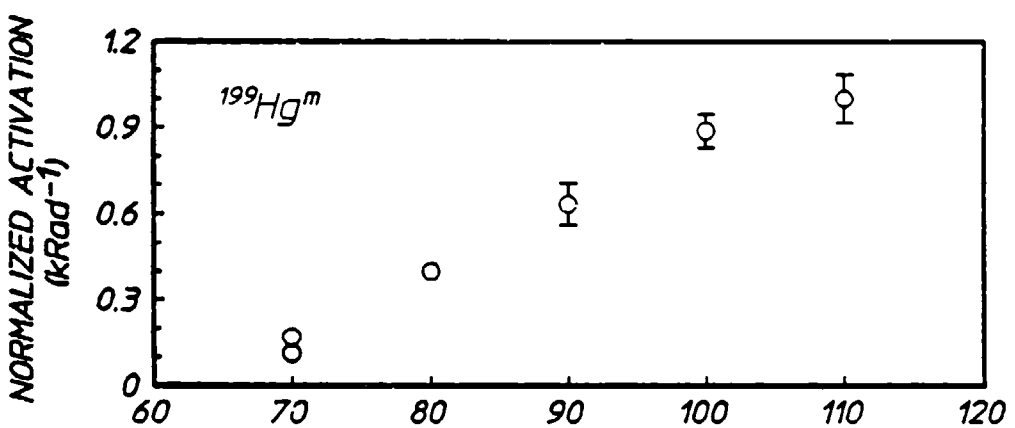
NORMALIZED ACTIVATION (kRad-1)
199Hgm
1.2
0.9
0.6
0.3
0
60
70
80
90
100
110
120
CHARGE VOLTAGE (kV)

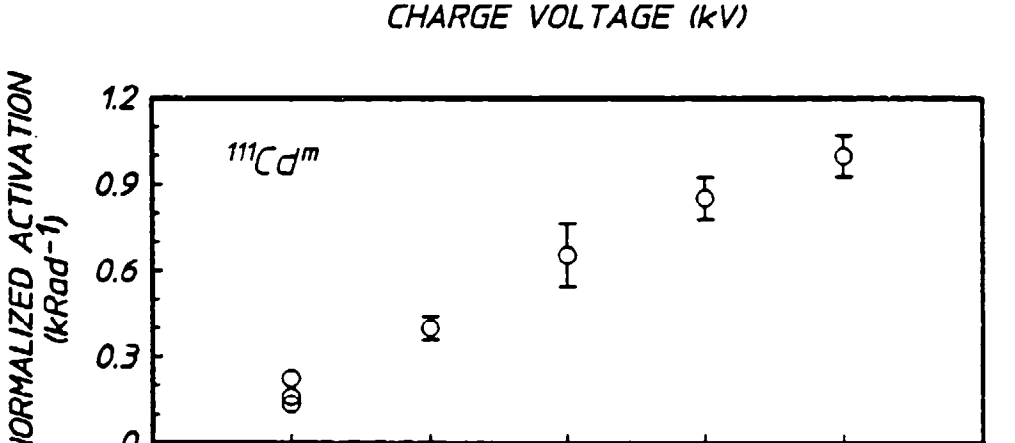
NORMALIZED ACTIVATION (kRad-1)
111Cdm
1.2
0.9
0.6
0.3
0
60
70
80
90
100
110
120
CHARGE VOLTAGE (kV)

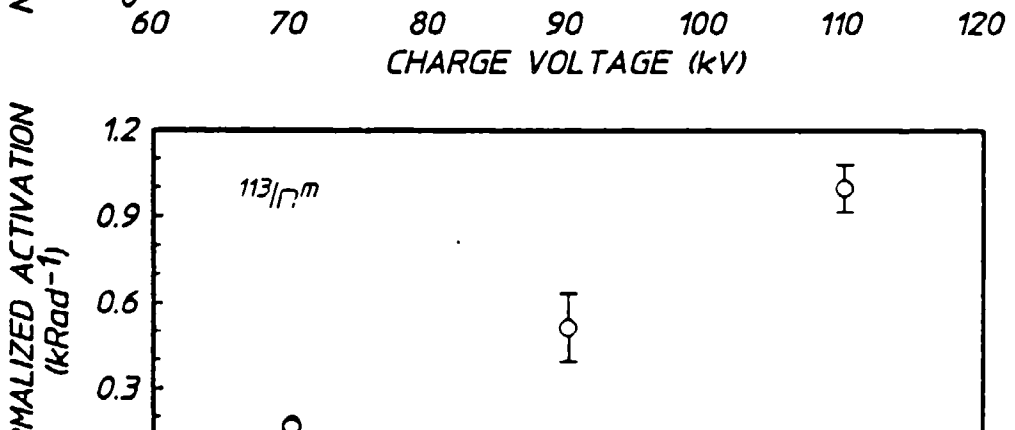
NORMALIZED ACTIVATION (kRad-1)
113Inm
1.2
0.9
0.6
0.3
0
60
70
80
90
100
110
120
CHARGE VOLTAGE (kV)

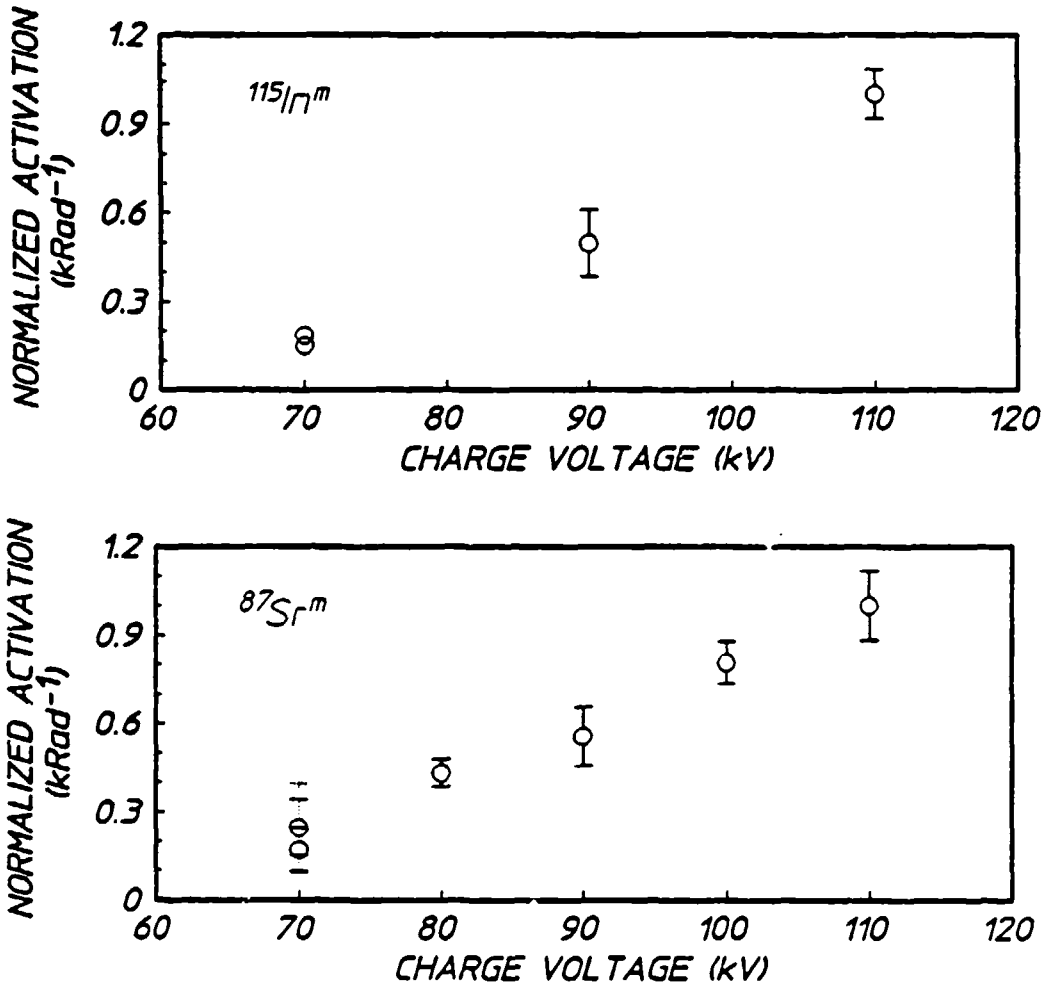

Figure 5: Isomeric activation per kilorad of dose normalized to the activation at 110 kV, as a function of the DNA/AURORA charging voltage for the following nuclei:
a), b), and c) (preceding page): $^{199}Hg^{m}$, $^{111}Cd^{m}$, *and* $^{113}In^{m}$:
d) and e) (above): $^{115}In^{m}$ *and* $^{87}Sr^{m}$.
Where no error bars are shown, the error is commensurate with the symbol size. For $^{87}Sr^{m}$, *the dashed error bar indicates the largest extent of the error associated with the cluster of points.*

Conclusions

The general agreement between the calculated and measured values of spectral fluence from DNA/AURORA shown in Fig. 3 are both surprisingly good and disturbingly inconsistent. Since the dominant gateway energies of the ^{115}In and ^{113}In components of the target are not known, deviations between theory and experiment of less than an order of magnitude are most heartening. This is the first and most overriding conclusion.

Finer details are troublesome. Not having access to a variable energy LINAC, the calibrating values of the integrated cross sections for indium activation had been obtained earlier by fitting calculations of LINAC spectra to dosimeter measurements for comparison to measured yields of fluorescence. Rather surprisingly the calculated spectra for the 6 MeV LINAC were extremely close to those for DNA/AURORA charged to 90 kV. Because of that, it would have seemed unlikely that the activations were proceeding through gateways at different energies, one being preferred in the LINAC case and the other in AURORA. As a consequence, it would seem that the differences seen in Fig. 3 should have accrued only from variances in counting accuracy and dosimeter calibrations and thus, should have been far smaller. The most attractive speculation is that in fact, gateways were accessed at different energies because one or the other of the two sources had a tail of higher energies more intense than computed. Such a possibility emphasizes the need for more definitive calibration of the sampling targets.

The survey data pursuant to the second objective is interesting in that evidence for individual gateways may be appearing at the lower charging voltages. Mercury seems to show a sharper onset between 70 and 80 kV than does cadmium. If better data confirms this trend it will indicate that the dominant gateway lies at higher energies in ^{111}Cd than in ^{199}Hg. In the latter case the onset would have occurred at even lower charging voltages than tested here and the sharp part of the increase in fluorescence would have passed before 70 kV were reached.

The present data is of such a cursory nature that only speculations can be supported about detailed mechanisms. What is clear is that there is a strong case for the efficacy of calibrating such a large accelerator as DNA/AURORA with the nuclear activation technique we proved at lower x-ray energies. Success would be certain if a variable energy

LINAC were available to first determine the gateway energies of the sampling targets. Without such a device, the present results suggest that a repetition of the "bootstrap" process which succeeded at lower energies has a reasonable chance of succeeding at these higher energies.

Acknowledgement

The help, advice, and support of the AURORA team at Harry Diamond Laboratories is gratefully acknowledged and in particular F. J. Agee, K. Kerris, G. A. Huttlin, and D. A. Whittaker.

References

1. J. A. Anderson and C. B. Collins, Rev. Sci. Instrum. 58, 2157 (1987).

2. J. A, Anderson and C. B. Collins, Rev. Sci. Instrums 59, 414 (1988).

3. C. B. Collins, F. W. Lee, D. M. Shemwell, B. D. DePaola, S. Olariu, and I. I. Popescu, J. Appl. Phys. 53, 4645 (1982).

4. Evaluated Nuclear Structure Data File (Brookhaven National Laboratory, Upton, New York, 1986).

5. C. B. Collins and J. A. Anderson in Center for Quantum Electronics Report #GRL/8701, University of Texas at Dallas, 1987 (unpublished) pp. 35-53.

6. C. D. Eberhard, J. W. Glesener, Y. Paiss, J. A. Anderson, C. B. Collins, W. L. Hodge, E. C. Scarbrough, and P. P. Antich, Phys. Rev. C. (pending).

7. C. B. Collins, J. A. Anderson, C. D. Eberhard, J. F. McCoy, J. J. Carroll, E. C. Scarbrough, and P. P. Antich in Center for Quantum Electronics Report #GRL/8703, University of Texas at Dallas, 1988 (unpublished) pp. 37-56.

8. C. B. Collins in Center for Quantum Electronics Report #GRL/8703, University of Texas at Dallas, 1988 (unpublished) pp. 1-20.

9. E. Browne and R. B. Firestone, Table of Radioactive Isotopes, edited by Virginia S. Shirley (Wiley, New York, 1986).

10. K. G. Kerris in Harry Diamond Laboratories Report No. HDL-TM-81-18, Harry Diamond Laboratories, 1981 (unpublished).

11. J. H. Hubbell, Photon Cross Sections, Attenuation Coefficients, and Energy Absorption Coefficients from 10 keV to 100 GeV, NSRDS-NBS-29, (U.S. Gov. Printing Office, Washington, D.C., 1969).

12. R. Mohan, C. Chui, and L. Lidofsky Med. Phys. 12, 595 (1985).

N00014-86-C-2488
UTD #24522-964

A FREQUENCY MODULATION SPECTROMETER FOR MOSSBAUER STUDIES

by P. W. Reittinger, T. W. Sinor, S. S. Wagal, and C. B. Collins

Introduction

As early as 1960 it had been noted that radiofrequency (Rf) sidebands to the hyperfine structure of ^{57}Fe could be observed with a Mössbauer spectrometer.[1] The six lines (Parent Transitions) in a normal absorption spectrum of ^{57}Fe in iron (Fig. 1a) are accompanied by additional absorption peaks (Rf sidebands) when the absorber is subjected to an Rf field (Fig. 1b). In 1960 Ruby and Bolef reported the observation of Rf sidebands in iron produced by mounting a ^{57}Co Mössbauer gamma ray source on an ultrasonic transducer driven at MHz frequencies.[1] It should be noted that the Rf transducer was used in addition to a long period oscillator which provided the energy range for the Mössbauer spectrum by introducing controlled Doppler shifts. In 1968 Perlow reported the generation of Rf sidebands in iron directly, by subjecting the gamma-ray source an Rf field without the involvement of any external ultrasonic source.[2] In that same year Heiman, Pfeiffer and Walker reported observing Rf sidebands in iron as a result of subjecting the iron foil absorber to an Rf field.[3] Finally, in 1976 Chien and Walker presented a method for producing Rf sidebands in a nonferromagnetic stainless steel absorber with an Rf field, by using nickel as a ferromagnetic non-absorbing driver.[4] In all cases, the Rf sidebands appeared at integral multiples of the frequency of the applied Rf (Fig. 2). Figure 2 shows Rf sidebands produced in a stainless-steel foil driven by a nickel foil immersed in Rf fields of different frequencies. The frequency dependence of these Rf sidebands can be utilized to make a high resolution adaptation of Mössbauer spectroscopy which is freed from many of the mechanical constraints tending to limit conventional devices.

In 1967, Bolef and Mishory reported the development of a spectrometer which was based upon Rf sidebands induced in a Mössbauer source with an rf electromechanical transducer (an X-cut quartz crystal).[5] As the frequency of the applied Rf was changed, the energies of the sideband gamma ray emissions changed. This phenomenon enabled Bolef and Mishory to obtain an absorption spectrum as a function of the frequency of the applied rf. In 1985 DePaolo, Wagal and Collins reported success in

developing a spectroscopic technique using Rf sidebands induced in a ferromagnetic absorber by an Rf field.[6] Modulating the absorber has numerous advantages over modulating the source. It is easier and safer to work with a stable isotope, and it is also easier to interpret a spectrum from a single line source, as opposed to a Zeeman split source or a source with Rf sidebands. Therefore, we have improved the technique for a modulated gamma-ray absorption cross section spectroscopy which we call Nuclear Frequency Modulation Spectroscopy (NFMS).

The technique reported by DePaolo, Wagal and Collins was slow and laborious, with data collection times on the order of months for tens of data points. We would like to report the automation of this technique, with resulting data collection times of two days for 1024 data points and a signal to noise ratio of 8:1 for a signal that represents a relative absorption of 3%. This article describes the NFMS apparatus, describes the interface to an Apple computer which automates NFMS data collection, and presents some typical NFMS data.

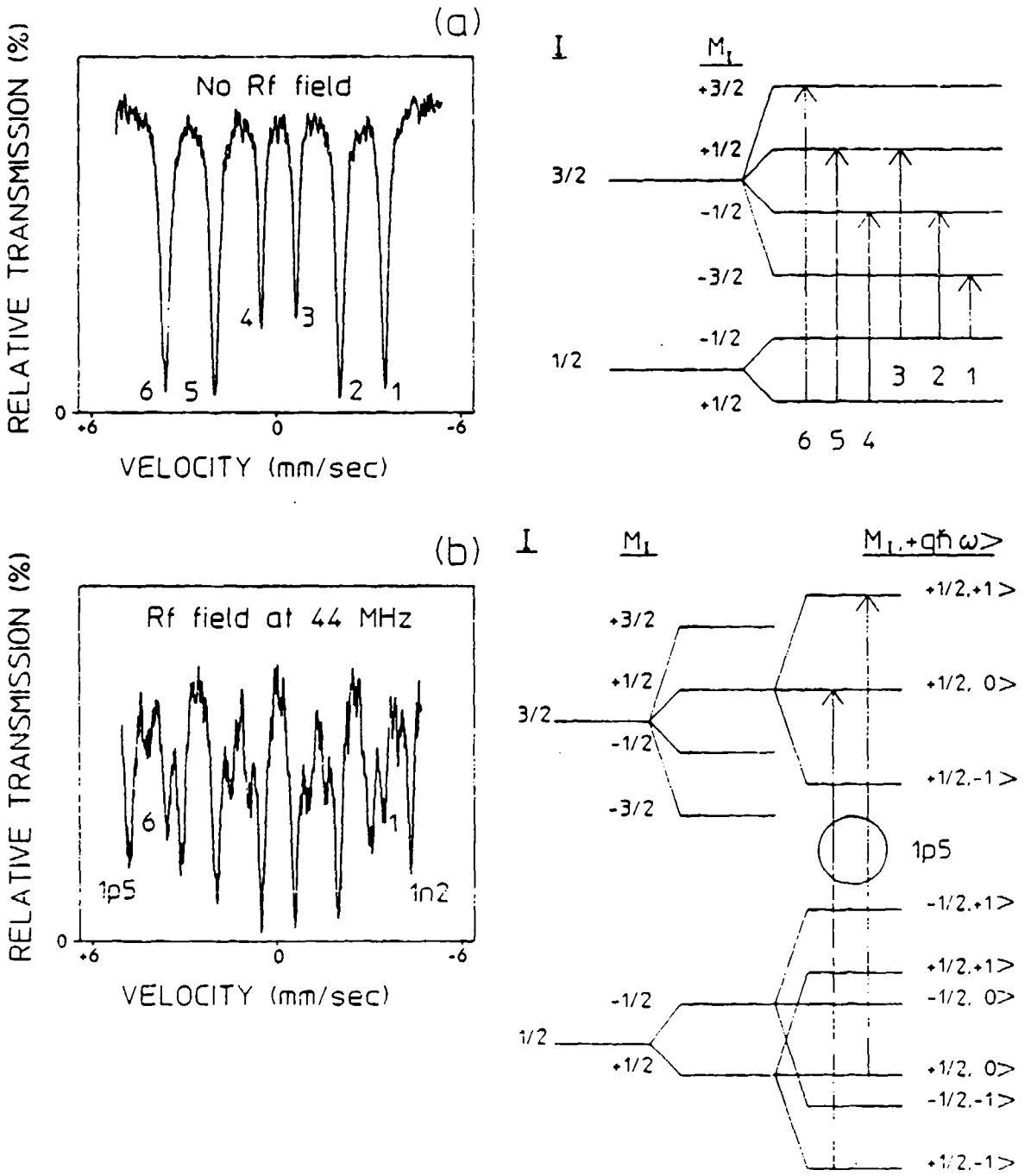

Figure 1: Mössbauer absorption spectra and energy level diagrams for ^{57}Fe in iron, a) with no Rf field at the absorber, and b) with a 4 Oersted Rf field applied to the absorber at a frequency of 44 MHz, showing the effect of the Rf field.

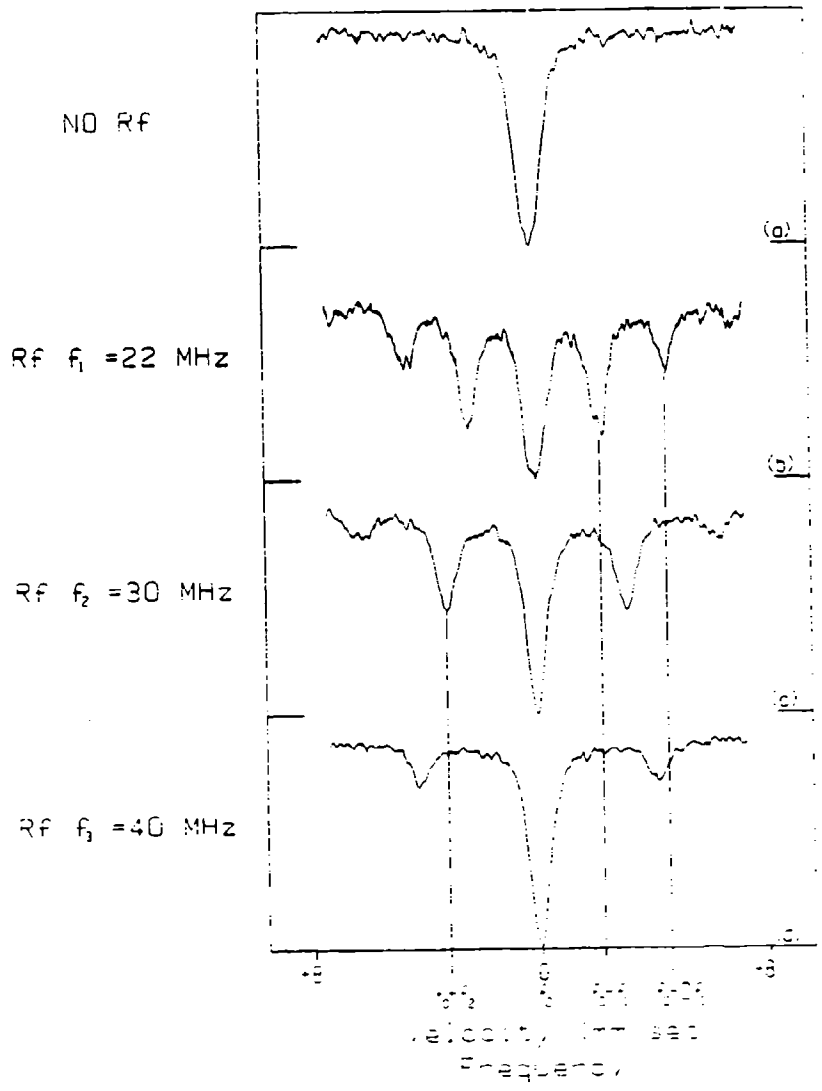

Figure 2: Mössbauer absorption spectra of ^{57}Fe in 310-stainless steel driven by a nickel foil, showing the effect of an Rf field applied to the absorber-nonabsorber sandwich at frequencies of b) 22 MHz, c) 30 MHz, and d) 40 MHz in comparison to a) a no Rf spectra. It can be seen from the figure that sidebands appear at integral multiples of the frequency of the Rf field.

Spectrometer Design

The NFMS is a modification of a conventional Mössbauer spectrometer comprised of the equipment in the dotted box in the schematic of Fig. 3. A Kr gas filled proportional counter (ASA PC-KR-1) biased with 1.8 kV from a Bertran Associates model 303 DC voltage supply was used as our gamma-ray detector. The signal from the detector was amplified by an ASA CSP-400A preamp and ASA LA-200 amplifier. The amplified signal was then fed into an ASA LG-200 linear gate which produced 1 μsec TTL pulses for counting.

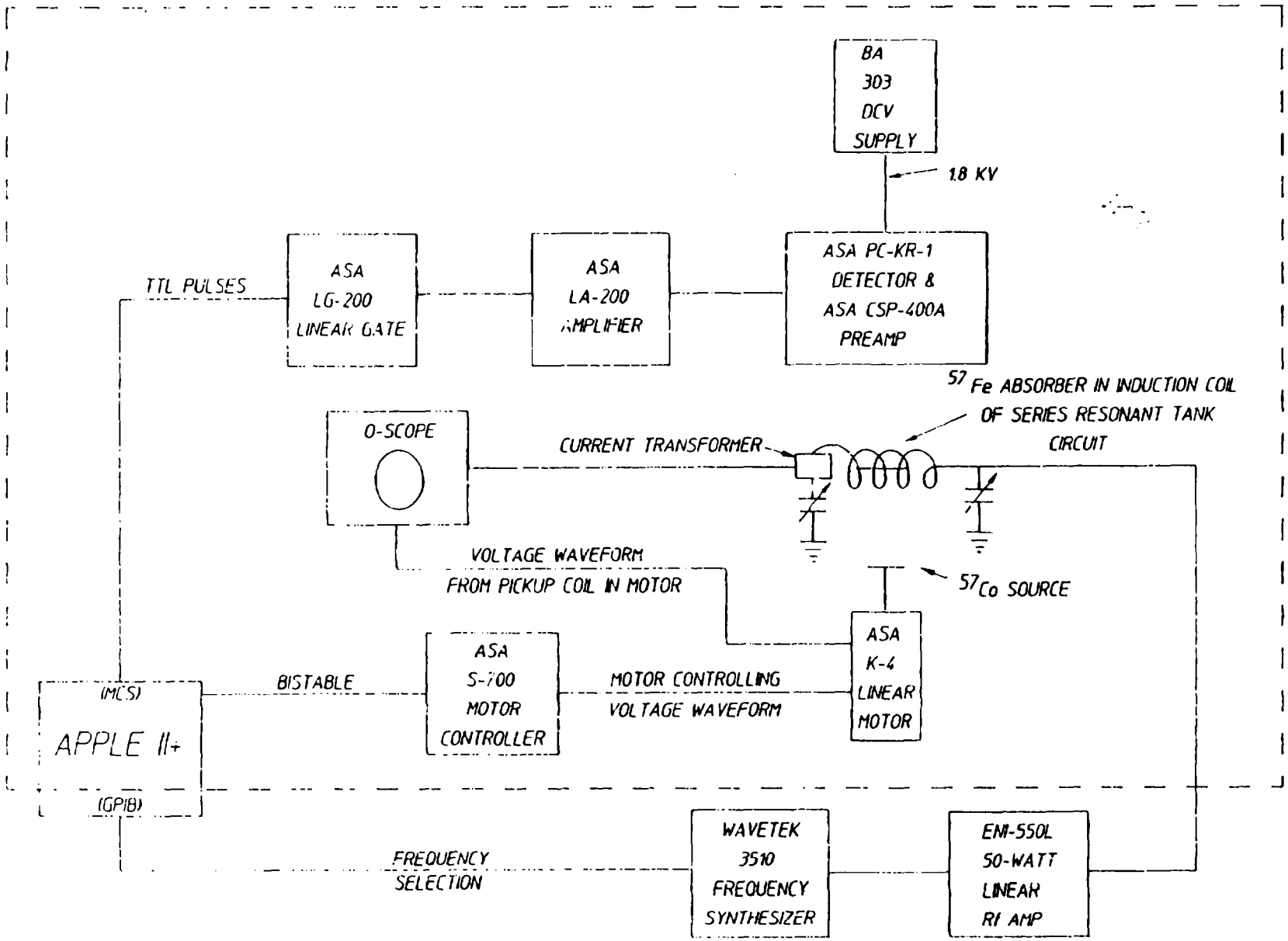

Figure 3: This schematic shows the NFMS, while the portion of the apparatus which is in the dotted box can be used as a conventional Mössbauer spectrometer.

A 10 mCi ^{57}Co Mössbauer source in a Pd matrix was mounted on an ASA K-4 linear motor capable of operating at a constant velocity or with constant acceleration. A stable means of Doppler shifting the energy of the emitted gamma ray is needed, therefore an ASA S-700 motor controller is used to produce the voltage waveforms which drive the linear motor. The constant acceleration voltage waveform is derived from a 5 Hz square wave which must be provided by the multi-channel scalar (MCS). If the motor is driven at a constant velocity, then the motor controller gates off data to the MCS while the motor is rewinding.

The key to NFMS is the presence of the Rf field at the absorber, for which a very stable Rf signal generator and amplifier are needed. A Wavetek 3510 signal generator, with a frequency range of 1 MHz to 1GHz, and a 100 Hz resolution with a 500 Hz/(10 min) stability, was used. The Rf amplifier was an ENI 550L 50 watt linear amplifier with a range of 1.5-400 MHz. There were two basic circuits used to generate the Rf field at the absorber. One was a series LC circuit in parallel with an impedance matching capacitor (Fig. 3). This series-resonant tank circuit was designed to have either a low Q when used in a narrowband NFMS, or a high Q when used to obtain a Mössbauer spectrum in the presence of a single frequency Rf field. It should be noced that narrowband in these instances refers to a 12 Mhz or less bandwidth. The other circuit, used in the wideband NFMS, simply incorporated an inductor in series with an impedance matching non-inductive load. The absorber was then mounted in the induction coil of the appropriate circuit and subject d to field intensities on the order of 1-5 Oersteds.

In order to monitor the field intensity in the coil, a Pearson 2877 current transformer was used to measure the current flowing into the induction coil. This transformer outputs 1 V/Amp with a usable range of 300 Hz to 200 MHz and an insertion impedance of 0.02 Ohms. In order to monitor the velocity of the motor, there is a pickup coil mounted in the linear motor. The output from this pickup is used to stabilize the driving voltage waveform, but it can also be monitored on an oscilloscope. The velocity of the motor was established by correlating the pickup coil voltages to the positions of the peaks in the 6 line spectrum of ^{57}Fe. Currently work is underway building an interface to an Apple II+ from an ASA LC-9A laser interferometer. This interface will enable the computer to display real time velocity information as well as track any drifting.

The heart of the NFMS, however, is the MCS/GPIB interface (Fig. 4). It enables an Apple II+ computer to be used for data acquisition and real time data display with either the conventional Mössbauer spectrometer (constant acceleration mode), or with the NFMS (constant velocity mode with GPIB interface to signal generator). The MCS is a card designed around two VIA's, or Versatile Interface Adapters (6522's). The GPIB, or IEEE-488 General Purpose Interface Bus (9914), is a commercially available interface card available for the Apple computer. The GPIB is necessary only for scanning frequencies of the signal generator. Therefore, the GPIB is not needed if one intends to use only the Mössbauer spectrometer.

The central components of the MCS are the two 6522's, the multiplexing logic, and a 12-bit counter. Each 6522 is a 40 pin chip which has a 16-bit counter with a 16-bit latch, a 16-bit counter with an 8-bit latch, two 8-bit parallel ports, and a serial port. The counter with the full latch can be set to count down in a free running mode and generate interrupts. In other words, the 6522 can be set to generate evenly spaced interrupts so that the Apple's CPU need not be wasted keeping track of time. The counter with the half latch can be set to count negative logic pulses at one of the pins of the 6522. The multiplexing logic is an assortment of gates which channel the pulses to be counted to one of the 6522's while channeling the Apple's data bus to the other 6522. When an interrupt is generated, the pulses to be counted are gated to the other 6522 while the Apple's data bus is then channeled to the first 6522. As a result, the time it takes the Apple's CPU to add a count to the proper channel is not dead time for the MCS. The twelve bit counter, actually three 4-bit counters, is needed to count 512 interrupts. This counting produces the 5 Hz square wave which is used by the motor controller to generate a constant acceleration voltage waveform for the linear motor. Therefore, the time between interrupts, hence the dwell time per channel, must be 195 μsec for a 1024 data point Mössbauer spectrum. The NFMS, on the other hand, does not require an accelerating source. Therefore, when using the MCS in an NFMS the dwell time can be user selected. The optimum dwell time minimizes the total dead time, which arises from the time needed to allow the Rf signal to stabilize each time the frequency is changed, without compromising the stability of the signal.

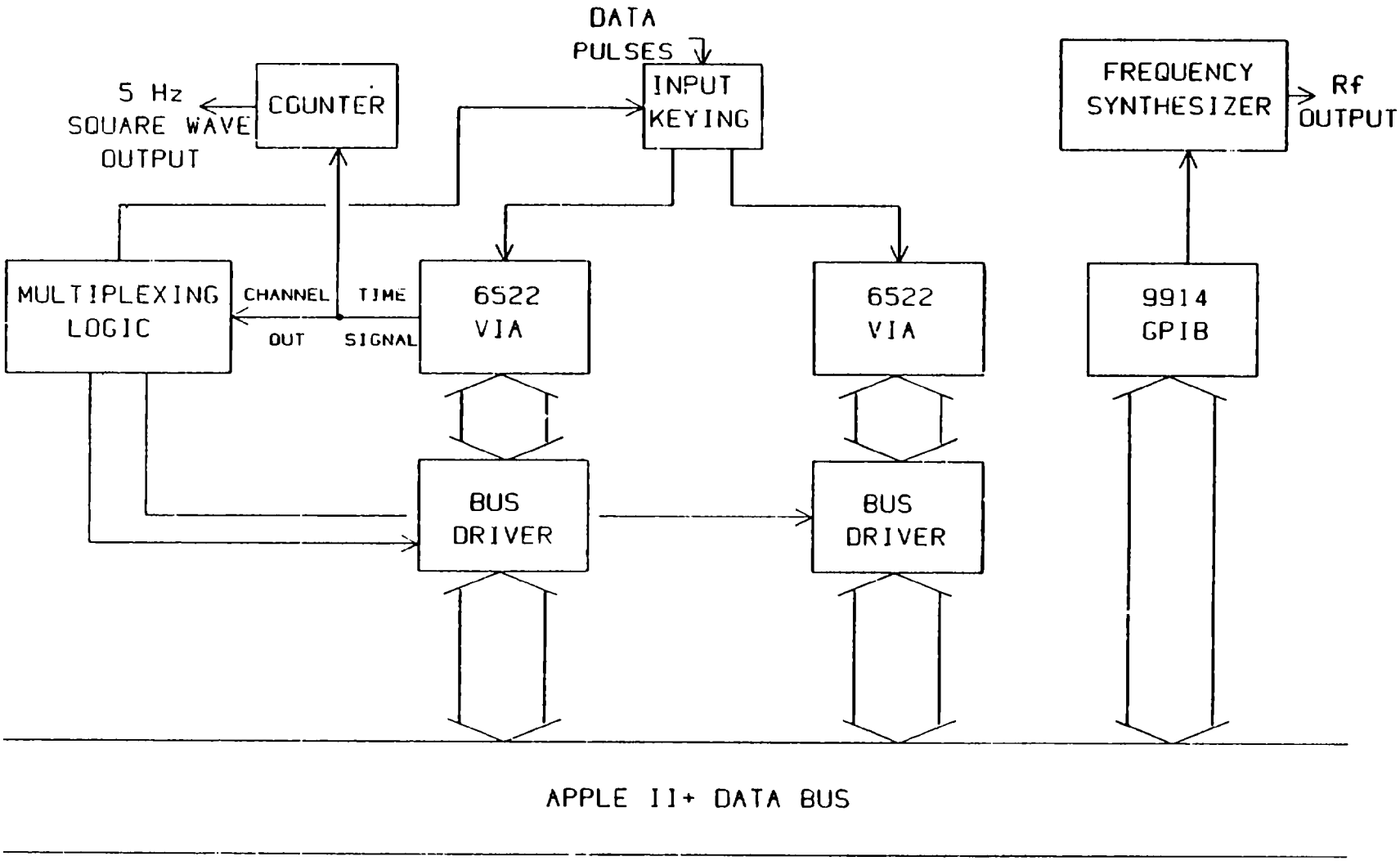

Figure 4. This block diagram shows the basic components of the interface to the Apple II+ computer. This interface enables the computer to be used for automatic NFMS data acquisition, or it can enable one computer, with two cards, to control and collect data from up to two Mössbauer spectrometers.

MCS/GPIB INTERFACE

Use of this hardware as an NFMS or a Mössbauer spectrometer is determined by the software. Written in 6502 assembly language, the software for the two spectrometers is similar in principle but different in particulars. In both spectrometers the MCS transfers data to the Apple on an interrupt basis. Both programs consist of four basic routines: an initialization routine, a display routine, a keyboard interpreting routine, and an interrupt routine. The initialization routine uses the multiplexing logic on the MCS card to address each of the 6522's and set the appropriate registers. The display routine has two options. The data can be displayed graphically at different resolutions, or counts can be displayed as counts per channel and total counts per sweep. The graphics data display uses table look up and two graphics screens to provide a real time data display. The initialization routine generates a table in memory which stores the address for a given vertical coordinate on the screen in a memory location which is correlated to the value of the vertical coordinate. The value of the horizontal coordinate is correlated to the memory address of the channel to be displayed. As the display routine scans through memory at the data, the data value and the channel value are used to address indirectly the appropriate graphics screen coordinate through this table. Therefore, by using table lookup, all of the mathematical operations necessary to obtain the appropriate screen addresses (including a division by seven) are performed only once. While one graphics screen is displayed, the other is cleared and plotted with the current data. The updated screen is then activated and the first screen is cleared and replotted, and so on. The keyboard interpreting routine allows one to change the display, change the resolution of the graphics display, or stop the spectrometer and store the data on a disk, all with single key codes. A table of these key codes is displayed at the bottom of the counts display screen, the default display. Finally, the interrupt routine collects the count from the currently accessible 6522 and stores it in the appropriate three byte location. The display and keyboard routines for the two spectrometers are identical, but the initialization and interrupt routines for the two spectrometers are necessarily very different.

In the Mössbauer spectrometer, the initialization routine must enable the MCS card to generate interrupts at 195 μsec intervals. Next, the interrupt routine must be capable of pushing all values in the CPU's registers to the stack, accessing the count from the appropriate 6522

and adding it to the appropriate memory locations, and then reloading the CPU's registers with their initial values, all in less than 195 μsec, with enough time left over to update the display between interrupts. This feat was best accomplished by using four separate interrupt routines. Since the spectrometer has 1024 channels, the data is stored in twelve 256-byte pages for three bytes per channel. Each interrupt routine addresses a channel comprising three bytes through the sum of base addresses plus a counter value. Upon completion, each routine stores the address of the next interrupt routine in the interrupt vector. The fourth routine stores the address for the first routine in the interrupt vector and increments the addressing counter. The result is an interrupt routine that lasts 50-60 μsec from interrupt to return, depending on the number of bytes which must be incremented. As a result, one Apple II+ computer can easily handle two Mössbauer spectrometers with a real time data display for each.

In the NFMS, the initialization routine enables the MCS card to generate interrupts at 1/20 of a second intervals. This routine also initializes the signal generator through the GPIB. The interrupt routine must then translate the number of interrupts generated into an elapsed time and compare this time to the selected dwell time. In addition, this interrupt routine must perform all of the functions of the Mössbauer spectrometer interrupt routine. After the elapsed dwell time, the interrupt routine must step the frequency of the signal generator and change the address (channel) for data storage. When the frequency of the signal generator is changed, and for a time thereafter, the data to the MCS must be gated off and the timing stopped until the signal is stabilized. In the NFMS the speed of the interrupt routine is no longer a major concern due to the significant increase in the time between interrupts and the fact that the data is gated off while the interrupt routine is delaying for the signal generator. Unfortunately, however, the time required to change the frequency is unavoidable dead time. Yet the total dead time in a run can be minimized by selecting a sufficiently long dwell time which does not allow the signal to drift significantly.

Data and Discussion

Figures 1 and 2 show data collected with our Mössbauer spectrometer and processed with a 5 point running average. These figures show Rf

sidebands in an iron foil absorber, and the frequency dependence of the Rf sideband energies in a stainless steel foil absorber. All NFMS spectra to be shown were obtained from a 1.5 cm x 0.85 cm x 2.5 μm iron foil absorber enriched with 95% ^{57}Fe. This foil is the same absorber which gave us the spectra in Fig. 1. All spectra shown were obtained from an absorption geometry, using a ^{57}Co source in a Pd matrix. All NFMS spectra have been processed with a five point running average.

The first set of NFMS data concentrates on the first order sidebands from the 1 and 6 parent transitions (Fig. 5). The nomenclature for identifying the Rf sidebands is as follows. The first digit corresponds to the order of the sideband. Rf sidebands of the j'th order from a given parent transition are found at the sum and difference frequencies of the static field, or Zeeman splitting, and j times the frequency of the applied Rf field. The letter after the first digit, either an "n" or a "p", indicates whether the sideband is a negative or positive sideband respectively. A negative sideband appears at an energy lower than the energy of the parent transition, while a positive sideband is at a higher energy. The last digit identifies the parent transition of the sideband. There are six allowed transitions for ^{57}Fe in a metallic iron foil, of which the lowest energy transition is identified as parent transition one and the highest energy transition is identified as six. The energy difference between parent transitions one and six is 123 MHz, therefore, at 61.5 MHz the 1n6 and 1p1 sidebands should overlap at the transition center of the spectrum. If the gamma ray source is stationary, then the energy of the gamma rays emitted differ from the energy of the transition center of the absorber by the isomer shift. Therefore, a stationary source should provide an NFM spectrum of the 1n6 and 1p1 sidebands displaced from 61.5 MHz by plus and minus the isomer shift respectively (Fig. 5a). The source used was in a Pd lattice, which has an isomer shift of -0.185 mm/sec relative to metallic iron. If the source is then given a constant velocity, the 1n6 and 1p1 sidebands should be displaced from 61.5 MHz by plus and minus (isomer shift - velocity) respectively (Fig. 5b-g). The sign convention is to define a velocity as negative when the source and absorber are moving away from each other. Note that the Rf sideband 1n5, which appears in Fig. 5, should be separated from 1n6 by 25.9 MHz, the excited state splitting frequency in metallic iron.

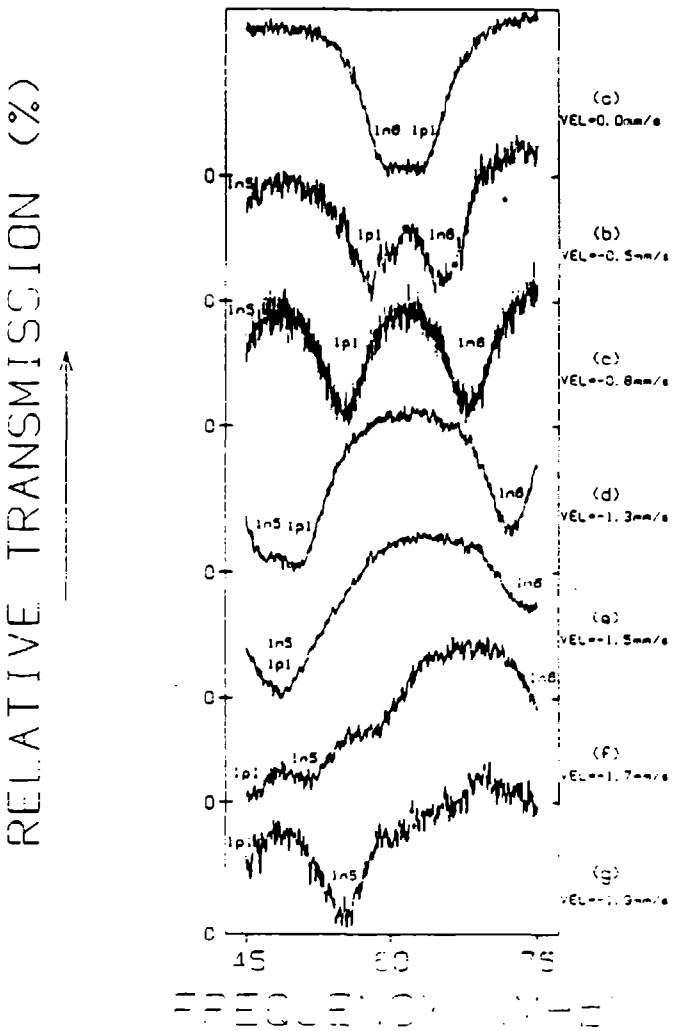

Figure 5: Typical NFMS data showing first order sidebands from the highest and lowest energy transitions of ^{57}Fe in iron, 1n6 and 1p1 respectively, a) in the vicinity of the transition center of this Zeeman split absorber. An "n" in the sideband label indicates that the sideband is at a lower energy than its parent transition, whereas a "p" indicates that the sideband is at a higher energy. As the velocity of the source is decreased b)-g), the energy of the probing radiation is decreased, and as a result the sideband from the lower energy transition, 1p1, appears at lower frequencies. The sidebands from the higher energy transitions, 1n5 and 1n6, appear separated by the excited state splitting frequency of ^{57}Fe in iron, 26 MHz.

The second set of NFM spectra (Fig. 6a-c) were obtained at a lower frequency range. Higher order sidebands add together at these lower frequencies and present significant cross sections. These particular spectra are comprised of 24 different sidebands, if one takes into

account sidebands out to the fifth order. Following the spectra are computer generated simulations (Fig. 7a-c). The model, a simple algorithm, shows remarkable agreement with the data. The frequency at which a sideband will appear is

$$F_{j,ord}(MHz) = [vel-(P_j+iso)]*K/ord \quad , \qquad (1)$$

where Pj is the position of the j'th parent transition in mm/sec, vel is the velocity of the source in mm/sec, iso is the isomeric shift between the source and absorber, ord is the order of the sideband, and K is a conversion factor = 11.6 MHz/(mm/sec) for the 14.4 keV gamma ray being detected. The linewidth of the sideband in the NFM spectrum is

$$\Gamma_{j,ord} = (\Gamma_{pj}+\Gamma_g)/ord \quad , \qquad (2)$$

where ΓPj is the linewidth of the sideband's parent transition and Γg is the linewidth of the 14.4 keV gamma ray emitted by the source. The apparant linewidth's dependence on sideband order can be understood by realizing that an n'th order sideband will be displaced by n frequency units while a first order sideband is displaced by one frequency unit. Since we were concerned only with the relative amplitudes of a sideband within a given NFM spectrum the amplitude of a sideband in a spectrum was assumed to be

$$A_{j,ord} = A_{pj}/ord \quad , \qquad (3)$$

where APj is the amplitude of the sideband's parent transition. By using this equation we have assumed that our spectra were not exhibiting the saturation effects discussed in Ref. 6. This assumption was a convenient mechanism for introducing a sideband amplitude dependence on the relative amplitudes of the parents. For the iron foil used, the relative amplitudes of the parents were taken as 2:2:1:1:2:2 (Fig. 1a). The NFMS is a tool for directly measuring Rf sideband position, width, and amplitude. This model shows that the NFMS is a powerful means of indirectly measuring isomeric shifts and the positions and relative amplitudes of the parent transitions.

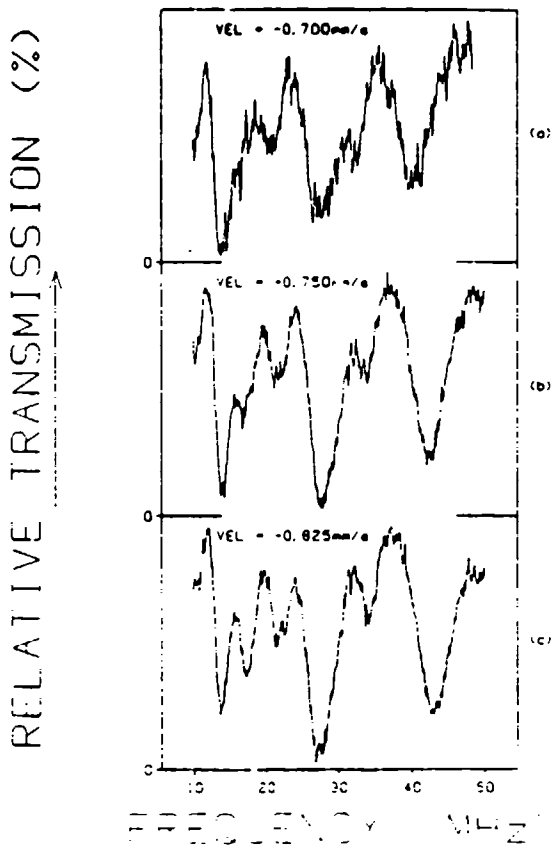

Figure 6: NFMS data obtained at lower frequencies has an appearance which belies the underlying complexity of the spectra. Sidebands add together to produce composite sidebands which have amplitudes, widths, and lineshapes with a high degree of dependence upon the energy of the probing radition. As a result, a small change in the source velocity can lead to a significant change in the appearance of a spectrum.

The NFMS apparatus is versatile. This apparatus is a conventional Mössbauer spectrometer with or without an Rf field, as well as an Rf sideband spectrometer. A conventional Mössbauer spectrometer is not capable of measuring Rf sidebands when they overlap a parent transition, and resonances have been predicted for certain such overlappings. The NFMS enables one to observe the behavior of Rf sidebands in the vicinity of a parent transition, with high enough resolution to discern any fine structure in the sideband which might result from such resonances, because in NFMS the parent transition appears only as a baseline due to its lack of any frequency dependence. With the NFMS it is also possible to observe directly the effect of the Rf field intensity on sideband position, amplitude, and width. It should also be noted that the MCS

described in this paper may also be used in a spectrometer similar to the type described by Bolef and Mishory in Ref. 5.

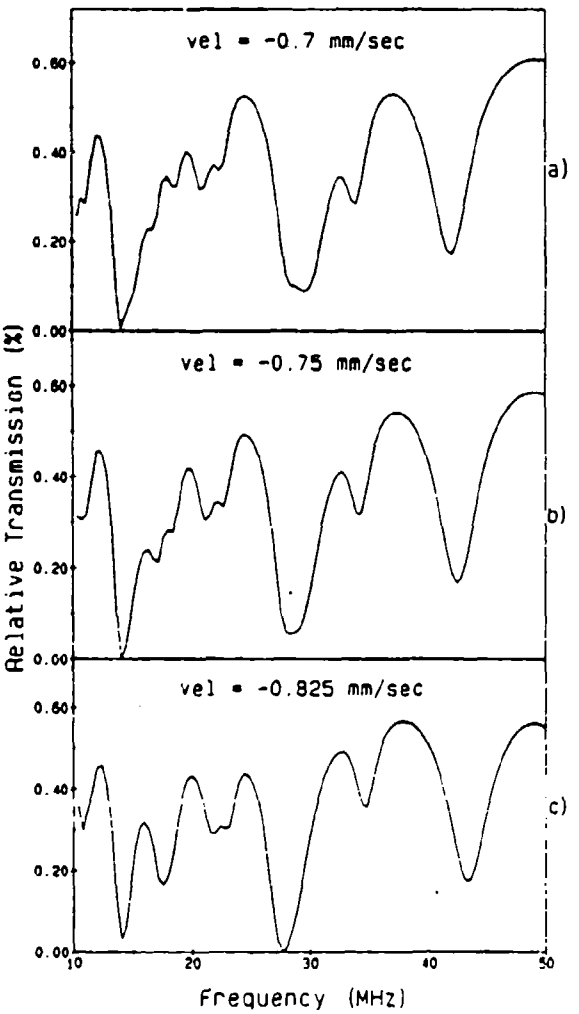

Figure 7: Computer generated simulations of the NFM spectra in Fig. 6 obtained from equations (1-3). Each simulation is composed of 24 different sidebands.

References

1. S. L. Ruby and D. I. Bolef, Phys. Ref. Lett. 5, 5 (1960).

2. Gilbert J. Perlow, Phys. Rev. 172, 319 (1968).

3. Neil D. Heiman, Loren Pfeiffer, and J. C. Walker, Phys. Rev. Lett. 21, 93 (1968).

4. C. L. Chien and J. C. Walker, Phys. Rev. B 13, 1876 (1976).

5. D. I. Bolef and J. Mishory, App. Phys. Lett. 11, 321 (1967).

6. B. D. DePaolo, S. S. Wagal, and C. B. Collins, J. Opt. Soc. Am. B 2, 541 (1985).

N00014-86-C-2488
UTD #24522-964

COMMENT ON MOSSBAUER SIDEBANDS FROM A SINGLE PARENT LINE

by C. B. Collins, P. W. Reittinger, and T. W. Sinor

Foils composed of alternating layers of ferromagnetic and nonmagnetic materials immersed in magnetic fields oscillating at radiofrequencies display sidebands on Mössbauer transitions from the nuclei contained in the nonmagnetic regions. Attributed by Chien and Walker [Phys. Rev. B13, 1876 (1976)] to the transfer into the nonmagnetic layer of acoustic phonons excited by magnetostriction in the ferromagnetic layers, this accepted cause of such effects is challenged by new data resulting from a reexamination and extension of that classic experiment.

The paper of Chien and Walker[1] was of such critical importance that it warrants comment over a decade later. Generally perceived as reporting an unarguable proof of a certain basic proposition, it has now been found to have rested upon a demonstrably false assumption. A reexamination of the original experiment shows it to have been so flawed that any conclusions drawn from it must now be considered unproven.

The point of inception had been the original proposal of Mitin[2,3] that Mössbauer transitions could be excited as part of a multiphoton process in nuclei immersed in intense radiofrequency (rf) fields. In those cases the Mössbauer spectrum was expected to show additional sum and difference frequency lines displaced from the normal lines by integral multiples of the perturbing frequency. In appearance such multiphoton spectra are expected to resemble the transmission spectra which Ruby and Bolef[4] obtained by imposing periodic Doppler shifts of purely mechanical origin upon the Mössbauer source. This unfortunate similarity in appearance between phenomena arising from such different origins provided the basis for years of critical controversy seemingly resolved by the work of Chien and Walker.[1] The purpose of this comment is to report new data from a repetition and extension of the Chien and Walker experiment that shows their conclusions to be unjustified. Without the force of conviction conveyed by their work, the controversy must be reopened to further investigation.

The earliest experiment in radiofrequency sideband production, reported by Perlow[5] in 1968, focused upon the components of the 14.4 keV transition in ^{57}Fe. Several ^{57}Co sources diffused into ferromagnetic hosts were immersed into intense magnetic fields oscillating at radiof-

requencies. Those results were explained[5] as the magnetodynamic modulation of the hyperfine fields and generally conformed to the Mitin hypothesis for multiphoton transitions. Two of the three groups who initially documented this phenomena favored the magnetodynamic explanation which required no mechanical action[5,6,7] while the other group began to develop an alternative based entirely upon magnetostriction.[8,9] Most of the actual experiments had used ferromagnetic hosts to enhance the applied magnetic fields, and such materials are almost invariably magnetostrictive. In the model finally synthesized, periodic Doppler shifts were assumed to be driven by acoustic phonons which were excited by magnetostriction along the greatest dimensions of the material and scattered onto the axis connecting source and absorber. To be effective, this mechanism required the sample to have a large acoustic Q so that displacements of the active nuclei could build to significant values.

Despite the accretion over the years of a large body of phenomenology presumed to describe rf sidebands on Mössbauer transitions, the magnetostrictive-acoustic theory never quantitatively predicted the amplitudes of the sidebands as functions of either applied power or frequency. However, the magnetodynamic models of that time fared no better, and attention turned to "proving" a magnetostrictive origin by distressing the alternative explanations.[10] The obvious difficulty with proving a theory by distressing the alternatives is that those other explanations may not have reached comparable levels of maturation. The magnetodynamic models of the late 60's were relatively easy to destroy.[10] However, the recent successes of ferromagnetodynamics[11,12] show the early models[5] of sideband formation to have been inspired, but inadequate approximations. These models simply did not embody the level of sophistication necessary to describe the complex switching behavior of magnetization in ferromagnetic foils subjected to various combinations of static and oscillating fields in those geometries employed.

More recent experiments[13,14] have shown that the applications of such oscillating magnetic fields to Mössbauer nuclei embedded in nonmagnetic hosts do produce radiofrequency sidebands by directly modulating the phases of the nuclear states involved in the transitions. However, amplitudes were rather small in those experiments because the driving forces depended only upon the value of applied field, $\mu_o H$. In 1984, we extended such approaches further by deriving the phase modulation of a nuclear state in a magnetic material.[15] In this case driving forces

proportional to the magnetization $\mu_o M$ and effects were found to be large.[15,16,17] It appears that many prior results attributed exclusively to acoustic effects driven by magnetostriction could have also benefited from an unrecognized contribution from direct phase modulations of the nuclear states involved.

From a current perspective it is the experiment reported by Chien and Walker[1] that forms the bulwark of the magnetostrictive-acoustic explanation of Mössbauer sidebands. In that experiment an absorbing foil composed of ferromagnetic and nonmagnetic layers was used to study transport of the causitive agent from the ferromagnetic layer into the nonmagnetic region where the sidebands were produced upon Mössbauer transitions of embedded ^{57}Fe nuclei. Very clear evidence showed that the cause did arise in the ferromagnetic Ni layers, producing sidebands in the nonmagnetic stainless steel layers. The most ready explanation at that time was a transport of phonons from one layer to the next with a high acoustic Q. Those experiments were repeated in the work reported here, but with extensions which contradict the classic interpretation of Chien and Walker.[1]

Although not unique for all sidebands in a spectrum,[1] the idea of a modulation index m as a measure of the strength of the development of the sidebands offers practical convenience for descriptions. For a magnetostrictive origin,[1]

$$m = x_0/\lambda \quad , \tag{1}$$

where x_0 is the amplitude of the periodic displacement of the nuclei and $\lambda = 0.137$ A for the 14.4 keV line of ^{57}Fe. In the corresponding magneto dynamic model,[15]

$$m = bH \quad , \tag{2}$$

where H is the applied magnetic field and b provides proportionality between M_s, the saturation magnization of the medium, and H. For relatively small m, the ratio of the magnitude of the first order sidebands to the intensity in the original parent line is proportional to m^2, which in turn is proportional to P, the applied radiofrequency power.

One of the most compelling results presented by Chien and Walker[1] was a demonstration supposed to show the enhancement of m^2 afforded by

tighter acoustic coupling of the layers. They found that electroplating Ni upon a stainless steel foil produced much higher values of m^2 in absorption experiments than could be obtained by gluing a Ni foil to the stainless foil. They attributed the difference to the obviously poorer acoustic properties of the glue. However, as part of this report we observe that their stainless steel foil was electroplated on <u>both</u> sides with Ni while the epoxied bond was used to join a <u>single</u> Ni foil to one side of the stainless absorber. While the m defined by Eq. (1) for a single foil could not be additive if produced in different magnetostrictive layers, in principle the M_s upon which m depends in Eq. (2) could add coherently. Two sources of m arising from distinctly separate sources could give a resulting modulation of $4m^2$ in a magnetodynamic model. Chien and Walker failed to recognize[1] that even in the magnostrictive model two sources of m generated in the two electroplated layers should give a modulation index of $2m^2$ in the absorber foil. Instead, they attributed the increased sideband intensity developed by the two plated sources in comparison to the one glued source only to the advantage they assumed for a plated contact over a glued interface. They reported no comparison of the effects of gluing or plating the *same number of ferromagnetic layers to the absorber foil.* Reported here is a repetition of the Chien and Walker experiment which showed that the effect of two foils varied from two to four times that produced by a single foil joined in the same fashion, depending upon the static magnetic bias applied.

In our experiment the absorber was a 2.5 μm paramagnetic stainless steel (SS) foil with 90.6% enrichment of ^{57}Fe. For the nonabsorbing ferromagnetic drivers, 2.5 μm Ni foils were used, all of which were cut from a single sheet of polycrystalline Ni. The stainless-steel absorber was sandwiched between two Ni foils and held in rigid contact by mounting the foils between glass cover slides of 100 μm thickness. A conventional Mössbauer spectrometer, modified for rf experiments, Fig. 1, utilized a 25 mCi source in a Rh matrix to obtain the ^{57}Fe absorption spectra. The 14.4 keV gamma rays were detected with a Kr gas filled proportional counter biased with 1.8 kV.

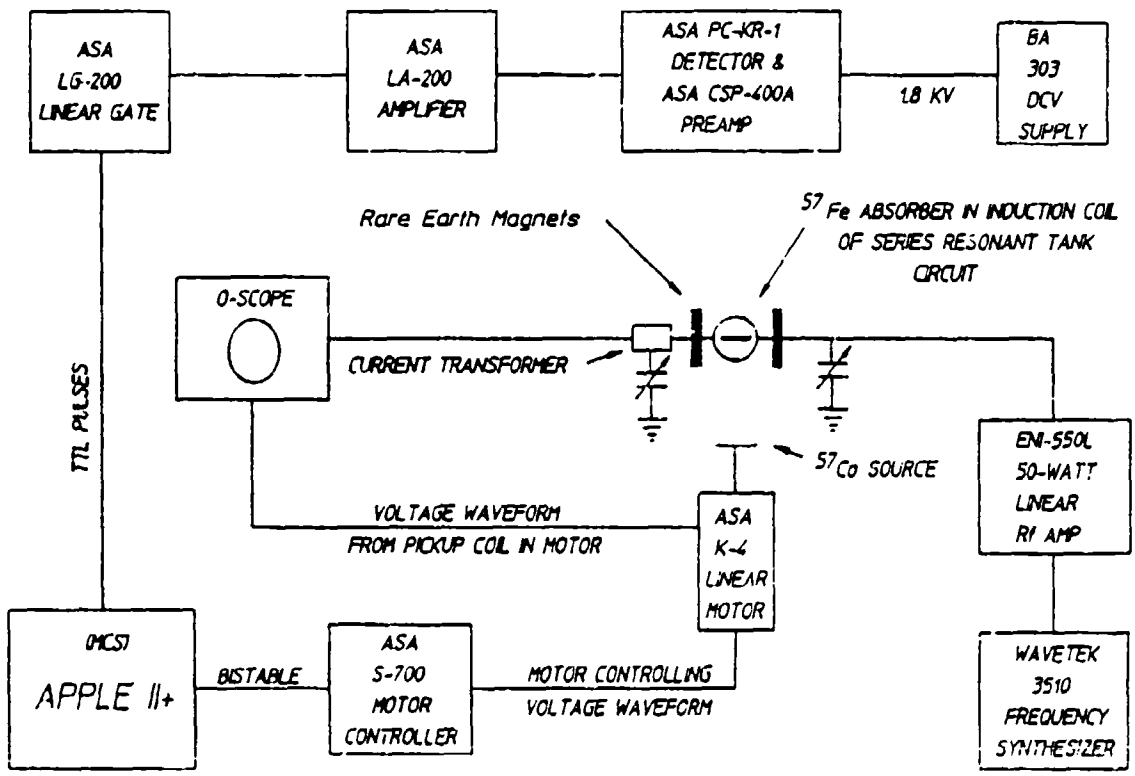

Fig. 1: Schematic drawing of the experimental arrangement used.

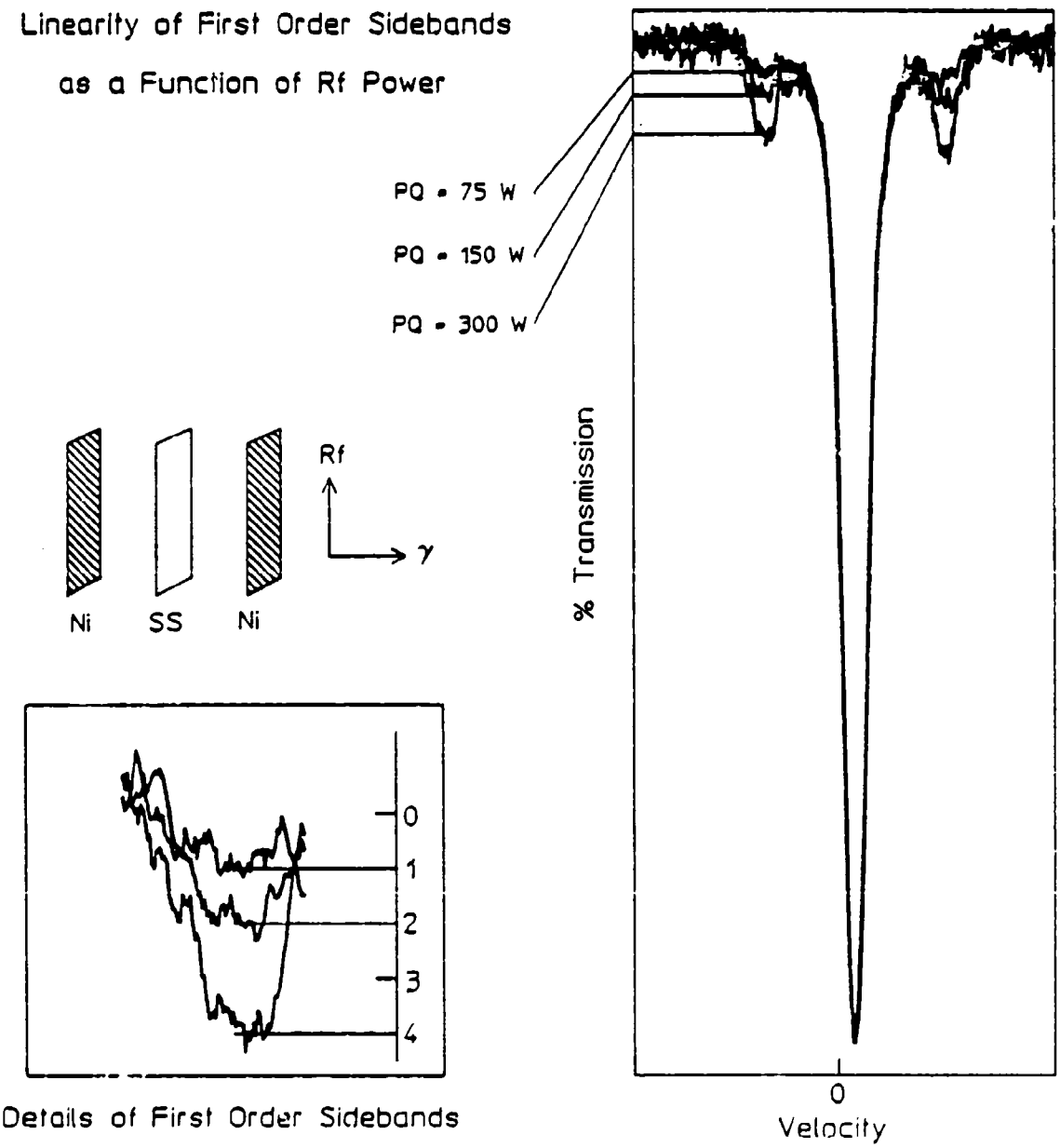

Fig. 2: Experimental verification of the linearity of the first order sidebands at 25 MHz as a function of the applied rf power. The product of the applied rf power, P, and the quality factor, Q, of the circuit are used to insure reproducibility of the rf field strengths.

A 25 MHz rf magnetic field was applied by mounting the foils in the cylindrical induction coil of an L-C tank circuit. In obtaining data for a direct comparison between the effect of one Ni driver versus two, the product of the applied rf power P and the electrical Q of the circuit containing the rf induction coil was maintained at constant values. Elementary analysis shows that if PQ is constant the rf current in the coil of such a circuit is also constant and hence the two absorber arrangements are subjected to applied fields of the same intensity H. The results of the first experiment verified the linearity of the first order sideband amplitudes at 25 MHz for SS with two Ni drivers with PQ products of 75, 150, and 300 W Fig. 2. The spectra are scaled so that the intensity of the central Mössbauer absorption peak of ^{57}Fe in SS is held constant in order to make direct comparisons of the sideband amplitudes.

Having established the linearity of the first order sidebands in the Ni-SS-Ni sandwich, one of the Ni drivers was removed and the experiment was repeated with the same PQ products as before. Figure 3 shows a comparison of the sideband amplitude for two Ni drivers versus one; in this configuration two Ni drivers give twice the effect of one driver foil.

In the next experiment a comparison between the effect of one source of excitation with that from two sources when both were biased with a static magnetic field. Rare earth magnets were placed about the induction coil such that the static magnetic field was mutually orthogonal to the rf magnetic field and the direction of gamma-ray propagation.

The linearity of the sideband amplitudes at 25 MHz as a function of PQ was again established (Fig. 4) to insure that the introduction of the static magnetic field did not introduce any nonlinearities to the system. The scale thus established was used to measure the decrease in the sideband amplitude when one of the sources of excitation was removed from this biased sandwich. As is clearly shown in Fig. 5, the sideband amplitudes obtained with two driver foils are four times the amplitudes obtained with one driver foil. Therefore, with the application of a static B-field, two sources of excitation give four times the effect.

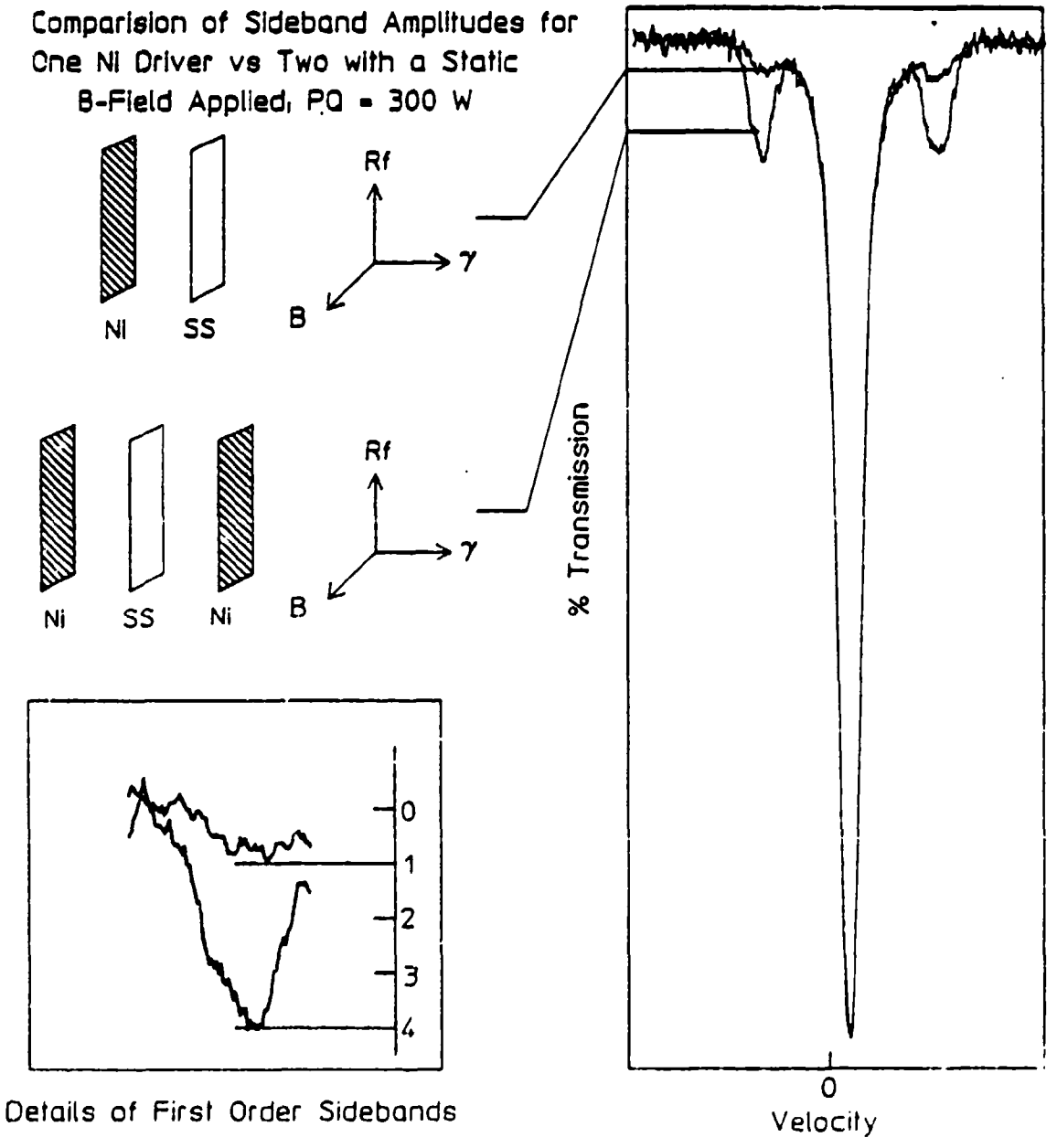

Fig. 3: Comparison of first order sideband amplitudes for one Ni driver foil versus two at 25 MHz with a PQ product of 300 W.

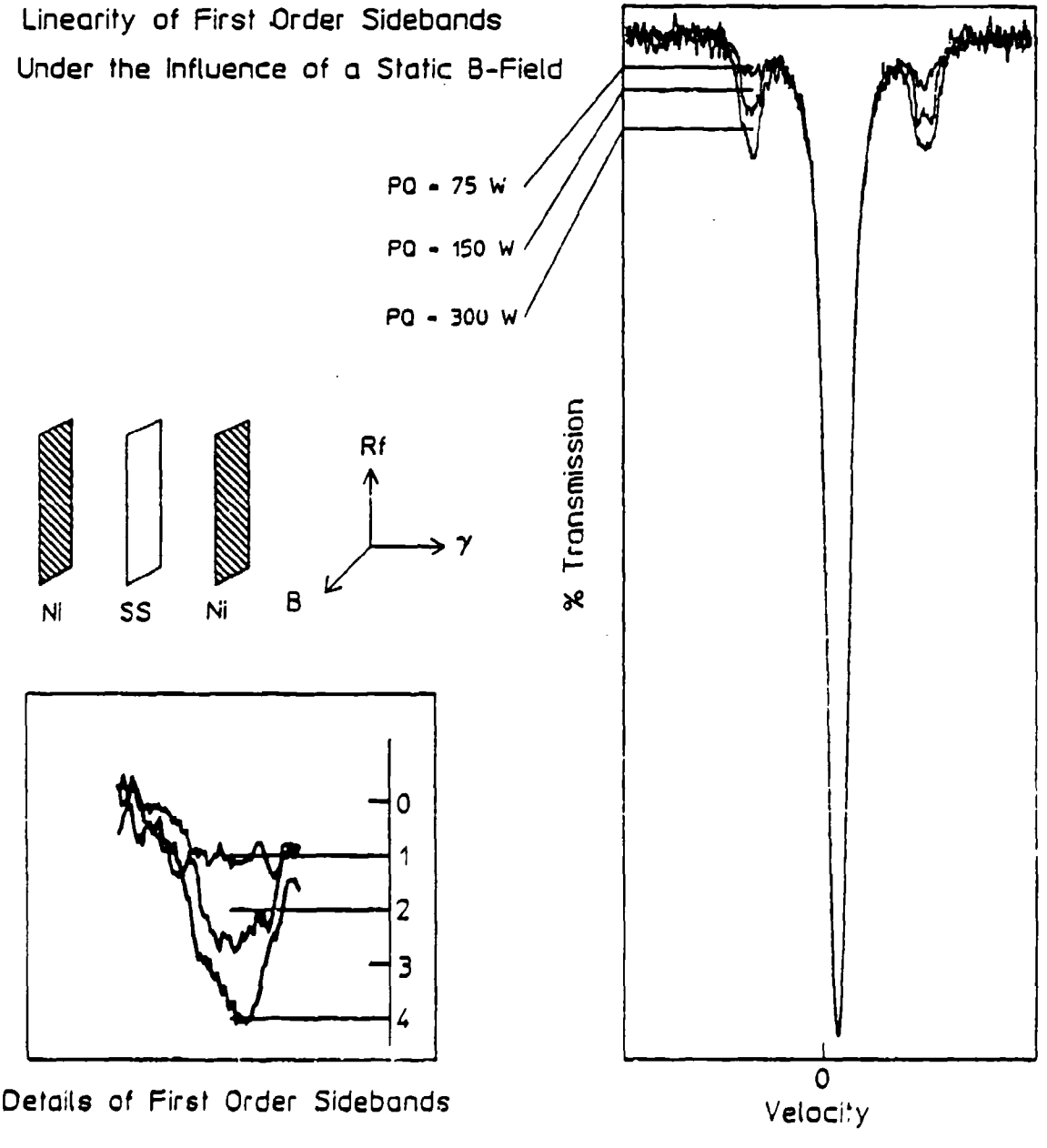

Fig. 4: Establishment of linearity of the first order sidebands at 25 MHz with PQ = 75, 150 and 300 W when the foils are biased with a static B-field.

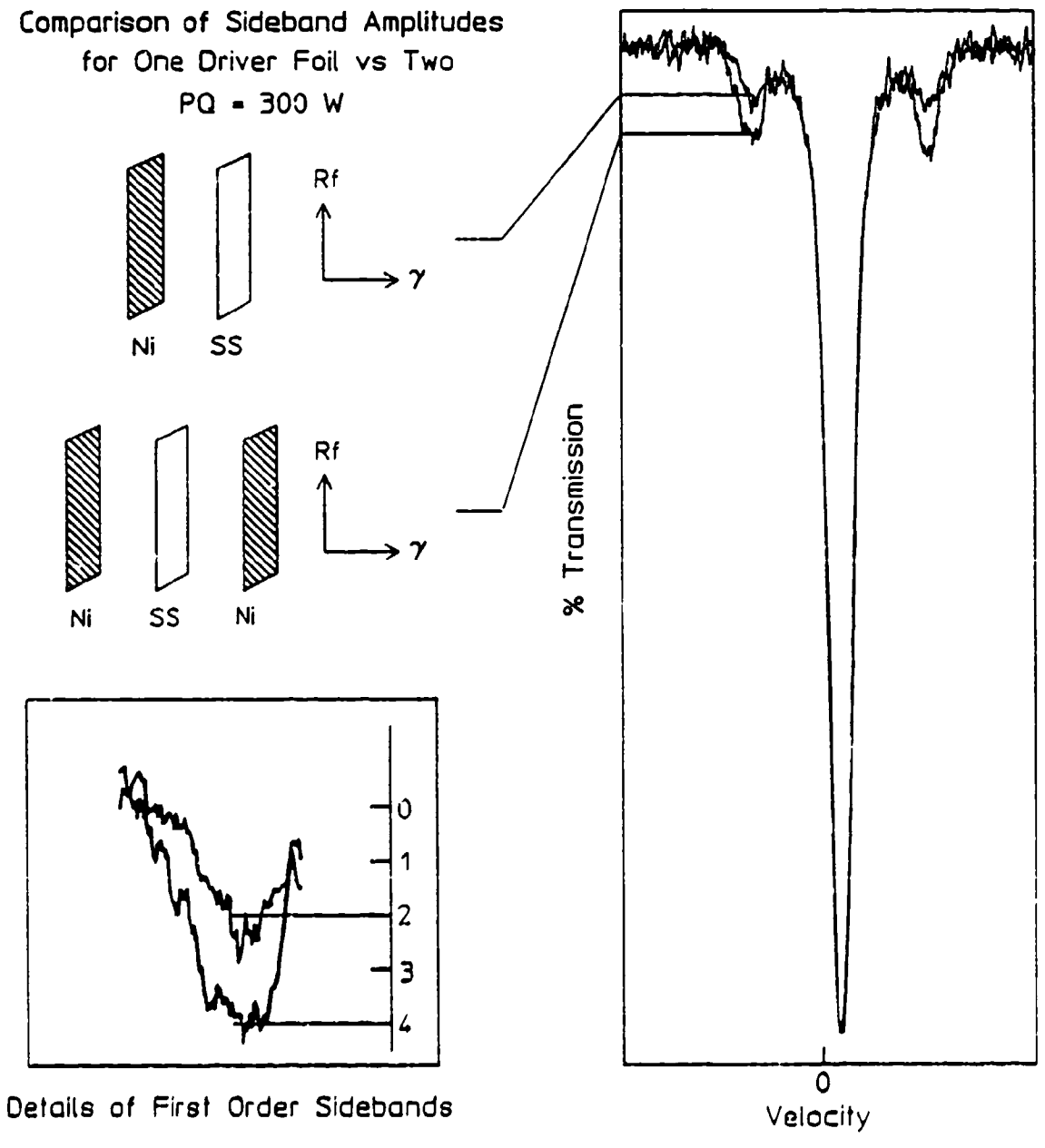

Fig. 5: Comparison of sideband amplitudes for one driver foil versus two when both are biased by a static B-field with PQ = 300 W. Here two foils give four times the effect of one thus giving a modulation index of $4m^2$.

The results of this reexamination of the Chien and Walker experiment support only the first conclusion reached in that original work, namely that the causitive agent of rf sidebands can be produced in a ferromagnetic layer and then transported into a nonmagnetic layer. Their other conclusion is completely refuted by this demonstration because the effects they attributed to the type of coupling between layers most probably resulted from the relative numbers of magnetic and nonmagnetic layers.

These new results go beyond the propositions tested by Chien and Walker[1] and display behaviors completely inconsistent with the traditional magnetostrictive-acoustic origin of Mössbauer sidebands. In experiments such as these, acoustic phonons are the bosons associated with vector fields driven by tensor forces, *not vector forces*. Without invoking stimulated emission, we can conceive of no way in which tensor sources which are physically separated can produce coherent vector fields in a space between them, even if they are temporally synchronized. The stimulated emission of phonons to produce coherent additions of the displacements arising from the different sources would imply the existence of a threshold of power, above which two modulation indices of m would give an effect of $4m^2$ and below which only $2m^2$. No such threshold was suggested by data similar to that of Fig. 5 which was obtained over an adequate range of powers.

In view of the growing number of successes of the model for the direct modulation of the phases of the nuclear states and these new results which question the validity of the conclusions of the Chien and Walker[1] experiment, it would appear that the controversy over the origin of Mössbauer sidebands must be reopened.

The authors gratefully acknowledge the support of this work by the Office of Naval Research, by the Naval Research Laboratory, and by the Innovative Science and Technology Directorate of the Strategic Defense Initiative Office.

References

1. C. L Chien and J. C. Walker, Phys. Rev. B 13, 1876 (1976).

2. A. V. Mitin, Sov. Phys. JETP 25, 1062 (1967).

3. A. V. Mitin, Sov. Phys. Dok. 15, B27 (1971).

4. S. L. Ruby and D. I. Bolef, Phys. Rev. Lett. 5, 5 (1960).

5. G. L. Perlow, Phys. Rev. 172, 319 (1968).

6. G. Asti, G. Albanese, and C. Bucci, II Nuovo Cimento 57B, 531 (1968).

7. G. Asti, AB. Albanese, and C. Bucci, Phys. Rev. 184, 260 (1969).

8. N. D. Heiman, L. Pfeiffer, and J. C. Walker, Phys. Rev. Lett. 21, 93 (1968).

9. N. D. Heiman and J. C. Walker, Phys. Rev. 184, 281 (1969).

10. L. Pfeiffer, N. D. Heiman, and J. C. Walker, Phys. Rev. B 6, 74 (1972).

11. T. H. O'Dell, Ferromagnetodynamics (Wiley, New York, 1981), Chap. I.

12. C. W. Chen, Magnetism and Metallurgy of Soft Magnetic Materials (North-Holland, Amsterdam, 1977).

13. P. J. West and E. Matthias, Z. Phys. A 288, 369 (1978).

14. E. Ikonen, P. Helistö, J. Hietanieni, and T. Katila, Phys. Rev. Lett. 60, 643 (1988).

15. C. B. Collins and B. D. DePaola, Optics Lett. 10, 25 (1985).

16. B. D. DePaola and C. B. Collins, J. Opt. Soc. Am. B 1, 812 (1984).

17. B. D. DePaola, S. S. Wagal, and C. B. Collins, J. Opt. Soc. Am. B 2, 541 (1985).